The Sound Insulation
of
Cavity Walls

A thesis submitted in fulfilment of the

requirements for the Degree of

Doctor of Philosophy

at the

University of Canterbury

by

Jason E. Cambridge

University of Canterbury
Christchurch, New Zealand
2012

Table of Contents

List of Figures

List of Tables

Acknowledgements

I would like to thank my supervisor Dr John Pearse for giving me the opportunity to do this work. Thank you for all of your support, advice, input, time, patience and understanding during the course of this research.

I wish to extend my special thanks to Dr John Davy for all the time and effort spent answering the questions which I had along the way. Dr Davy's input was invaluable and I am grateful to him for introducing me to Gösele's paper.

I would also like to thank Dr Stefanie Gutschmidt for her timely input, observations and comments which enhanced the overall development of this work, as well as Brian Donohue for discussing different ideas regarding the research at various times.

I also wish to acknowledge the support of the Foundation for Research, Science and Technology who funded this research through the Technology for Industry Fellowship (TIF) program in conjunction with Winstone Wallboards Ltd.

To my New Zealand family (Nick, Jenny, John, Emma, Eliot, Jessica, Lynelle, Ben and Dana) who supported me throughout my research; the Cousin's family (Brian and Linda), my Caribbean family (Fernandez, Greg, Josh, Trudy, Vannesa, Ghislaine, Annette and Yvette), College House, Arise Church and special friends (Anastasia, Marie, Sharia, Elsabe, Tanuja, Rod, Tykes, Cameron, Kuda, Rohan and Taz) thank you for your overall support as we faced earthquakes and other personal challenges together during this research.

Finally, I would like to thank my father (Patrick Cambridge) who always believed in me, never gave up and provided the support which I needed. My grandparents (Cuthbert and Mary James) who set the foundation of my life. The Pascal family (Junior, Monica, Afyia and Akilah) who I lived with during my teenage years. The Alexander family (Dexter and Debbie) for all their support and making me feel at home while I studied in the USA and to all of my other family members who helped to shape me along the way.

Thank you Dr Nearon and everyone else in Trinidad, Washington D.C, New York, Sweden and South Africa who made this possible. I am extremely grateful for all of your support.

Abstract

Lightweight building materials are now commonly employed in many countries in preference to heavyweight materials. This has lead to extensive research into the sound transmission loss of double leaf wall systems. These studies have shown that the wall cavity and sound absorption material placed within the cavity play a crucial role in the sound transmission through these systems. However, the influence of the wall cavity on the sound transmission loss is not fully understood.

The purpose of this research is to obtain a comprehensive understanding of the role played by the wall cavity and any associated sound absorption material on the sound transmission loss through double leaf wall systems. The research was justified by the fact that some of the existing prediction models do not agree with some observed experimental trends.

Gösele's theory is expanded and used in the creation of an infinite and finite vibrating strip model in order to acquire the desired understanding. The sound transmission loss, radiated sound pressure and directivity of double leaf systems composed of gypsum boards and glass have been calculated using the developed model. A method for calculating the forced radiation efficiency has also been proposed. Predictions are compared to well established theories and to reported experimental results.

This work also provides a physical explanation for the under-prediction of the sound transmission loss in London's model; explains why Sharp's model corresponds to Davy's with a limiting angle of 61° and gives an explanation for Rindel's directivity and sound transmission loss measurements through double glazed windows. The investigation also revealed that a wide variety of conclusions were obtained by different researchers concerning the role of the cavity and the properties of any associated sound absorption material on the sound transmission loss through double wall systems. Consequently recommendations about the ways in which sound transmission through cavity systems can be improved should always be qualified with regard to the specific frequency range of interest, type of sound absorption material, wall panel and stud characteristics.

1 Introduction

In many countries the problems associated with the shift from heavy to lightweight building materials has led to extensive research into the sound transmission loss of double leaf wall systems. These studies have shown that the wall cavity and sound absorption material placed within the cavity plays a crucial role in the sound transmission of these systems. However, a full understanding of the influence of the wall cavity on the sound transmission loss has not been obtained.

The sound insulation/sound transmission loss though the wall system in buildings is the primary means by which the noise exposure of the inhabitants is controlled. Epidemiological studies have shown links between population exposure to environmental noise and cardiovascular disease, cognitive impairment in children, sleep disturbance, tinnitus and annoyance; as a result noise exposure should not only be considered to be a source of nuisance but of public and environmental health (World Health Organization regional office for Europe, 2011). Legal, engineering and educational noise management measures as recommended in the World Health Organisation's "Guidelines for Community Noise"(World Health Organization, 1999) are all aimed at reducing the public's exposure to noise and the protection of their health. The establishment of legal measures for the acoustic properties of buildings are included within the recommended noise management measures within this report. Consequently many nations within Rasmussen's (2010) survey have developed building codes with legal stipulations outlining the requirements for sound transmission loss. Examples of some of the regulations existing in different countries are given in Table 1.

Table 1 Building requirements in three European countries and New Zealand

Country	Descriptor	Multi-storey housing requirement (dB)	Row housing requirement (dB)	Class denotation
Germany	R'_w	≥ 53	≥ 57	III/II/I
Sweden	$R'_w + C_{50-3150}$	≥ 53	≥ 53	A/B/C/D
UK[1]	$D_{nT,w} + C_{tr}$	≥ 45	≥ 45	-
New Zealand	STC	≥ 55	≥ 55	-

From (Rasmussen, 2010) and (New Zealand Department of Building and Housing, 2006)

Although the descriptors, requirements and classifications vary internationally, it is universally agreed that appropriate sound transmission loss of wall systems is important for the health and well being of a population. The implementation of different standards in countries is partly related to each country's attempt to deal with low frequency noise, the complexities of sound sources and the realization of the importance for having an evaluation system which works equally well for both heavy and lightweight structures (Rasmussen and Rindel, 2005). The shift from heavy to lightweight building materials has lead to extensive research into the sound transmission loss of double leaf wall systems over the past decades. These studies have shown that high sound transmission loss can be obtained when using a double leaf wall system, even when composed of lightweight materials.

A typical double leaf wall system separating two rooms can be seen in Figure 1. In such systems the sound transmission through the flanking path, studs or wall connections and wall cavity are the three main paths through which sound is transmitted.

[1] England and Wales only. Scotland and Northern Ireland use different descriptors and performance levels

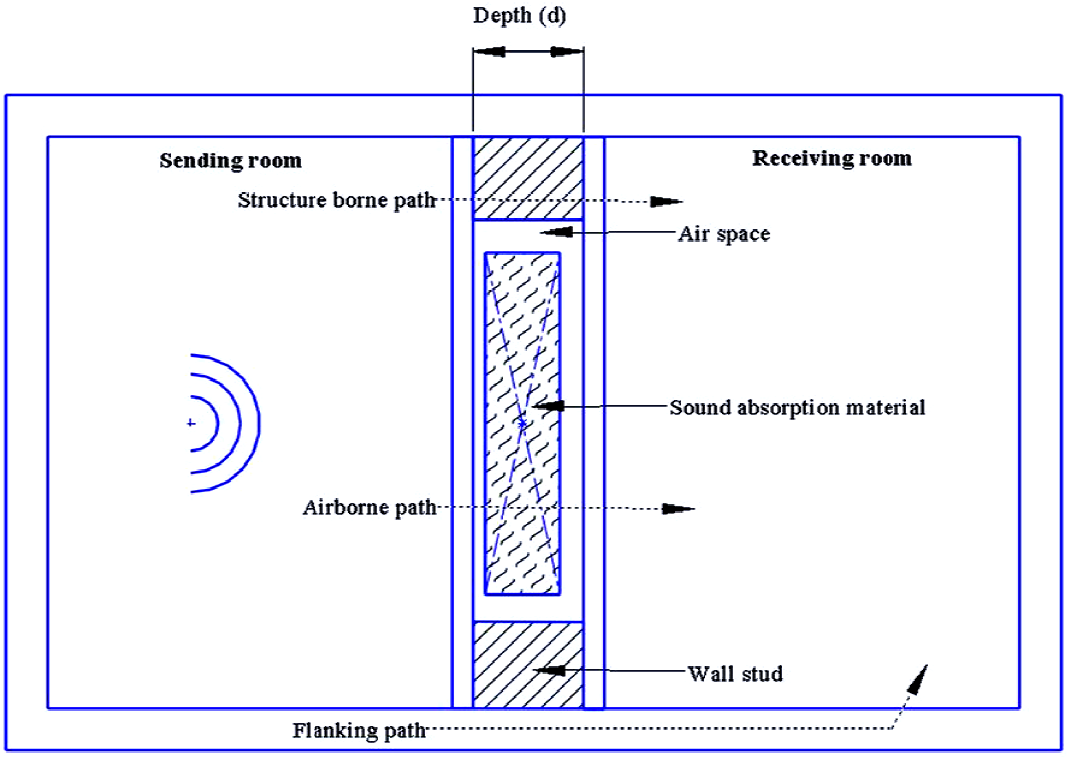

Figure 1 Sound transmission paths through a double leaf wall system separating two rooms

The study of the sound transmission through different flanking paths is the fundamental basis of the European EN 12354-1:2000 (EN12354-1:2000) standard. This standard is limited to adjacent rooms and the type of elements is mainly restricted by the available information on the vibration reduction index of monolithic and lightweight double elements (EN12354-1:2000). The vibration reduction index gives a measure of the attenuation of sound that occurs due to vibrations at the junctions. Calculation of the vibration reduction index is based on Gerretsen's (1979; 1986) measurements and prediction model. When only homogenous building materials are used, the vibration reduction index is frequency independent; however a slight frequency dependence can be seen in lightweight double leaf constructions (Gerretsen, 1986). Accurately predicting the vibration reduction index when lightweight double leaf constructions are used has been a challenge. As a result an alternative method for calculating the velocity level difference (which is used in the calculation of the vibration reduction index) and flanking transmission loss has been proposed by Mahn and Pearse

(2008). Research in this area especially with regard to lightweight double leaf constructions is ongoing.

Measurements and prediction models for the structure borne sound transmission via the wall studs have been conducted by many authors. Sharp (1978) developed a theory to account for both point and line connected steel studs; Gu and Wang (1983) for resilient steel studs; Rindel (2006) combined the effect of different boundary conditions, stud and connection types into one formula to account for the change in sound transmission loss due to the studs; while Craik and Wilson (1995) developed a theoretical model for sound transmission across metal ties in cavity walls. These are just a few of the authors who have developed theories relating to the structure borne transmission. Sound transmission via the wall studs is relatively well understood.

Airborne sound transmission through the wall cavity is the subject of this thesis. The wall cavity is considered to be the space through which airborne sound transmission occurs and where any sound absorption material is placed (see Figure 1). Although sound transmission through the studs is greater than through the cavity (Davy, 2009c) and the amount of flanking transmission depends on the flanking path; the sound transmission through the cavity plays a crucial role in the overall sound transmission loss of the entire wall system and special consideration must be given to it if suitable sound transmission loss (STL) is to be obtained. As a result this thesis looks at the influence of the wall cavity on the STL from experimental investigations and explains why some existing prediction models do not agree with some observed experimental trends.

1.1 Experimental investigations

Experimental investigations into how different elements within the wall cavity affect the STL have been conducted by authors such as Bravo et al. (2002), Hongisto et al. (2002) and Loney (1971; 1973). These investigators studied the effect of changing different parameters (such as the amount of sound absorption material) on the STL under laboratory conditions. Their work provide useful information about trends associated with varying these parameters and are usually supported by the more theoretical approach by authors such as Sharp (1978). For example, Sharp (1978) discussed the effect of having sound absorption material and studs within the wall system on the STL. Without sound absorption material within the wall cavity,

Sharp concluded that modal coupling between the wall panel and the cavity could produce a similar effect as having a direct mechanical connection. As expected, such coupling would reduce the STL of the system. However, as Sharp mentioned, if sound absorption material were placed within the cavity, the magnitude of the standing waves would be reduced, thus giving an increase in the STL. Loney (1971) verified these trends by reporting the difference in the STL with and without sound absorption material within the wall cavity. He also went one step further, by showing that the first inch (25 mm) of absorbent material has the greatest influence on the STL.

With regards to the characteristics of the absorption material within the cavity, Narang (1993) showed that fibreglass with an airflow resistance of 400 $\mathrm{Ns/m^3}$ was sufficient for optimum STL; while his experimental results indicated that increasing the airflow resistance of the fibreglass beyond this point had negligible effect on the STL. Narang (1995) also showed that placing polyester in the cavity increased the STL by an amount similar to fibreglass even though the airflow resistance of the polyester was 20% less.

Although extensive experimental investigations have been conducted into the sound transmission loss through double leaf wall systems over the past decades a summary of the conclusions from these investigations has not been produced. Consequently, questions are still being asked about the influence of the material characteristics, amount and placement within the wall cavity on the sound transmission loss.

1.2 Prediction models

Prediction models of the STL have been used extensively to explain the different trends observed from experimental data. Consider the National Research Council of Canada (NRCC) (Halliwell *et al.*, 1998) measured STL results shown in Figure 2 for a 16 mm double leaf gypsum plasterboard double wall system with 65 mm steel studs at 406 mm centres without sound absorption material within the cavity. In this figure the mass air mass resonance (f_0), limiting (f_l) and critical (f_c) frequencies are all shown.

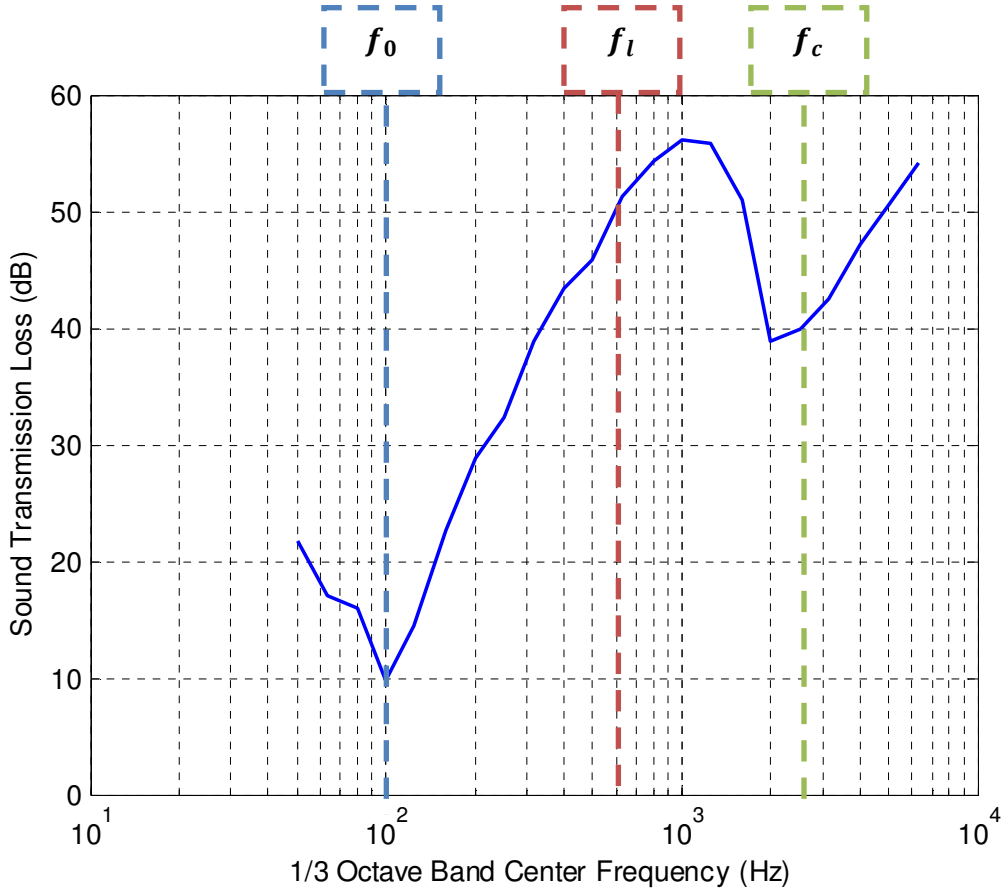

Figure 2 NRCC's STL measurements for a 16 mm double leaf wall system with 90 mm steel studs at 406 mm centres

The mass air mass resonance frequency (f_o) is the frequency where maximum sound transmission occurs in double leaf wall systems (Fahy, 1985);

$$f_o = \frac{c}{2\pi}\sqrt{\frac{\rho_o}{d}\left(\frac{m_1 + m_2}{m_1 m_2}\right)} \qquad \text{1-1}$$

where c is the speed of sound in air, ρ_o is the density of air, d is the depth of the wall cavity and m_1 and m_2 are the mass of the two leaves of the double leaf system.

The STL below f_0 is primarily based on the mass of the wall panels; the cavity has little influence within this frequency range (Sharp, 1973). The limiting frequency (f_l) shown in Figure 2 corresponds to the frequency at which the Helmholtz wave number of one with

respect to the wave number of sound in air and the cavity width occurs. Helmholtz wave number is equal to k. Therefore the Helmholtz wave number of one with respect to the wave number of sound in air and cavity width corresponds to $1/(kd)$, which is equal to $c/(\omega d)$. An approximate expression for the limiting frequency was found by Sharp (1973) such that

$$f_l = \frac{55}{d}. \qquad \textbf{1-2}$$

At frequencies greater than the limiting frequency, the wavelength of the sound wave within the cavity becomes comparable to and less than the panel separation (Sharp, 1973). The cavity resonance perpendicular to the wall panels plays a major role in the sound transmission within this frequency range. Finally the critical frequency (f_c) is the frequency where the wavelength of the bending waves on the panel is equal to the wavelength of air.

$$f_c = \frac{c^2}{2\pi}\sqrt{\frac{m}{B}} \qquad \textbf{1-3}$$

where B is the bending stiffness of the wall panel. At f_c a region of a reduction in the STL begins.

The prediction and understanding of the STL through double leaf wall systems over all of the frequency ranges has dramatically improved since the development of the early classical prediction models developed by Beranek and Work (1949) and London (1950). Hongisto (2006) provided a detailed survey of more than 20 of the well known prediction models that are currently being utilized and concluded that there is a high degree of variability in the results produced from these models and no single model was capable of predicting the STL for the entire spread of commercially available walls.

The prediction of the STL above the critical frequency for double leaf walls has been well understood due to the insights obtained from work done on single thin panels from authors such as Cremer (2005) and Jose and Lamure (1964). In this frequency range sound transmission is dominated by the free bending waves. The wavelength of these waves is greater than the wavelength of air. However, below the critical frequency the free bending

waves are inefficient radiators. As a result the sound transmission is controlled by the forced bending waves below the critical frequency. The complexity of the calculations required for the radiation efficiency of the forced bending waves is generally more complicated than those required for the free bending waves. As a result some analytical models such as Sharp's (1973) use unexplained empirical correction factors and techniques in order to improve the accuracy of their prediction models.

Cremer (1942) showed that the sound transmission coefficient (τ) at a specific angle of incidence (θ) for an infinite panel can be found from

$$\tau_\theta = \frac{1}{\left|1 + \frac{Z cos\theta}{2\rho_0 c}\right|^2} \qquad \text{1-4}$$

where Z is the bending wave impedance of the wall and $\rho_0$is the density of air.

In order to determine the sound transmission coefficient for excitation by a reverberant sound field it is generally assumed that all angles of incidence are equally probable and that the average value of the coefficient is given by integrating τ_θ, multiplied by an appropriate weighting factor, over all angles of incidence in the range from 0 to $\pi/2$ radians (Sharp, 1978). The result obtained by integrating over all angles of incidence from 0 to $\pi/2$ radians under-predicts the STL; as a result the upper limit of the integration is often limited by some authors in order to improve the STL prediction. However, instead of limiting the upper limit of the integration, Sharp (1973) used the "effective mass" of the wall within his prediction model.

Sharp (1973) showed that the "effective mass" of a single panel for the sound transmission loss below the critical frequency can be obtained by dividing the actual mass by 1.9. Sharp's deviation came from Jose and Lamure's (1964) single panel STL model for one third octave bands below the critical frequency. For double leaf walls with sound absorption material in the cavity, Sharp used this effective mass for each leaf and assumed that the normal STL

could be used for all angles of incidence to account for integrating over all angles of incidence, a result which matches Davy's (1990a; b) theories with a fixed limiting angle of

incidence of 61° (Davy, 1998). Although it may be reasonable to suppose that a cavity with a large amount of absorption reduces the range of angles at which sound can propagate effectively across the cavity (Davy, 1998); the use of the normal sound transmission loss in this manner has been an unexplained technique. Consequently the reason why Sharp's (1973) and Davy's (1990a; b) model with a limiting angle of 61° are successful at predicting the sound insulation of cavity walls with sound absorption material in the cavity remains unknown.

Sharp's (1973) and Davy's (1990b; a) models are extensions of London's (1950) infinite model. London's model underestimates the STL of finite wall systems. In order to obtain satisfactory results with measurements, London (1949; 1950) used an empirical correction factor which was determined from experimental observations. However no physical explanation was given for the use of this empirical correction factor either by London or within the literature. As a result, physical explanation for the reason why London's model underestimates the STL remains unknown.

STL prediction models for double leaf wall systems can also be applied to double glazed windows. Rindel (1975) measured sound transmission through double glazed systems for different angles of incidence. Rindel's prediction models for both the STL and the directivity of the transmitted sound did not compare well to his measured results. As a result, a model and an explanation for Rindel's measured STL and directivity data have not been forthcoming.

1.3 Aim and methodology

The aim of this research is to obtain a comprehensive understanding of the role played by the wall cavity and any associated sound absorption material in the STL of double leaf wall systems. The methodology utilized is based on first establishing the observed experimental trends; then once these trends are established a model is created to explain why London's (1950) infinite model underestimates the sound transmission loss. It is believed that once this explanation is found, this model can then be adopted for the finite case which in turn can be used to explain some of the observed experimental trends. Consequently the desired understanding is achieved by:

- A review, supported by some experimental measurements of the results of previous investigations in order to determine the influence of the material characteristics, amount and placement within the wall cavity on the STL
- Developing a model which provides a physical explanation for the reason why London's model under-predicts the STL of double wall systems.
- Developing a model which addresses why Sharp's (1973) model corresponds to Davy's (1990b; a) model with a limiting angle of 61°
- Using the developed model to provide an explanation for Rindel's (1975) measured STL and directivity

1.4 Thesis outline

Gösele's (1977) work is expanded within this research to create a two dimensional vibrating strip model. This expansion is used to calculate the sound transmission loss, radiated sound pressure and forced radiation efficiency of the double leaf wall systems. The developed model is also used in the prediction of the STL and directivity of transmitted sound through double glazed windows. The study begins by looking at the influence of the wall cavity and sound absorption material on the STL from reported experimental results in Chapter 2.

In Chapter 3 a survey of the existing approaches used in predicting the sound transmission loss is given in relation to whether they can be used to explain the under-prediction in London's model or in determining the role of the wall cavity on the STL through double leaf wall systems.

In Chapter 4 Gösele's (1977) work is expanded and the governing equations used to describe the sound pressure within the wall cavity is derived and solved. The results from Chapter 4 are then used to derive the STL for the infinite model in Chapter 5. Comparisons are made to London's (1950) model and an explanation given for the reason why London's model under predicts the STL.

In Chapter 6 a two-dimensional vibrating strip model is developed and used to determine the forced radiation efficiency. A two-dimensional version of Davy's (2009b) model for the forced radiation efficiency into a two-dimensional space is also given within this chapter. The developed model is then used to determine the STL of double leaf wall systems in Chapter 7;

while descriptions of all the numerical techniques and integration methods used within this thesis are given in Chapter 8. An analysis of the convergence of the solution for the radiation efficiency of the forced reflected waves within the wall cavity is also given.

In Chapter 9 the developed model is used to find the STL through double glazed window systems, Rindel's measured STL at different angles of incidence and the directivity of transmitted sound through double glazed windows. Finally in Chapter 10 conclusions are given about the role played by the cavity in the STL through double leaf wall systems and double glazed windows.

Extensive references have been made throughout this thesis to other models and alternative approaches used by other researchers. The aim of this approach is to give a holistic vantage point of the overall scope of the amount of work that has been conducted within this area and to demonstrate how the research presented in this thesis relates to research conducted by others. By doing this, a comprehensive understanding of the influence of the wall cavity and any associated sound absorption material on the STL has been obtained.

2 The influence of the wall cavity on the sound transmission loss of wall systems-experimental trends

2.1 Introduction

Numerous experimental investigations have been conducted into the STL of wall systems. It has been observed that the amount, location and properties of the sound absorption material placed within the cavity directly affect the resonant component of sound transmission. Consequently, characteristics such as the damping of the modes within the cavity as well as the extent of modal coupling between the panels and wall cavity are directly influenced by the amount, location and properties of the sound absorption material placed within the wall cavity. On the other hand the size of the cavity directly affects the resonance frequencies, pressure distribution as well as the position of the axial, tangential and oblique modes.

A quantitative comparison of the numerous experimental investigations by different researchers is difficult due to the differences which occur in experimental laboratory facilities and measurement technique. Fausti et al. (1999) conducted round robin tests and showed that differences up to 12 dB can occur between measurements in the mid-frequency range; while comparisons between the intensity and conventional two room method showed that differences do occur between these two measurement techniques especially in the low frequency range as discussed by Jacobson and Ding (1996), Ding and Jacobson (1994) and Lai et al. (1991) among others. Consequently these differences make absolute quantitative comparison of the experimental data difficult. However, a qualitative comparison of the conclusions obtained from the experiments conducted by different researchers can be carried out.

This chapter summarizes the significant experimental observations and conclusions made by different researchers concerning the influence of the wall cavity and any associated sound absorption material on the STL of double leaf wall systems. The analysis is based on three distinct frequency ranges:

- Low frequency range, above the mass air mass resonance frequency (f_0) but below the limiting frequency (f_l)

- Middle frequency range, above the limiting frequency but below the critical frequency (f_c)
- High frequency range, above the critical frequency.

The influence of the material's airflow resistivity, density, thickness, amount and location as well as the type of material and size of the cavity on the STL with respect to these frequency ranges will be addressed. Throughout this discussion experimental measurements made by the author at the University of Canterbury will be used in order to support these findings. A summary of reported work used during this discussion as well as the specific areas investigated can be seen in Table 2. It should be noted that throughout this discussion the generic name of the materials will be used instead of the trade names; for example mineral-wool will be used to refer to rock-wool and glass-fibre for fibreglass. As a result the name of the materials used in the original documents by the authors listed in Table 2 may be different from those used in this analysis.

Table 2 Reported experimental investigations

Author	Year	Sound Absorption Material Properties					Cavity Parameters	
		Airflow resistivity	Thickness	Amount	Density	Type	Location	Size
Meyer	1935						✓	
London	1950			✓				✓
Ingerslev	1952						✓	
Bazley	1966			✓				
Ford	1967			✓			✓	
Zaborov	1967							✓
Utley	1968							✓
Northwood	1968		✓		✓	✓		
Utley	1969			✓			✓	
Loney	1971		✓	✓	✓	✓	✓	✓
Mulholland	1971			✓	✓	✓		✓
Loney	1973		✓			✓		✓
Gösele	1977	✓		✓			✓	
Green	1982			✓				✓
Novak	1992	✓	✓	✓		✓		
Quirt	1993	✓	✓	✓		✓	✓	
Narang	1993	✓	✓		✓			
Warnock	1995	✓	✓			✓		
Narang	1995	✓			✓	✓		
Bolton	1996						✓	
Uris	1999				✓			
Uris	2000		✓		✓			
Uris	2001		✓					✓
Kurra	2001		✓	✓	✓			✓
Hongisto	2002	✓	✓	✓	✓			
Royar	2007	✓	✓	✓	✓			

2.2 Airflow resistivity

The airflow resistance/resistivity can be used to describe the sound absorption properties of the materials placed within the wall cavity. The airflow resistance of fibrous materials is due to friction between the fibres and the air particles moving between the fibres, hence it can depend upon: size of fibres, shape/type of fibres (e.g. crimped, hollow), density of fibres, number of fibres per unit volume and the fibre orientation/distribution (e.g. random, stratified/layered, stratified with higher fibre density near the surface of the sheet) (Hopkins, 2007). Allard (1993) noted that fibrous materials are generally anisotropic and the fibres generally lie in planes parallel to the surface of the material. As a result the normal airflow resistivity (Ξ_n) which is measured perpendicular to the planes of the fibres is different from the planar airflow resistivity (Ξ_p) which is measured parallel to the directions of the planes. Although Hopkins (2007) gave measurements of both the normal and planar airflow resistivity, measurement of the planar airflow resistivity occurs less frequently within the literature. In the proceeding discussion it is assumed that the airflow resistivity reported by the different authors refers to the normal airflow resistivity.

Mathematical studies have shown that when porous sound absorbent material is placed within the wall cavity an airflow resistivity of approximately 5000 to $10\,000$ $\mathrm{Ns/m^4}$ is needed to achieve maximum damping of the modes within the cavity (Gösele and Gösele, 1977). The results of these mathematical studies were verified by Gösele's (1977) measurements which indicated that increasing the airflow resistivity from 6500 to $28\,000$ $\mathrm{Ns/m^4}$ resulted only in a slight improvement in the STL. On the other hand, Narang's (1993) experimental investigations with glass-fibre within the wall cavity suggested that an airflow resistance of 500 $\mathrm{Ns/m^3}$ is sufficient to damp the cavity vibration modes provided that the cavity is nearly completely filled with glass-fibre(for a 100mm depth cavity this corresponds to an airflow resistivity of 5000 $\mathrm{Ns/m^4}$). Experimental investigations conducted by Royar (2007) with mineral-wool as an infill also indicated that the damping limit is reached once the airflow resistivity of 5000 $\mathrm{Ns/m^4}$ is obtained. Furthermore experimental investigations conducted by Narang (1995) with polyester infill showed that STL values similar to when glass-fibre was used can be obtained even though the airflow resistivity of polyester was 20% less than glass-fibre. Narang (1995) also observed that small changes in the airflow resistivity had only a minor effect on the STL; thus confirming Gösele's observation (1977).

Although both Narang's (1993) and Royar's (2007) suggestion for the required airflow resistivity is supported by Gösele's (1977) observation based on mathematical studies; other experimental investigations provide additional insight into the effect of the airflow resistivity on the STL. Novak (1992) measured the STL with different infill within the cavity with different densities and airflow resistivity. These infill materials included one glass-wool, four different mineral-wool, one cellulose and two polyethylene/dacron materials. All of the materials except cellulose produced a similar STL within the low frequency range. The STL with the cellulose material as an infill was lower than the others even though its density ($50\ \mathrm{kg/m^3}$) and its airflow resistivity ($9700\ \mathrm{Ns/m^4}$) were higher than some of the other materials investigated. Novak (1992) indicated that this observation could not be explained from either its density or airflow resistivity. For the middle and high frequency ranges Novak (1992) obtained similar STL values for cavity infill with airflow resistivity greater than $5000\ \mathrm{Ns/m^4}$: In these frequency ranges the STL of the wall system was proportional to the airflow resistivity of the infill material for materials with airflow resistivity less than $5000\ \mathrm{Ns/m^4}$. Novak's (1992) results for the middle and high frequency ranges agree with both Narang's (1993) and Royar's (2007) supposition that an airflow resistivity of at least $5000\ \mathrm{Ns/m^4}$ is needed to sufficiently damp the modes within the cavity.

Novak's (1992) work was conducted at the Royal Institute of Technology in Sweden; interestingly Quirt (1993) and Warnock's (1995) work which was conducted at the National Research Council of Canada showed a slightly different trend to Novak. Quirt (1993) measured the STL of a 3 mm plastic double leaf wall with a cavity depth of 150 mm with seven different 100 mm thick fibrous material cavity infill. No significant correlation occurred between the STL and the material's airflow resistivity or density for both the high and low frequency ranges. However, for the mid frequency range (i.e. 500 to 2000 Hz) the r-squared correlation was between 0.8 to 0.9 for the airflow resistivity but below 0.4 for the density. As a result Quirt concluded that these results suggested that the airflow resistivity, rather than the density is a significant characteristic which determines the effectiveness of the absorptive material placed within the cavity.

On the other hand Warnock (1995) measured and took multiple regression lines from 360 wall tests containing sound absorption material and studied the dependence of both the STC

and R'_w on the mass of the gypsum board layers (M_g), cavity depth (d), airflow resistance (R) and stud spacing (S_{oc}). The resulting equations for these regression lines were;

$$STC = -69.8 + 33.5\, log_{10}\, M_g + 32.2\, log_{10}\, d - 7 \times 10^{-4} R + 0.017\, S_{oc}\,, r^2 = 0.903$$

and

$$R'_w = -60.3 + 29.5\, log_{10}\, M_g + 32.2\, log_{10}\, d - 2.1 \times 10^{-4} R + 9.2 \times 10^{-3} S_{oc}\,, r^2 = 0.924$$

The negative correlation between both the STC and R'_w and the airflow resistance (R) from these regression lines was apparent and surprising. Warnock (1995) gave two plausible explanations for this occurrence. Firstly, for the low frequency range both the mineral fibre and cellulose fibre material performed poorly; this could be due to the fact that for some of the materials used the increase in airflow resistance also increased its density and rigidity therefore an increase in the structural transmission through the material was possible. Secondly, at 2000 Hz and above Warnock suspected that the dominance of the structural transmission through the resilient metal stud or channel over the airborne sound transmission was the reason for the poor correlation in this range. As a result of the negative correlation obtained for the airflow resistance, Warnock (1995) concluded that factors other than the airflow resistance of the material needs to be considered; a conclusion which also agrees with Novak's (1992) measured results.

It can be concluded that for the middle and high frequency ranges increasing the airflow resistivity up to approximately $5000\ \mathrm{Ns/m^4}$ will lead to an increase in the STL once the structural transmission through the wall system isn't increased due to an increase in the rigidity of the material as a result of the increased airflow resistivity. Once the airflow resistivity goes above approximately $5000\ \mathrm{Ns/m^4}$ further increases in the airflow resistivity will lead to little improvement in the STL as most of the modes within the wall cavity are sufficiently damped. Correlation between the STL and the airflow resistance/resistivity is poor for the low frequency range; as a result other factors need to be considered.

2.3 Density

While discussing Quirt's work within section 2.2 it became apparent that there was some discussion within the literature about whether the density or airflow resistance/resistivity of the material in the wall cavity was the important factor which influenced the STL of the wall system. Quirt (1993) indicated that the density didn't have a significant effect on the STL since the r-squared correlation between the density and the STL was only 0.4 as opposed to 0.8 for the airflow resistivity within the mid-frequency range (i.e. 500 to 2000 Hz). On the other hand Warnock (1995) in his final summary indicated that using sound absorption material with high airflow resistivity and density was beneficial for the high frequency range but not for the low frequencies which determine the single rated STC and R'_w values.

Warnock's (1995) conclusion about the effect of the density of the material on the STC ratings is supported by Loney's (1971) findings which indicated that slight but significant increase in the STL due to increased density in the mid frequency range was not reflected in the overall STC since this frequency range was not important in determining the STC. Loney (1971) used glass-fibre and mineral-wool for the infill of his cavity; his measurement results showed that the STL when using the thinnest, densest material was less than the instance when the thicker sample with equal surface density was used. Consequently, Loney (1971) concluded that the thickness rather than the density of the material is a more reliable general indicator of a material's effect on the STL. Furthermore, Mulholland's (1971) investigation showed how unreliable the use of the material's density as the only indicator of the materials effectiveness on the STL can be. Mulholland's (1971) results presented in Figure 3 and Figure 4 showed that the lightweight double leaf gypsum plasterboard wall system with denser mineral-wool as an infill, produced

higher STL than polyurethane or polystyrene as an infill in the 50 and 100 mm cavity: However, the polyurethane infill produced higher STL than the polystyrene even though the densities of both materials were the same (i.e. 1 and 2 $\mathrm{kg/m^2}$ in the 50 and 100 mm cavity respectively).

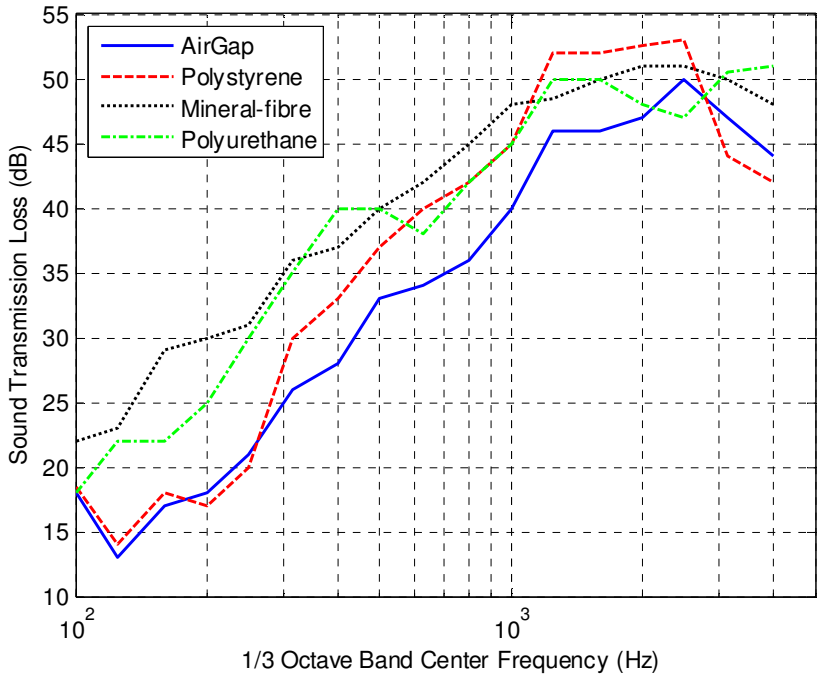

Figure 3 Mulholland's (1971) measured STL through an 11 mm thick double leaf gypsum wall system with a 50 mm cavity depth and various infill

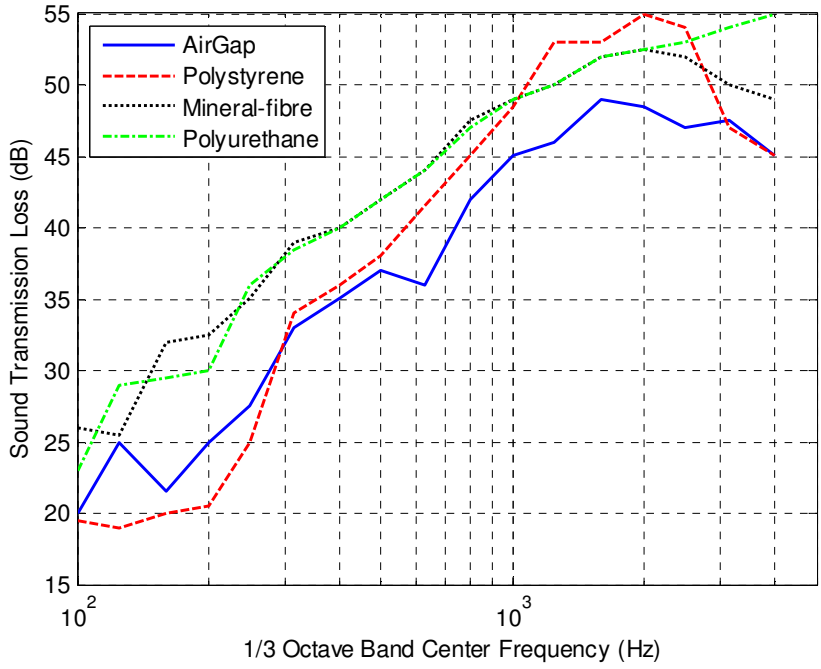

Figure 4 Mulholland's (1971) measured STL through an 11 mm thick double leaf gypsum wall system with a 100 mm cavity depth and various infill

The difference in the STL results with polyurethane and polystyrene, as well as the poor correlation which occurred between the STL and density for a variety of materials as in

Quirt's (1993) investigation suggests that an analysis of the effect of density based on the specific type of material used within the wall cavity would be beneficial.

Uris et al (1999) utilized a gypsum plasterboard double leaf wall system with a 50 mm deep cavity and three mineral-wool infill of different densities (120, 70 and 40 $\mathrm{kg/m^3}$). Uris showed that below the mass air mass resonance frequency (i.e. $f_0 = 125$ Hz) the 120 $\mathrm{kg/m^3}$ mineral-wool performed better than the 70 and 40 $\mathrm{kg/m^3}$ infill as shown in Figure 5.

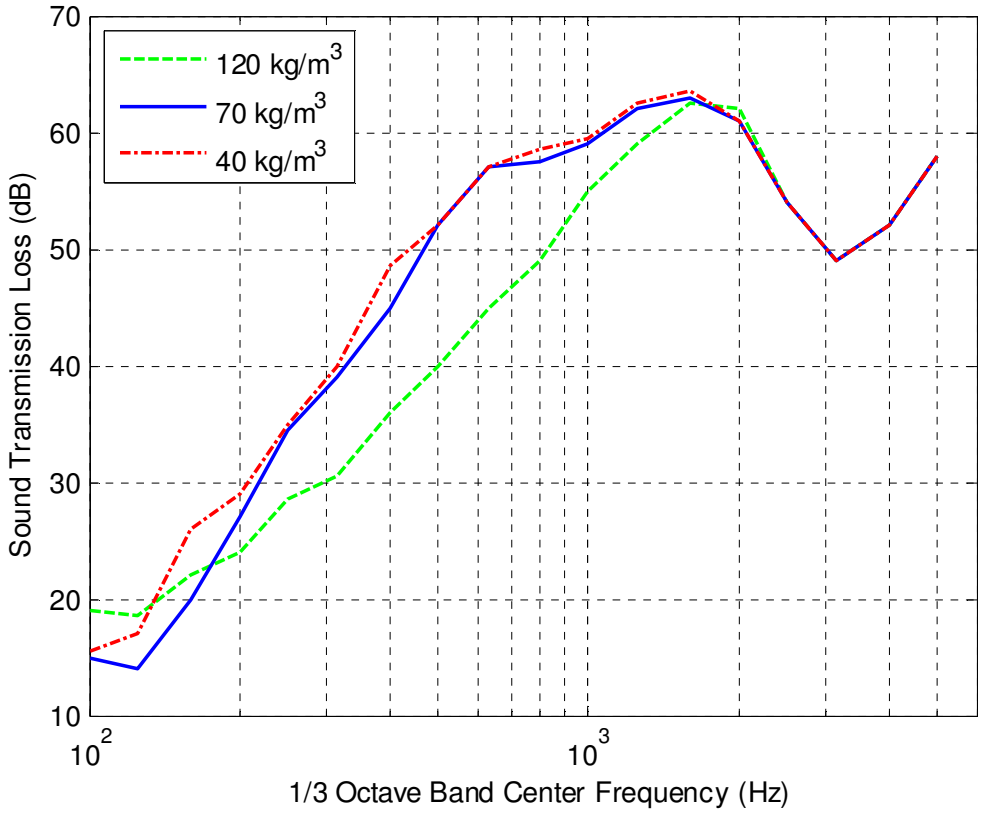

Figure 5 Uris et al. (1999) measured STL through a 13 mm gypsum plasterboard double leaf wall system with 50 mm cavity depth and mineral-wool infill of different densities

Uris et al (1999) concluded that this trend occurred because the lower density mineral-wool didn't have sufficient inertia to remain motionless under the excitation of the sound waves and the effect of the mineral-wool was to provide resistance and mass inertia to the sound waves passing through it. Within the middle frequency range (i.e. 125 to 1250 Hz) the 120 $\mathrm{kg/m^3}$ mineral-wool performed significantly worst than the 70 and 40 $\mathrm{kg/m^3}$ mineral-wool; with the less dense 40 $\mathrm{kg/m^3}$mineral-wool performing slightly better than the 70

kg/m^3 sample. Little difference occurred for the STL in the middle and high frequency range. On the other hand, Royar's (2007) experimental results with the density of mineral-wool varied from 18 to 125 kg/m^3 showed that increasing the density of the cavity infill did not result in an increase in the STL for all frequency ranges if the airflow resistivity had reached a value of $5000\ Ns/m^4$. Royar (2007) noted that further increases in the density only lead to an increase in the cost of production. Furthermore, while investigating the use of mineral-wool and glass-fibre Northword (1966) observed that his results were not critically sensitive to the material's density.

These trends were different from Uris et al's (2000) investigation using 60, 80 and 120 kg/m^3 dense polyurethane foam as the infill. This investigation showed that within the measured low frequency range (i.e.100 to 315 Hz) increasing the density of the polyurethane foam did not increase the STL. However, for the middle and high frequency ranges increasing the density of the polyurethane foam did result in an increase in the STL.

Narang's (1993) results with glass-fibre agreed with Northword's (1966) conclusion that the STL was not critically sensitive to the material's density; as his results showed the STC rating exhibited asymptotic behaviour as a function of density and a high density is not required if the STC is the only criteria parameter of interest. No significant improvement occurred in the STC rating beyond a density of approximately 30 kg/m^3 (Narang, 1993); while Irvine (1998) recommended that the density of the sound insulation material should not be less than 40 kg/m^3. Narang's (1993) results also showed that the thickness of the material had a significant effect on the STL; and it would be more cost effective to use a 75 mm thick low density glass-fibre in a 64 mm cavity than to use a 50 mm thick high density glass-fibre.

It can be concluded that the effect of the density of the material on the STL is highly dependent on the type of material used and the frequency range of interest. Similar to the case discussed with regard to the effect of the airflow resistivity/resistance the increase of the density of some materials can result in an increase in their rigidity and may result in an increase in the structure borne transmission. This explains the reason why the correlation between the STL and the density of the material is low when comparisons between different materials are made. A material density of at least approximately 40 kg/m^3 is recommended and the potential increase in production cost by increasing the density of the infill material

has been noted. Once an airflow resistivity of $5000\ \mathrm{Ns/m^4}$ is obtained, increasing the density will not lead to any significant increase in the STL.

2.4 Thickness

The thickness rather than the density of the material is a more reliable general indicator of a materials effect on the STL (Loney, 1971). The question however remains; to what degree does the thickness of the material influence the STL.

Novak's (1992) experimental results showed that if the ratio of the thickness of the material to cavity depth was less than 0.5, then the smaller thickness to cavity ratio performed worse than a material with a greater thickness to cavity depth ratio. Novak also noted that no significant increase occurred in the STL after a certain thickness was reached. Loney (1971) explained this trend by noting that the STL varies as the logarithm of the thickness rather than linearly; a conclusion which can explain the observed results from other researchers.

Northwood (1966) noted that the STL was not critically sensitive to the thickness while Uris et al. (2000) recognized that increasing the thickness of polyurethane foam from 100 to 150 mm did not significantly increase the STL below 1000 Hz. The greatest effect was obtained for frequencies above 1000 Hz where the wavelength of the sound waves in the polyurethane foam became comparable to its thickness (Uris *et al.*, 2000). Quirt's (1993) measurements on the other hand showed a continual increase in the STL with increasing thickness. Quirt's results were obtained for 50, 100 and 200 mm thick sound absorption material placed within a 205 mm cavity. The steady increase in the STL with increasing thickness of the sound absorption material could be due to the ratio of the material thickness to the cavity depth being less than 0.5 in the 50 and 100 mm case. These results also support Novak's findings with regard to the relationship between the cavity depth and thickness of the material.

Further support for Novak's (1992) findings that no significant improvement in the STL occurs once a certain thickness of material is used, can be seen from the author's measurements in Figure 7. For the results shown in Figure 7 one sheet of glass-fibre with different thicknesses (i.e. dimensions 1.140*0.80*0.075 m and 1.140*0.8*0.1 m) was suspended in turn within a 106 mm depth cavity within a 10 mm gypsum double leaf wall as shown in Figure 6.

Figure 6 Mechanism used to suspend the glass-fibre within the 106mm deep cavity

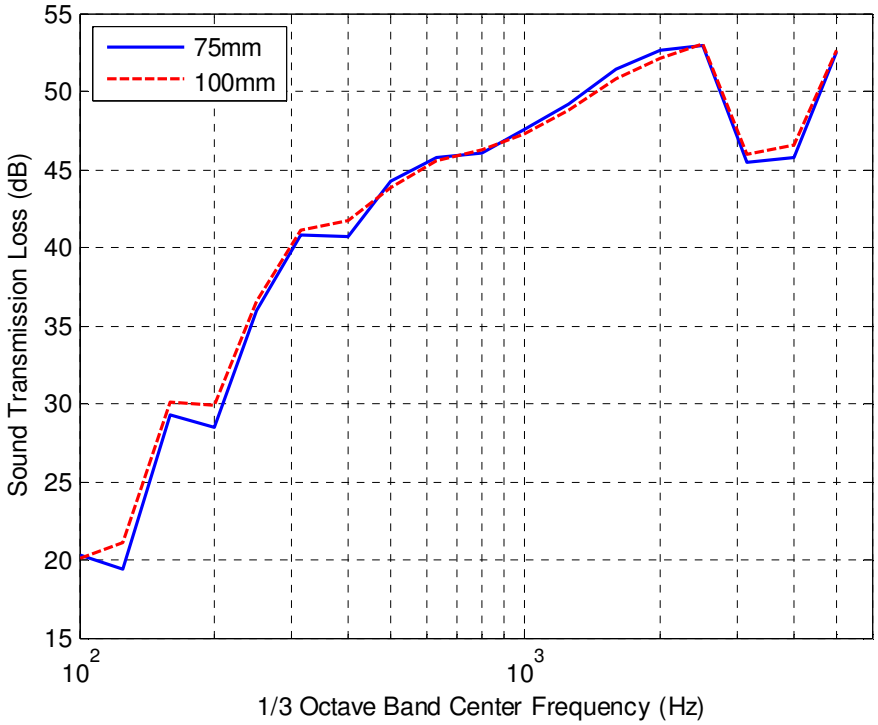

Figure 7 Cambridge's measurements showing the effect of having 75 mm and 100 mm glass-fibre within a 105 mm depth cavity

The results in Figure 7 showed that only slight improvement in the STL occurred when the thickness of the glass-fibre was increased from 75 mm to 100 mm with the greatest improvement occurring in the low and high frequency ranges.

In conclusion the STL increases with increased thickness of the material placed within the cavity until a certain thickness to cavity depth ratio is obtained. Once this ratio is obtained, only slight improvement in the STL occurs with an increase in the thickness of the material. Loney summarized this trend by stating that the STL varies as the logarithm of the thickness rather than linearly.

2.5 Amount

The effect of the amount of sound absorption material in the cavity from different experimental investigations is discussed within this section. Ford's (1967) experimental investigation showed little difference could be seen between the results obtained for the completely filled and partially filled case; only 1 dB difference occurred between the overall mean in both cases. The increase in the STL due to the doubling of the amount of sound absorption material within the cavity, can be seen from Bazley's (1966) reported results shown in Figure 8.

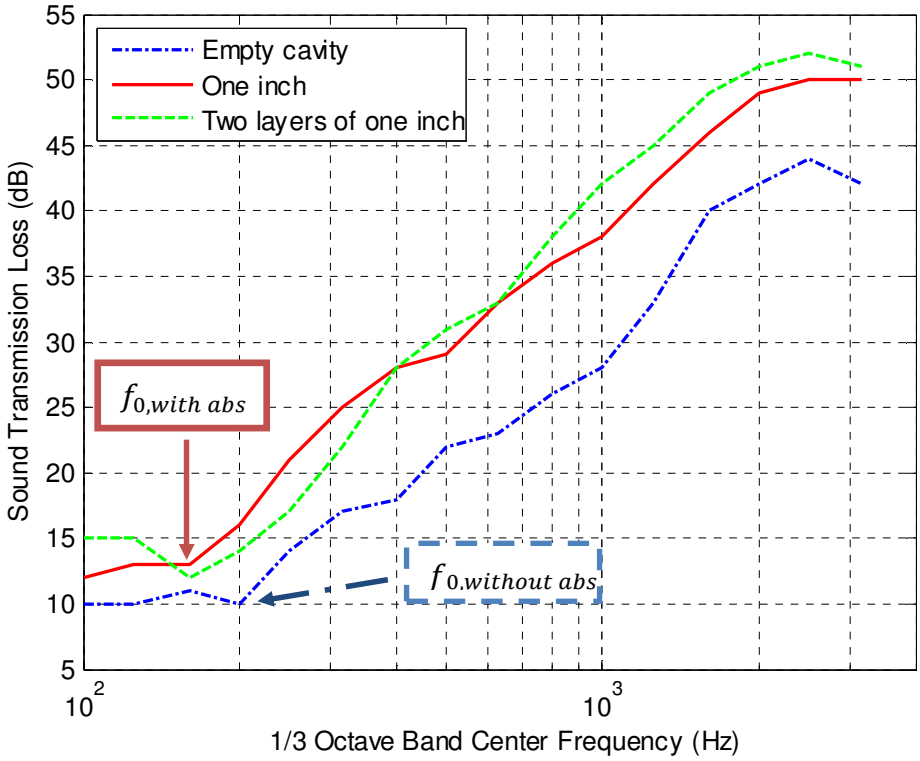

Figure 8 Bazley's (1966) reported results showing the effect of doubling the amount of sound absorption material within a 2 inch (50 mm) cavity

The results shown in Figure 8 are for a ¼ inch (6.35 mm) plywood double leaf wall system with two 2 inch (50.8 mm) wooden studs at 2 ft (609.6 mm) centres. Mulholland (1971) commented on these results and speculated that it is possible that complete filling of the cavity will not only dampen the cavity resonances, such as the mass spring mass resonance and the various standing waves, but it will also add a degree of damping to the panel resonances and the coincidence effect. On the other hand Quirt (1993) viewed the complete filling of the cavity as causing a lateral shift in the STL for the lower frequencies, with the mass air mass resonance frequency shifting to a lower frequency in this case; Kurra (2001b) also observed this lateral shift in the mass air mass frequency. This lateral shift in the mass air mass frequency due to the presence of sound absorption material within the cavity can also be seen in Figure 8. Narang (1993) gave the explanation for the lateral shift of the mass-air-mass resonance frequency by noting that the presence of glass-fibre makes the compressions and rarefactions at the low frequencies an isothermal process as opposed to an adiabatic process as in air. The resulting reduction in the speed of sound causes the mass-air-mass resonance frequency to shift to a lower frequency.

Loney (1971) investigated the effect of various amounts of sound absorption material within the cavity. His results showed that the first initial amount of sound absorption material has the greatest effect on the STL. Hongisto (2002) verified this trend and noted that increasing the filling ratio (i.e. the ratio of the thickness of the absorbent material to the depth of the cavity) from 0% to 24% gave a significantly larger increase in the STL than increasing the filling ratio from 24% to 88%. Despite the decreased gain in improvement of the STL after the first initial amount is added, as shown by Loney (1971) and Hongisto (2002), authors such as Quirt (1993) indicate that filling the cavity remains the most practical, while Gösele (1977) maintains that marginal damping (i.e. partially filling the cavity) is not a complete substitute for the fully damped case (i.e. completely filled). Quirt (1993) and Gösele's(1977) recommendation agree with Royar's (2007) finding that filling even the last 10% of the cavity improves its performance.

The author's measurements shown in Figure 9 provides evidence which support the view that partially filling the wall cavity is not a complete substitute for completely filling it with sound absorption material. The results in Figure 9 were obtained for a 10 mm double leaf gypsum plasterboard wall system with a 106 mm cavity depth. The sound absorption material for the 48 and 64 % filling ratio cases were suspended and placed within the cavity using the method shown in Figure 6; while the entire surface area of the cavity was covered for the case with 72 % filling ratio. Although the results shown in Figure 9 support Loney (1971) finding with regard to the initial amount of sound absorption material and Royar's (2007) conclusion regarding improved performance for the completely filled case; it should be noted that the both the effectiveness and the expected amount of improvement in the STL when sound absorption material is added to the cavity is directly dependent on the properties of the wall panels.

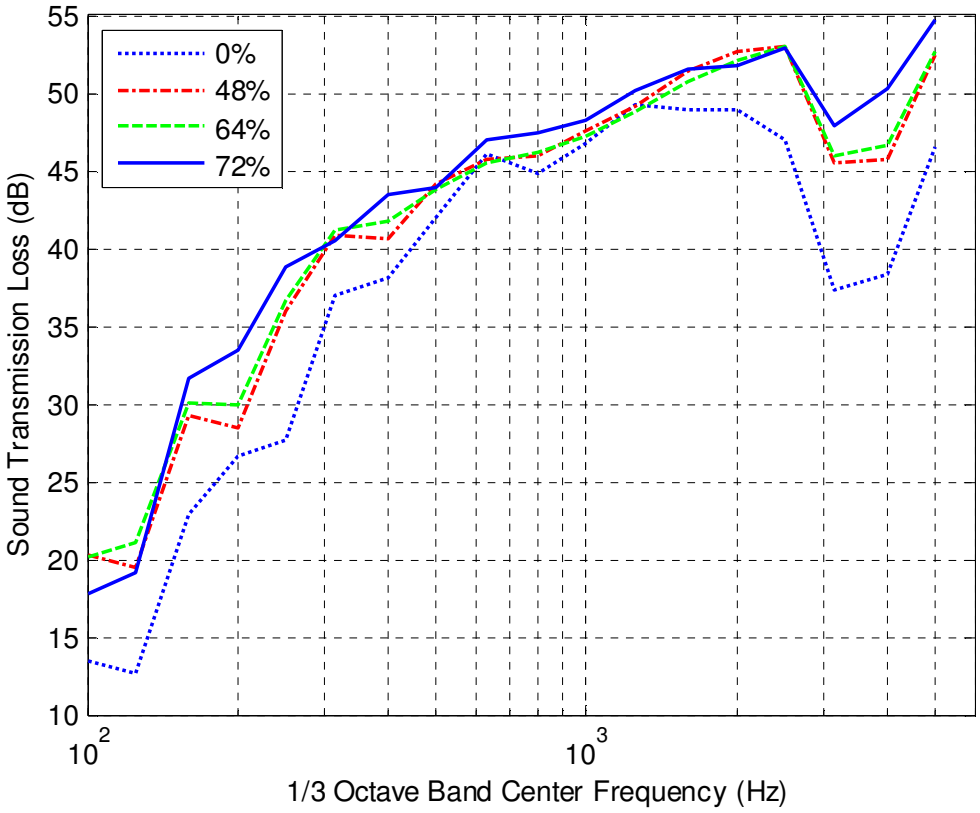

Figure 9 Cambridge's result for the effect of having different filling ratios of sound absorption material within the wall cavity

Mulholand's (1971) investigation showed that sound absorption material added to the wall cavity of the lightweight wall construction improved the STL of the system, but had no effect when heavy panels were used. Uris et al.'s (2001) investigation showed how the properties of the wall panels influenced the effect of the sound absorption material placed within the wall cavity. Uris et al (2001) placed mineral-wool within an uncoupled double leaf wall with one, two and three layers of gypsum boards symmetrically placed on each side of the cavity. His results showed a reduction in the influence of the mineral-wool within the cavity on the STL as the number of layers on each side was increased. The progressive increase in attenuation through the gypsum boards as the number of layers was increased was the explanation given for the reduced effectiveness of the mineral-wool within the cavity (Uris *et al.*, 2001).

Green and Cameron (1982a; 1982b; 1982c) measured the STL with and without glass-fibre within double leaf gypsum wall systems with steel and wooden studs which were either glued or screwed to the wall panels. Green and Cameron's (1982b) results for the double leaf wall systems with screwed steel studs showed decreased improvement in the both the STL and

STC when glass-fibre was added as the mass of the wall panels were increased. The decrease in the improvement in the STC can be seen from the extracted results shown in Table 3. Although the results shown in Table 3 show that the improvement in the STC was greater when the smaller 0.063 m stud was used, the trend of the decreased improvement in the STC is evident for both the 0.063 and 0.092 m stud size. As a result of these observations Green and Cameron (1982b) concluded that the heavier and stiffer the wall, the smaller the increase in the STL when glass-fibre is added to the cavity (i.e. with steel studs).

A slightly different trend occurred in the results of Green and Cameron (1982c) with wooden studs as shown in Table 4. These results show no increased improvement in the STC as the mass of the wall panels was increased when the wooden studs were screwed to the wall panels; as opposed to a slight increase in the improvement when the wooden studs were glued to the panels. Consequently, Green and Cameron (1982c) concluded that the cavity infill was more effective in multilayer partitions having a second layer attached to the first with adhesive than if screws were used.

Table 3 Extracted results from Green and Cameron (1982a; 1982b)showing the improvement in STC rating when glass-fibre is added to the wall cavity as the mass of the wall panels is increased .

Surface density (**kg/m^2**)	STC without absorption	STC with absorption	Increase in STC
0.092 m steel stud partition			
19	37	44	7
29	43	49	6
39	47	53	6
49	51	55	4
0.063 m steel stud partition			
19	36	44	8
29	42	49	7
39	46	52	6
49	49	54	5

Table 4 Extracted results from Green and Cameron (1982c) showing the improvement in STC rating when glass-fibre is added to the wall cavity with wooden studs as the mass of the wall panels is increased .

Surface density (**kg/m^2**)	STC without absorption	STC with absorption	Increase in STC
0.05*0.1 m wooden stud partition second layer screwed on			
29	36	40	4
39	39	43	4
49	41	45	4
59	42	46	4
0.05*0.1 m wooden stud partition second layer glued on			
29	37	41	4
39	41	45	4
49	43	49	6
59	46	52	6

It should be noted that increasing the thickness of the panels of a lightweight double wall construction does not lead to a major increase in the STC when sound absorption material is added to the cavity. Although increasing the thickness of the wall panel leads to an increase in its mass, which based on the mass law leads to an increase in the STL, an increase in the thickness of the wall panel also leads to a decrease in the critical frequency; both of which can be seen from the author's results shown in Figure 10. The effect of the increased mass and the decrease in the critical frequency often leads to similar STC or Rw values when comparing the STL of single panels which differ in thickness. On the other hand for double leaf wall constructions, the thickness of the wall panels only has a significant effect on the STC when there is no sound absorption material present within the cavity. This trend was observed by Loney (1973) when he reported a 3 STC increase when the size of his single panels in his double wall was increased from 1/2 inch (12.7 mm) to 5/8 inch (15.9 mm); but no increase in the STC when sound absorption material was added to the cavity. A similar trend can be seen from the reported results by Halliwell *et al.* (1998)in Figure 11. These results show the expected decrease in the critical frequency, but little difference occurs within the low and middle frequency regions for the different thicknesses. This resulted in a 1 dB decrease in the STC for the 16 mm gypsum plasterboard wall system as shown.

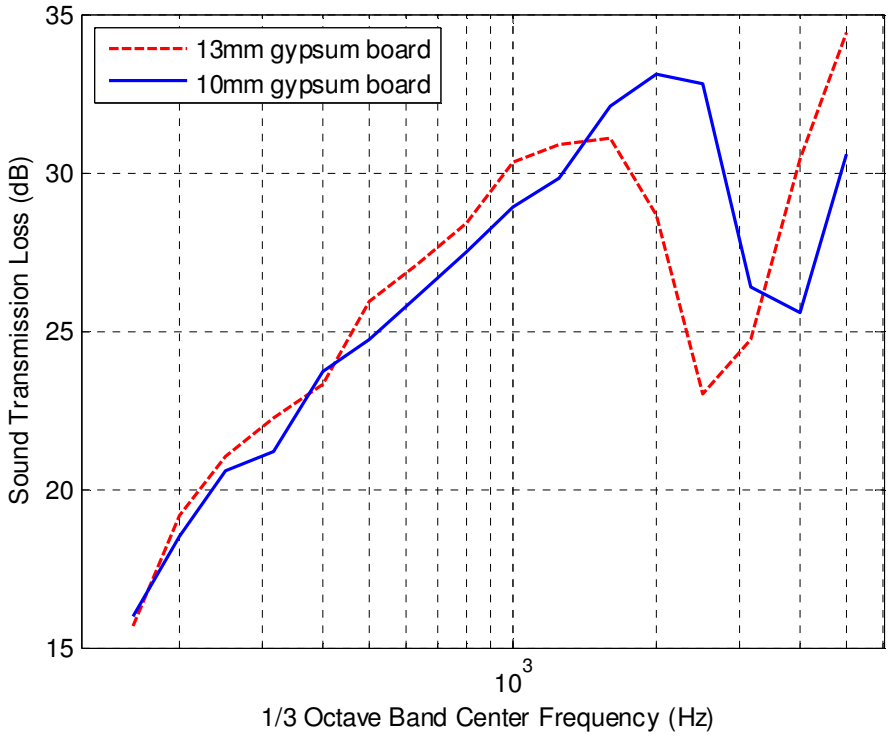

Figure 10 Cambridge's results for the effect of the panel thickness on the sound transmission loss of a 10 and 13 mm single panel gypsum board

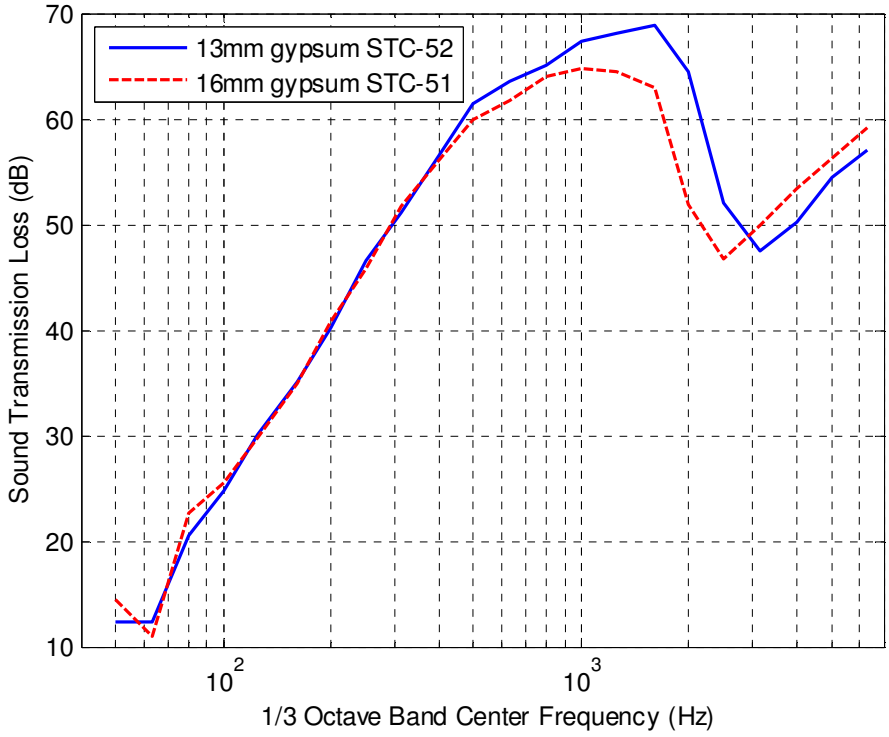

Figure 11 Reported sound transmission loss of a 13 and 16 mm double leaf wall with 150 mm steel studs at 610 centre and 150 mm of glass-fibre in the cavity (Halliwell *et al.*, 1998)

In conclusion the amount of sound absorption material needed within the wall cavity for optimum STL is dependent on the properties of the individual wall panels and the type of connections used. The recommendation by some authors of completely filling the wall cavity of lightweight double leaf wall systems has been noted. However, for heavy double leaf wall systems the effectiveness of the sound absorption material and conversely the amount of sound absorption material needed for optimum STL will decrease. The effectiveness of the sound absorption material can be increased if adhesive instead of screws are used to connect the wooden studs to the wall panel. Consequently the decision about the amount of sound absorption material needed for the cavity could be based on other factors such as the thermal rating and economic cost. Although filling the last 10% of the cavity will lead to improved performance (in light-weight double leaf walls), this improvement may not be justified by the cost associated with completely filling the cavity. In situations where an increase in the STC or R'_w rating can occur due to the filling of the last 10% of the wall cavity, filling this last portion of the cavity may be justified. However, if a sustainable building approach is taken, from an acoustic point of view, in terms of the STC or R'_w rating, completely filling the wall cavity may not be justifiable in some cases for lightweight constructions; and is not recommended for heavy double leaf wall configurations.

2.6 Type of material placed within the wall cavity

The effect of changing the material's airflow resistance, density, thickness and amount has been discussed within the previous sections. Although these discussions provided insight into how these material characteristics affect the STL a comparison of how different materials perform can be useful. The effect of using glass-fibre, mineral-fibre, cellulose, polyurethane foam, polystyrene and polyethylene/dacron as an infill is discussed in this section. The discussion is based on the observed trends of each material in the low, middle and high frequency ranges. Within each frequency range the ranking of each material appears in descending order with each bullet point representing a separate ranking as shown in Figure 12.

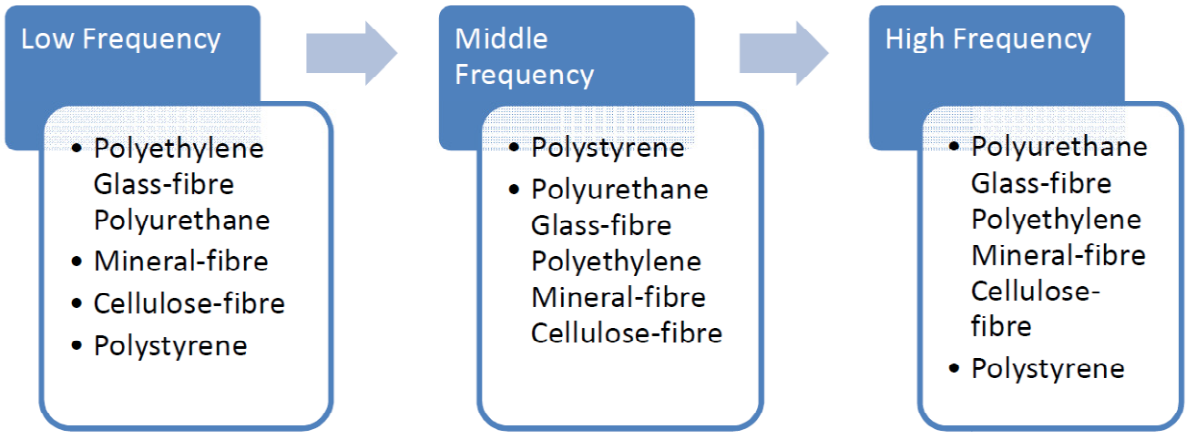

Figure 12 Cambridge's ranking of the effect of different material on the STL in the low, middle and high frequency range

In the low frequency range polyethylene, glass-fibre and polyurethane are all ranked as performing equally well. Although Mulholland's (1971) results showed that both mineral-wool and polyurethane foam performed equally well and significantly better than polystyrene; Warnock's (1995) and Quirt's (1993) work showed that mineral-fibre didn't perform as well as glass-fibre and polyethylene in the low frequency range. Novak's (1992) results showed that the higher density mineral-wool performed equally well when compared to the lower density mineral wool, glass-fibre and polyethylene/dacron; while Royar (2007) observed that the STL with mineral-wool infill didn't improve much when the density was varied from 18 to 125 kg/m^3. Novak's (1992) and Royar's (2007) results with mineral-wool infill were different from Uris et al's (1999) which showed that the low density mineral-fibre performed better than the high density material in the low frequency range. Consequently, as a result of the discrepancies in the experimental results found within the literature, mineral-fibre was ranked lower than polyurethane, polyethylene and glass-fibre. Cellulose-fibre was ranked lower than mineral wool as Warnock (1995), Quirt (1993) and Novak (1992) each observed that cellulose performed poorly within this frequency range. Novak (1992) suggested that because the mechanism by which cellulose-fibre works was totally different from that of glass-fibre and polyethylene it performed poorly in the low frequency range. Novak also noted the difficulty encountered with measuring the airflow resistance of the cellulose material due to the movements in the material. The potential movement of the cellulose-fibre within the cavity when excited may be the reason for its poor performance.

Finally, polystyrene was ranked as the worst material for the low frequency range as Mulholland's (1971) observed that it hardly made any contribution to the STL and even performed worse than the empty cavity situation for part of this frequency range as shown in Figures 4 and 5.

Within the middle frequency range Mulholland's (1971) experimental results showed that polystyrene performed better than polyurethane and mineral-fibre. Although polystyrene was ranked as the best material within this frequency range due to the significant improvement reported by Mulholland's (1971), the use of polystyrene within the wall cavity is generally not recommended for STL purposes. All of the other materials under investigation were ranked as performing equally well within the middle frequency range due to the high correlation between the material's airflow resistivity and the STL as discussed by Quirt (1993). The various reported experimental results all showed that once the recommended airflow resistivity was obtained for these materials, similar STL values were derived. Furthermore, this high correlation between the airflow resistivity and the STL is the reason why polyethylene, glass-fibre, polyurethane, mineral-fibre and cellulose were all equally ranked in the high frequency range. Polystyrene performed similarly to the empty cavity within the high frequency range; as a result polystyrene was ranked as the worst performing material.

2.7 Size of the wall cavity

The size of the wall cavity directly affects the resonance frequencies and pressure distribution as well as the position of the axial, tangential and oblique modes. Warnock's (1995) regression lines shown in Section 2.2 showed a positive correlation between the STC rating and both the depth of the cavity and the spacing of the studs; both of which affect the size of the cavity. Here, the focus will be on the depth of the cavity and not on the spacing of the studs. This is due to the belief that the increase in the STL as a result of an increase in the stud spacing is due to a reduction in the number of structural transmission paths (i.e. greater spacing equates to less studs for a given wall system): On the other hand the depth of the cavity (which is controlled by the size of the studs or wall frame) will be investigated since it directly affects the volume as well as the properties of the wall cavity.

The effect of the size of the cavity on STL is dependent on whether or not sound absorption material is present within the wall cavity. Loney's (1971; 1973) experimental investigations showed that significant increase in the STL due to the size of the stud occurs only in the case without sound absorption material: With sound absorption material the slight increase in the STL was limited to the low frequency range. Kurra and Arditi (2001b) observed a similar trend with only 1-2 units increase in R_w rating for the doubling of the cavity width with sound absorption material within the cavity as opposed to a 6-8 dB increase in the R_w rating for the empty cavity. Green and Cameron (1982b) also reported that no significant increase in the STL occurred when the size of the studs were increased with sound absorption material within the cavity.

These observations are well supported by Mulholland's (1971) work which showed that increasing the depth of the empty cavity from 50 to 100 mm resulted in a 3 dB mean STL increase but no increase when the depth was increased from 100 to 150mm. This result was similar to Utley and Mulholland's (1968) investigation which showed that with different cavity depths between 100 and 200 mm the STL may actually decrease with an increase in depth at particular depths. Further increases in the depth of the cavity at these points then led to an increase in the STL. Utley and Mulholland concluded that this trend for different cavity depths between 100 to 200 mm was due to the resonances of the standing waves within the cavity. Consequently, Utley and Mulholland (1968) considered a depth of 100 mm to be the optimum depth for their 0.035 inch (0.9 mm) thick aluminium double leaf wall system.

In conclusion, increasing the depth of the cavity may lead to a significant increase in the STL for the empty cavity especially at low frequencies, while smaller increases occur with increased cavity depth when sound absorption material is present within the cavity. The effectiveness of increasing the cavity depth is dependent on the resonances of the standing waves within the cavity; consequently a decrease in the STL can actually occur at certain cavity depths when the depth of the empty cavity is increased.

2.8 Location of the sound absorption material

The effect of the location of the sound absorption material within the wall cavity for the partially filled case has been investigated by some authors. Gösele (1977) acknowledged Meyer's (1935) suggestion that placing sound absorption material along the margins of the wall cavity could be used to prevent the occurrence of resonances within the cavity; the improvement over the empty cavity situation was noted by Gösele who however concluded that it is not a substitute for completely filling the cavity.

The concept of placing the sound absorption material along the margins of the cavity as well as along other strategic positions within the cavity was also investigated by Ford (1967). These results showed that placing the sound absorption material along the margins of the cavity resulted in a reduction in the low frequency performance of the wall system when compared to when the same amount of material was distributed over the entire volume of the cavity. On the other hand Loney's (1971) investigation showed little difference in the STL when the sound absorption material was moved closer to the wallboard on the source side, receiving side and directly to the centre of the cavity. Quirt's (1993) results also showed negligible change in the STL when the sound absorption material was moved from the centre of the cavity towards one of the faces of the wall panel. However, Quirt's measurements did indicate that the position of the absorption material does matter in the partially filled case; since the STL was consistently lower when the material was placed on the top or bottom of the wall cavity when compared to when the same amount was placed as one complete layer in the centre.

Further insight into the effect of the location of the sound absorption material within the wall cavity can be deduced from Bolton et al's. (1996) investigation. Bolton et al (1996) measured the STL of an aluminium double leaf wall with polyurethane foam within the cavity and found that having the sound absorption material unbound to the wall panel was generally preferred to having it bound. However, if improvement in the low frequency range is required then attaching the sound absorption material to the wall panel increases its stiffness and causes the first resonance to shift to a higher frequency range which results in an increase in the STL (Bolton *et al.*, 1996).

In conclusion the location of the sound absorption material within the cavity for the partially filled case does affect the STL. It is recommended that the sound absorption material be placed unbound from the panel in the centre of the wall cavity as one complete unit as opposed to along the lining or on the top/bottom area of the cavity. If improvement in the low frequency region is of prime concern, bonding sound absorption material to the face of one of the panels may be effective.

2.9 Summary and conclusions

The influence of the wall cavity on the sound transmission loss based on experimental evidence has been discussed. This discussion showed that the airflow resistivity of porous sound absorption material gives the best indication of how effective the material will be in enhancing the STL. The research from many authors has indicated that an airflow resistivity of approximately 5000 Ns/m^4 is needed to damp the modes within the cavity while a material density of at least approximately 40 kg/m^3 is recommended. For both the airflow resistivity and density caution must be taken in increasing these parameters as such increases may lead to an increase in the rigidity in some materials with the additional risk of an increase in structural transmission.

The effect of the thickness and the amount of sound absorption material within the cavity were also discussed. Previous work on these issues has shown that the STL increases with increased thickness of the material up until a certain thickness to cavity depth ratio; while the optimum amount of sound absorption material is dependent on both the mass of the wall panels and the type of structural connection used.

With regard to the size of the cavity, type and location of the material utilized. The literature suggests that significant improvement in STL can be gained by increasing the size of the empty cavity; while smaller improvement occurs when the size of the cavity is increased with sound absorption material within the cavity. The best material to be used is dependent on the frequency range of interest with the STL being sensitive to the location of the material placed within the wall cavity.

Finally the investigation has revealed that a wide variety of conclusions were obtained by different authors concerning the role of the cavity and the properties of any associated sound

absorption material on the sound transmission loss through double wall systems. Consequently recommendations about the ways in which sound transmission through cavity systems can be improved should always be qualified with regard to the specific frequency range of interest, type of sound absorption material, wall panel and stud characteristics.

3 Existing techniques used in the prediction of the sound transmission loss

3.1 Introduction

The prediction and understanding of the STL through double leaf wall systems over all of the frequency ranges has dramatically improved since the development of the early infinite prediction models developed by Beranek and Work (1949) and London (1950). Since these pioneering works the wave approach, Statistical Energy Analysis (SEA), the use of correction factors to improve the predictions obtained from different models, limiting the angle of incidence and the transfer matrix method have been utilized in the development of different STL models. A summary of some of the main contributors to each technique and a brief description of their contributions is given in Figure 13: The authors' contributions are listed in chronological order within each category.

In this chapter a survey of these existing techniques is given in relation to whether or not they can be used to determine the role of the wall cavity in both finite and infinite wall systems. The aim of the discussion is to determine the technique which can best provide a means for the explanation of the under-prediction in London's model for double leaf wall systems. This survey is different from other survey's such as Hongisto's (2006) survey which looked at the accuracy of different models as opposed to the whether or not they can be used to model both the infinite and finite wall systems. In this survey over forty different models are discussed; many of which were not included within Hongisto's (2006) survey, examples of such models are highlighted with an asterisk Figure 13

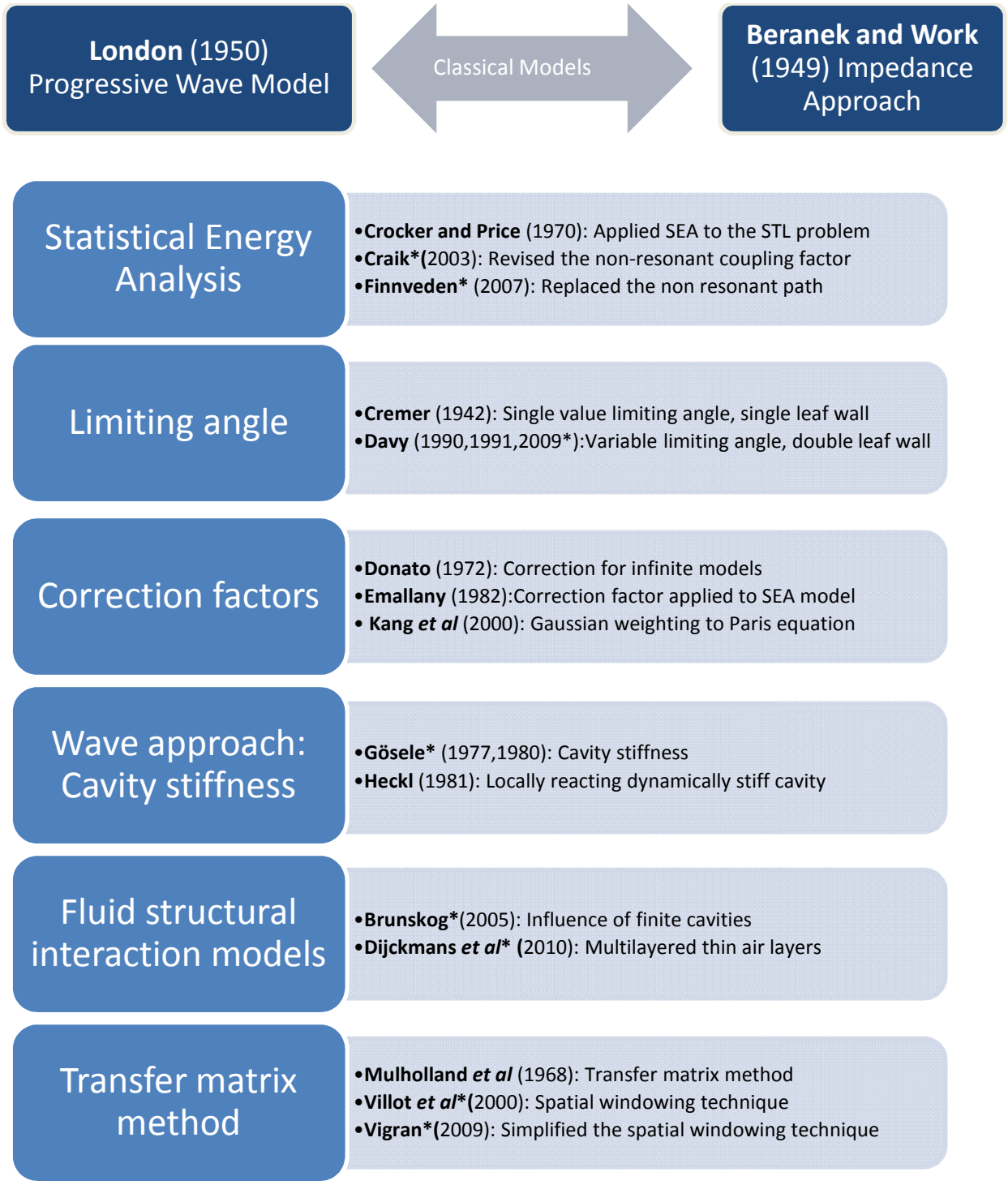

*Not included in Hongisto's *(2006)* survey

Figure 13 Survey of techniques used in predicting the STL of through double leaf systems

3.2 Statistical Energy Analysis (SEA)

The Statistical Energy Analysis (SEA) method has been used to predict the sound transmission through double leaf panels. This method has advantages over both the wave theory and modal approach as it reduces the complexity of the calculations required. According to Price (1970), London's (1950) wave theory approach only deals with non-resonant transmission and prior knowledge is needed of the real part of the complex acoustic impedance of the panel. On the other hand, the modal approach which is based on the superposition of modes in order to obtain the panels response, can have a high number of modes within the frequency band of interest which can make the calculations cumbersome, Kropp (2003). These factors along with the flexibility of being able to add different transmission paths and excitation sources makes the SEA model useful for studying the sound transmission through double leaf wall systems.

However, despite the many advantages of using the SEA approach, this method does not accurately predict the sound transmission into the wall cavity as observed by various authors. Donato's (1972) critique of White and Powell's (1965) work indicates that Maidanik's (1962) radiation efficiency expression which is based on SEA (see Chapter 6) may be used for externally radiated power but there is some doubt about the correct value of the energy radiated into the cavity. Maidanik's expression is also utilized in Price and Crocker's (1970) SEA model which showed negligible change in the STL when the cavity was varied from 1 to 40 cm. This unexpected result was also questioned by Donato (1972). Even the later SEA model produced by Craik (2001) who implemented Leppington's (1982) corrected solution for the radiation efficiency as opposed Maidanik's also showed poor agreement for empty smaller cavities. Consequently, Craik (2001) pointed out that the assumption that the non-resonant transmission and radiation into the cavity is the same as the transmission or radiation into a room was an assumption which only worked well for large cavities; a conclusion which is well supported by Smith's (1997) airborne level difference measurements into the wall cavity. A depiction of the transmission paths used within Price and Crocker's model which was also implemented in Craik's (2001) model can be seen in Figure 14.

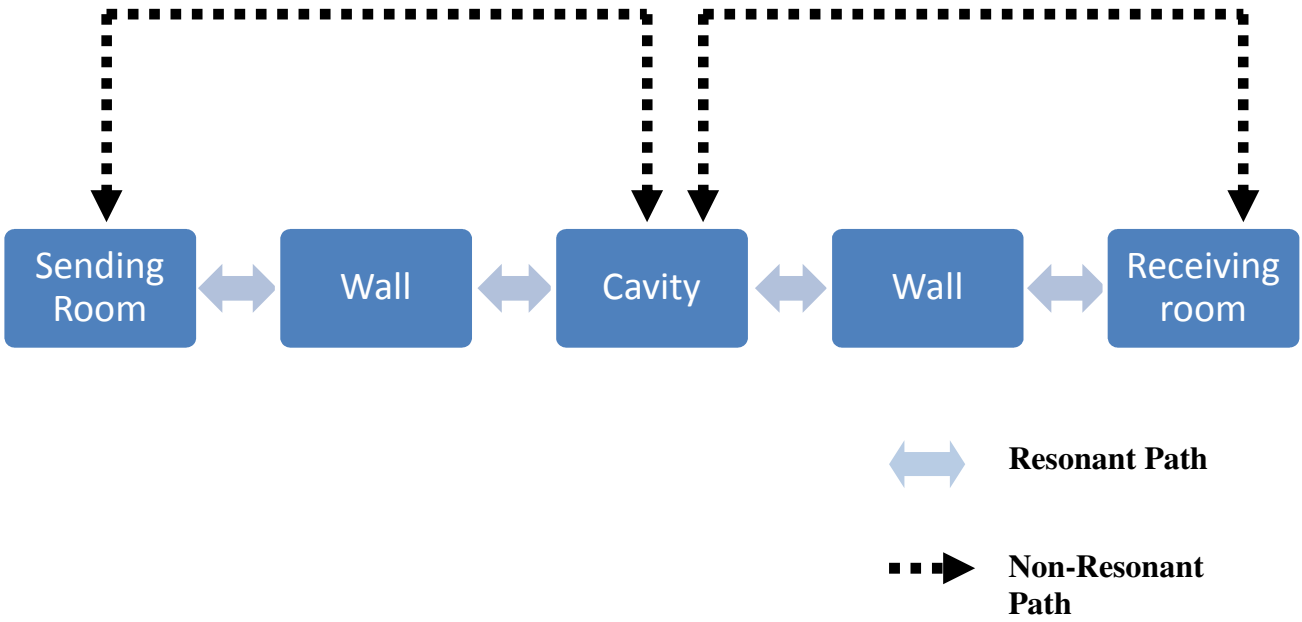

Figure 14 Depiction of the resonant and non-resonant transmission paths used within Price's (1970) SEA model

In order to improve the prediction of the STL of double leaf walls while using the SEA approach Craik (2003) developed a new non-resonant coupling loss factor between the room and cavity. This new loss factor gave better agreement to measured STL than the previous theory used by Price and Crocker (1970) for different cavity depths in most cases (Craik, 2003); as the previous theory underestimated the coupling from the room to the cavity. On the other hand Finnveden (2007) observed that the elements of an SEA model are not sub-structural but elements of vibro-acoustic response. Finnveden used this observation to improve the prediction of the STL of a double leaf wall system by creating two new separate SEA elements to deal with acoustic waves at the double wall resonance and the oblique cavity waves. These new elements made the traditional non-resonant transmission path obsolete (Finnveden, 2007).

Based on the above discussion it is clear that difficulties were encountered when modelling the STL of double leaf wall systems, with improvements only occurring when the non-resonant transmission path was modified from the traditional SEA approach.

3.3 Limiting angle

The transmission coefficient (τ) at a specific angle of incidence (θ) for an infinite panel by the classical models can be found from;

$$\tau_\theta = \frac{1}{\left|1 + \frac{Z cos\theta}{2\rho_0 c}\right|^2} \qquad 3\text{-}1$$

Where Z is the bending wave impedance of the wall, ρ_0 is the density of air and c is the speed of sound in air.

In order to determine the transmission coefficient for excitation by a reverberant sound field it is generally assumed that all angles of incidence are equally probable and that the average value of the coefficient is given by integrating τ_θ, multiplied by an appropriate weighting factor, over all angles of incidence in the range from 0 to $\frac{\pi}{2}$ radians. The result obtained by integrating over all angles of incidence from 0 to $\frac{\pi}{2}$ radians under-predicts the STL; as a result the upper limit of the integration is often limited by some authors in order to improve the STL prediction.

According to Rindel (1975) limiting the angle of incidence was used by Cremer (1942) to compensate for the discrepancies obtained between the measured and random incidence values for a single leaf wall panel. This was meant as a practical solution and not as a physical explanation to the problem (Rindel, 1975). However, in Sharp's paper the explanation for the use of the limiting angle given by different laboratory workers was that "the sound field within the reverberation chamber is not totally diffuse and little sound energy is incident to the panel at grazing angles of incidence. However there appears to be no experimental justification for this assumption." (Sharp, 1978). Such thinking may give the impression that the use of the limiting angle corrects the physical phenomenon related to the diffuse field on the panel. Based on Rindel's (1975) discussion this clearly isn't the case. Furthermore Leppington *et al.*(1987) described the use of the limiting angle as being *ad hoc* with no physical meaning and gave an explanation for its success.

The use of a limiting angle of incidence has been used in relation to prediction models which are based on the wave approach such as Davy's, and models which utilize the impedance transfer matrix method. In this section the use of the limiting angle of incidence in relation to the wave approach will be discussed, while the issues associated with this method in relation to the transfer matrix method will be discussed in Section 3.7.

The use of a limiting angle of incidence of between $78°$ and $85°$ has been used by different workers (Sharp, 1978). For single leaf wall constructions a single value limiting angle works well. However, for double leaf wall systems, the use of a single value limiting angle does not produce accurate results, due to the sensitivity of the STL to the limiting angle of incidence as it involves the square of the single wall sound transmission coefficient and thus vary with angle of incidence θ as $1/\cos^4(\theta)$ instead of $1/\cos^2(\theta)$ (Davy, 2009c). As a result, Davy (1991), (2009c) used a variable limiting angle of incidence based on Sewell's (1970) model in order to improve the prediction of the STL for double leaf systems.

Consequently, although the use of the variable limiting angle improves the prediction of the STL of the double leaf wall systems; based on the discussion given by Leppington *et al.*(1987) and Rindel (1975) it cannot provide a physical explanation for the reason why the infinite model under-predicts the STL. Furthermore, additional problems occur when this method is used for the empty cavity situation.

3.4 Correction factors

London utilized an empirical correction factor R, in order to improve the prediction obtained from his model. The use of this correction factor was criticised by Mulholand (1967) and White (1965) as no physical explanation for the use of this correction factor was given (Smith, 1997).

Donato (1972) on the other hand reformulated the classical approach used by London and Beranek and used the spatial Fourier transform in order to develop a low frequency correction factor to compensate for the finite size of the wall system. Elmallawany (1982), then applied Donato's correction factor to the SEA model in order to improve the accuracy of the predictions. However, none of these correction factors provided a physical explanation for the reason why London ascertained that above the mass air mass resonance frequency " some of

the waves will be totally transmitted resulting in a diminution of the transmission loss of the panel compared to that predicted by the normal incidence theory" (London, 1950). As a result a physical explanation for the reason why the infinite models under-predicted the STL of double leaf wall systems could not be obtained from these correction factors.

Kang et al. (2000) however developed a weighting/correction factor which deals with the distribution characteristics of the transmitted sound waves into the cavity. Kang's Gaussian distribution weighting to Paris's equation has a significant effect with the empty cavity situation but little effect when sound absorption material is included within the wall cavity; Kang et al.'s weighting can be applied to any model which utilizes Paris's equation (Hongisto, 2006). However, Kang's weighting only sheds light on the distribution characteristics outlined by Paris's equation and not on the calculation of the transmission coefficient and does not give an explanation for the reason why London's model under-predicts the STL.

3.5 Stiffness of the wall cavity

Modelling the stiffness of the wall cavity provides a means for investigating the role of the wall cavity in the STL. Craik and Wilson (1995) utilized this technique to model the air in the wall cavity as a stiffness connecting the two wall panels to a point in their SEA model. The reduction in the sound transmission through double leaf wall systems due to a reduction in the stiffness of the wall cavity when sound absorption material is added was also discussed by Craik and Wilson (1995).

Gösele (1977) also modelled the stiffness of the wall cavity and discussed the effect of the airflow resistivity, cavity depth and amount of sound absorption material in the cavity on the stiffness of both an infinite and finite cavity in relation to the STL. Gösele's (1977) original model did not consider the mass/impedance of the wall panels and as a result did not include the mass air mass resonance frequency. However, in a second publication Gösele (1980) did consider the mass air mass resonance frequency but only used the dynamic effective stiffness (s_o) as given by Equation 3-2.

$$s_o = \frac{\rho c^2}{d}, \qquad \text{3-2}$$

where ρ is the density of air; c the speed of sound in air and d is the depth of the wall cavity. The stiffness given by Equation 3-2 is only valid as long as the dimensions of the air layers in each direction are small as compared to the wavelength, (Gösele and Gösele, 1977). Gösele (1977) then further outlined that this criterion was fulfilled in building acoustics when considering the depth d, of the cavity only and not in the other dimensions of the cavity, as these dimensions are usually large in relation to the wavelength. The results from Gösele's (1977) work however showed that if the cavity is fully damped the stiffness of both the infinite ($S_{infinite}$) and finite (S_{finite}) cavity approximates to Equation 3-2 (since $\frac{S_{infinite}}{S_0} = \frac{S_{finite}}{S_0} = 1$ see Figure 5 in Gösele's (1977)); hence the reason why Equation 3-2 could be used in the fully damped case as in Gösele (1980). For any situation other than the fully damped case the use of Equation 3-2 implies that only the stiffness perpendicular to the wall cavity is being considered. By extension, this will also imply that only the modes perpendicular to the wall panels are being investigated. Considering only the modes perpendicular to the wall will lead to inaccurate results since these occur at high frequencies (i.e. $\lambda < \frac{d}{2}$) as discussed by Hongisto (2006) while outlining the innovations of Cummings (1968) and Mulholland's (1967) works; for low frequencies (i.e. below the first perpendicular cavity mode) the in-plane sound field is dominant (Hongisto, 2006).

The method used by Gösele (1980) to calculate the STL is similar to the one employed by Heckl (1981). In both approaches the double wall is modelled as a mass spring mass system. The bending wave equations for both panels are solved and the cavity is assumed to be locally reacting as specified by Heckl (1981). The locally reacting criterion is not valid for an empty cavity; as a result these models cannot be used in this situation.

3.6 Fluid structural interactions

The full effect of the wall cavity on the wall panels can be obtained by studying the fluid structural interaction between the wall panels and the cavity. Such studies usually involve modal analysis as opposed to the early locally reacting theories introduced by Morse (1939). The use of modal analysis has been used extensively to describe the cavity's reverberation time (Dowell, 1978; Pan and Bies, 1988; Pan and Bies, 1990; Sum and Pan, 2002), sound

absorption (Pan and Bies, 1990; Sum and Pan, 2003), forced response (Pan, 1992; Sum and Pan, 1998), radiation (Kihlman, 1967; Fahy, 1985) and sound transmission loss (Brunskog, 2005) of the wall system.

Although the cavity's reverberation time and sound absorption characteristics will not be discussed in great detail in this work, they are mentioned here as the techniques used by Pan and Bies (1990), (1988) are fundamentally similar to Brunskog's (2005) in his investigation into the effect that the cavity has on the STL but provides an alternative technique to Brunskog's. Both works represent the two major techniques used to solve the appropriate differential equations. For example, Pan and Bies (1990) used the wave equation to describe the sound field within the cavity, the equations of motion for the bending wave motion on the panel and Rayleigh's integral for the radiation from the panels. Pan and Bies then reduced each equation to their equivalent Green's function and used both the methods of orthogonal modal expansion and successive substitution to find the solutions. Brunskog (2005) also used the wave equation and the equations of motions to describe the bending waves on the panel, however the wave-number Fourier transform and periodic assumptions were used to find the solutions. Brunskog also considered the effect of the studs on the cavity sound field and solutions were applied directly to finding the STL of the wall system while Pan and Bies work was concerned with the reverberation time and sound absorption of the cavity without studs.

Regardless of whether a transform or integration method is used to determine the solution for the equations, once any form of modal analysis (modal summation, cosine expansion etc.) is required, this technique cannot be used to study both the infinite and finite cases. Modal analysis can only be used for the finite case, since no modes (or wave reflections) occur in the infinite direction within an infinite model. As a result a direct link between the infinite and finite models cannot be found by only considering modal analysis.

3.7 Transfer matrix method

Unlike the modal analysis method one alternative that can be used to study both the infinite and finite case that is not utilized in this work is the impedance transfer matrix method. This method is ideal for studying the infinite cases since it models each layer as being of infinite extent. The technique was first developed by Mulholland et al (1968) and further

improvements were made by Ookure and Saito (1978), Hamada and Tachibana (1985) and Au and Byrne (1987; 1990). The technique is fundamentally based on the Beranek and Work's (1949) model. Similar to London's infinite model, having the assumption that the layers are of infinite extent leads to discrepancies when compared to the finite system especially in the low frequencies.

In order to compensate for some of these discrepancies a high/unrealistic sound absorption is often used to obtain results which are more realistic when the layers are assumed to be infinite. One method utilized within the literature to compensate for the finite size of each layer, is the spatial windowing technique. Villot et al. (2001) developed this technique and showed that for the case of acoustic excitation spatially windowing both the pressure and vibration field before calculating the radiated field greatly improved the agreement between the measured and predicted results; therefore making the use of the transfer matrix method a viable option for modelling the STL through a finite double leaf wall. Vigran (2009) later simplified the spatial windowing technique and applied the spatial window to the pressure field only.

Alternatively, the use of a limiting angle of incidence or Kang's Gaussian distribution weighting has also been used to adjust the infinite layers used within the impedance transfer matrix method. Similar to techniques which are fundamentally based on the wave approach method, the use of the limiting angle and Kang's Gaussian distribution weighting works well for single panels as discussed in Sections 3.3 and 3.4. However, while comparing measurements to predictions obtained while utilizing Au and Byrne's (1987; 1990) impedance transfer matrix model; Kurra (2001a) showed that for various limiting angles of incidence the predictions did not compare well to measurements.

3.8 Summary and conclusion

A summary of the different techniques used in the prediction of the STL through both finite and infinite double leaf wall systems has been presented. On the basis of the review it can be concluded that the adjustments to the classical SEA model as well as the insights obtained through the development of the spatial windowing technique provides physical insight and good prediction of the STL. However, in order to evaluate the influence the wall cavity in both the infinite and finite wall systems, the wave approach using the stiffness of the cavity is

considered by the author to be the most effective method. Furthermore this evaluation will give insight into why London's model under-predicts the STL. This understanding could help to explain some of the problems associated with other prediction models and why *ad hoc* approaches such as use of the limiting angle of incidence are needed. This understanding may also explain why high/unrealistic sound absorption is needed when the layers are assumed to be infinite in the transfer matrix method.

4 Expansion of Gösele's model

Gösele (1977) explained different factors which influence the STL of double leaf wall systems by solving the differential equations for the acoustic pressure within the wall cavity. The explanation discussed the effect of the cavity size, airflow resistivity and amount of sound absorption material in the cavity in terms of the stiffness of both an infinite and finite cavity. However, Gösele's (1977) original model did not take into account the mass/impedance of the wall panels and as a result did not include the mass air mass resonance frequency (f_0) as discussed on Page 47. In this chapter the differential wave equation for the acoustic pressure within the wall cavity is derived and solved by taking into account the impedance of both wall panels. This initial expansion of Gösele's (1977) model is then further expanded and used in finding the radiated power, radiation efficiency and STL of the double leaf wall system in subsequent chapters. However, before the underlying differential equation is derived the mechanism for airborne sound transmission through the cavity will be considered.

4.1 Airborne sound transmission mechanism

The STL is defined simply as the logarithm of the incident energy upon the wall to the energy transmitted through it. A schematic which outlines the five stage mechanism in deriving the relevant formulas for the sound transmission through a double leaf wall system can be seen in Figure 15. Sound transmission through a double leaf wall system begins by the incident sound waves striking the wall at a range of angles of incidence (θ). These sound waves are either reflected into the sending room or transmitted into the wall cavity as shown in Figure 15.

The sound transmission into the wall cavity is due to the excitation of both free and forced bending waves within the wall panel adjacent to the sending room. The free bending waves are the waves generated by the reflection of the forced bending waves from the edge of the panel. Below the critical frequency the free bending waves are inefficient radiators as opposed to the forced bending waves which radiate efficiently within this frequency range. Consequently within this frequency range the forced bending wave exerts a force on the wall cavity. The resulting pressure due to this forcing action can be found by solving the

inhomogeneous wave equation for the cavity. In finite wall systems the forced bending wave within the wall panel adjacent to the sending room causes both forced and reflected waves to occur within the cavity (Step 3). These waves within the wall cavity cause the panel on the receiving room side to vibrate at a particular frequency. If porous sound absorption material is included within the wall cavity, the resistance to the force/pressure acting on the cavity can be modelled by using the flow resistivity of the cavity.

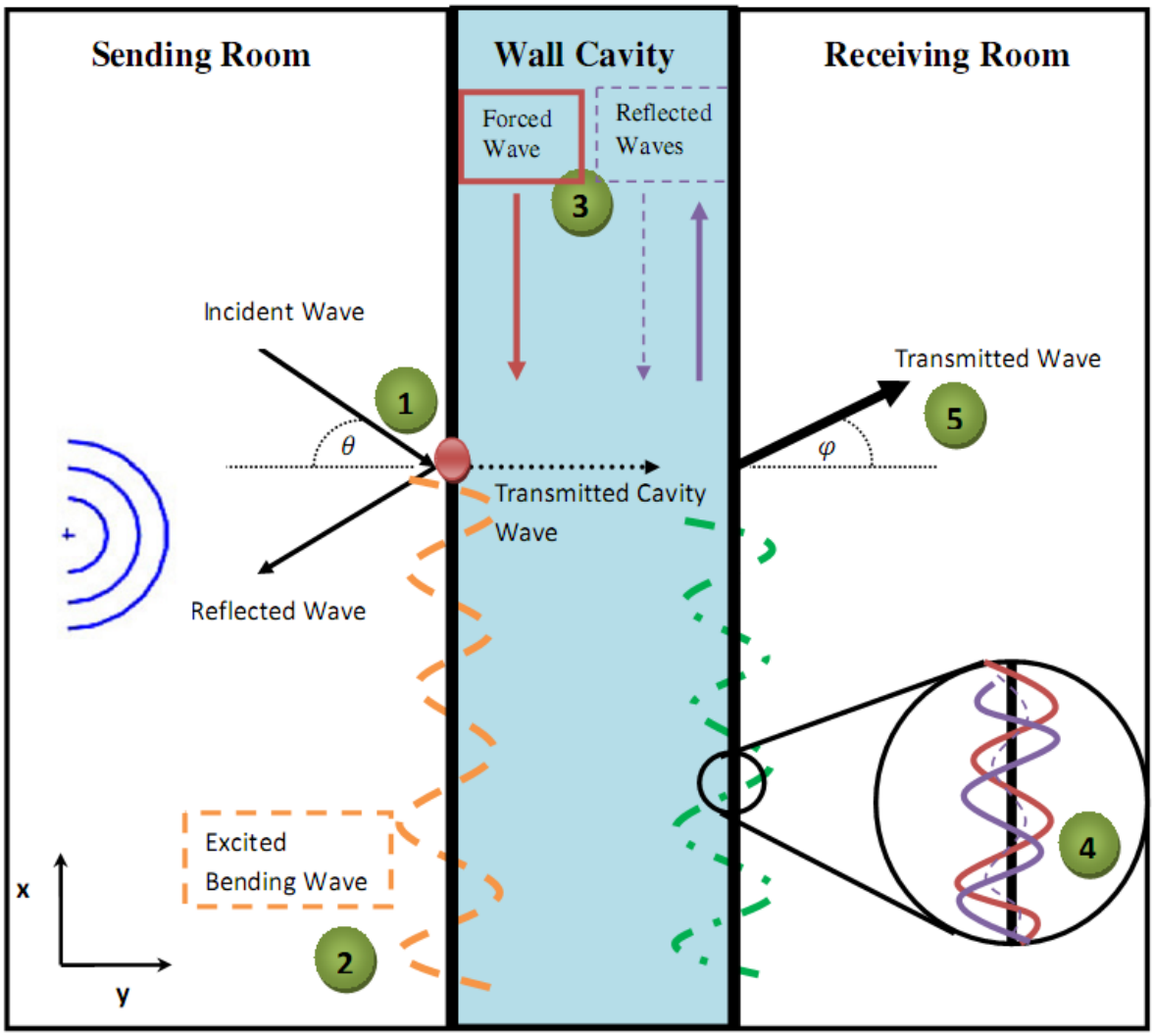

Figure 15 Mechanism of airborne sound transmission through double leaf wall systems

The total velocity of the panel adjacent to the receiving room is due to the sum of the excited bending waves caused by both the forced and reflected waves within the wall cavity as shown at Step 4 in Figure 15. These waves then radiate from this panel at angles of radiation φ into the receiving room as shown in Step 5. The extent of this radiation is determined by the

radiation efficiency of the bending waves excited by both the forced and reflected waves within the wall cavity. Assuming that this wall panel acts like a thin vibrating strip, the radiated power and efficiency can be determined and used in deriving the STL through the entire wall system.

This outlines the basic sound transmission mechanisms which will be used during the creation of the model developed within this research. All of the relevant assumptions and formulas will be explained and derived within the subsequent sections and chapters.

4.2 Governing equations

Consider the sketch of a double leaf wall system shown in Figure 16. The specific acoustic impedance (Z_i) of each wall panel can be found from the ratio of the sound pressure acting on it to its particle velocity (v_i).

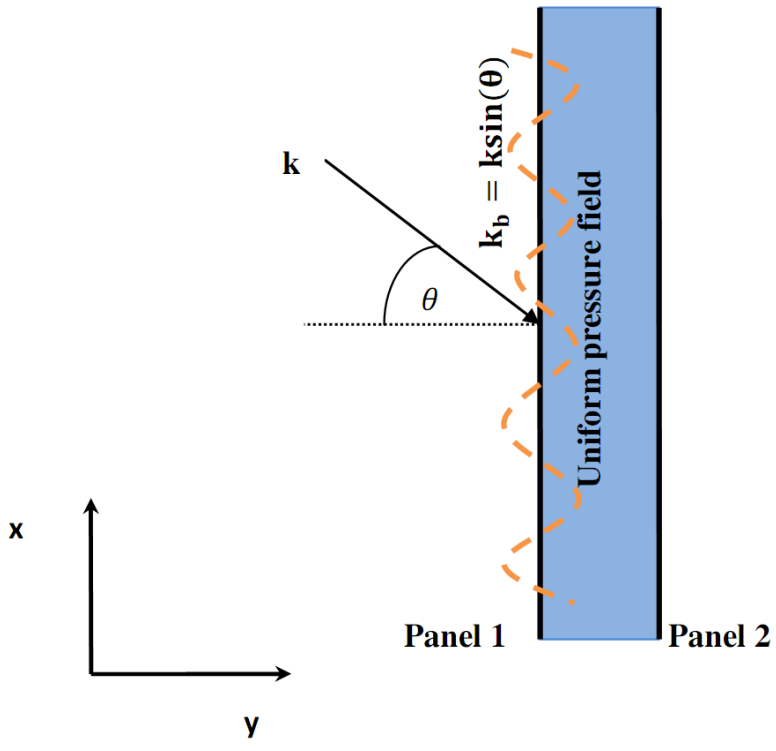

Figure 16 Co-ordinate system, incident and bending wave number used within the proposed model

Assuming that each wall panel acts as a limp mass; the fluid loading effect of the surrounding air on each panel can be taken into account by considering its radiation efficiency (σ_i) and the characteristic impedance ($\rho_0 c$) of the air such that

$$Z_i = j\omega m_i + \sigma_i \rho_0 c, \qquad 4\text{-}1$$

where the mass per unit area of each panel is m_i. The limp mass assumption means that there are not free bending waves within the wall panels and its bending stiffness is not considered. This assumption is only valid up to approximately half of the critical frequency of the panels. Assuming that a plane harmonic wave is incident on panel one, Gösele (1977) showed that once the depth of the wall cavity is small compared to the wavelength of incident sound waves a description of the air waves excited in the cavity parallel to the x direction is sufficient for the required analysis. Consequently the incident sound pressure can be modelled as

$$P_i(x,t) = \hat{P}_i e^{j(k_b x + \omega t)}, \qquad 4\text{-}2$$

where k_b is the wave number of the bending wave on the panel such that $k_b = ksin(\theta)$ as shown in Figure 16.

The magnitude of the sound pressure on the boundary of the first panel is twice the magnitude of the incident pressure due to the interaction between the incident and reflected wave. Further measurements and explanations which justify the assumption of this pressure doubling is given by Hart (2010). Consequently the specific acoustic impedance of panels one and two can be found from Equations 4-3 and 4-4 respectively

$$Z_1 = \frac{2P_i - P}{v_1}, \qquad 4\text{-}3$$

$$Z_2 = \frac{P}{v_2}, \qquad 4\text{-}4$$

where the cavity pressure (P) is created due to the motion of both wall panels. For frequencies below the first resonance frequency perpendicular to the wall panel Fahy (1985) showed that it can be assumed that the sound pressure within the wall cavity is uniform once the depth of the cavity is small compared to the wavelength of the incident waves. While Gösele (1977) showed that along the length of the cavity the sound pressure varies according to the position along the cavity within this frequency range.

Applying Newton's second law of motion to the air within the cavity, the sound pressure and acoustic particle velocity are related by

$$-\frac{\partial P(x,t)}{\partial x} = \rho_0 \frac{\partial v(x,t)}{\partial t}, \qquad \textbf{4-5}$$

where $v(x,t)$ is the particle velocity of the air within the wall cavity along the length in the x-direction. The particle velocity and cavity pressure can be written as

$$v(x,t) = v(x)e^{j\omega t}, \qquad \textbf{4-6}$$

$$P(x,t) = P(x)e^{j\omega t}, \qquad \textbf{4-7}$$

while Cremer (1982) showed that the cavity pressure is due to the compressibility factor (σ_c) such that

$$P(x,t) = \rho_0 c^2 \sigma_c(x,t). \qquad \textbf{4-8}$$

Within the wall cavity the rate of compression is due to the movement of the panel in the y-direction and the change in particle velocity in the x-direction, (Gösele and Gösele, 1977). As a result

$$\frac{\partial \sigma_c(x,t)}{\partial t} = -\frac{\partial v(x,t)}{\partial x} + q, \qquad \textbf{4-9}$$

where q is the volume addition per unit volume due to the movement of the panels in the y-direction. Combining Equations 4-3 and 4-4 gives

$$q(x,t) = \frac{v_1 - v_2}{d} = \frac{1}{d}\left(\frac{2P_i - P(x,t)}{Z_1} - \frac{P(x,t)}{Z_2}\right). \quad \textbf{4-10}$$

Consequently the rate of change of pressure with respect to time can be found. Equation 4-8 can be re-written as

$$\frac{1}{\rho_0 c^2}\frac{\partial P(x,t)}{\partial t} = \frac{\partial \sigma_c(x,t)}{\partial t}. \quad \textbf{4-11}$$

Substituting the rate of change of compression from Equation 4-9 into Equation 4-11 and solving for $\frac{\partial P}{\partial t}$ gives

$$\frac{j\omega P(x)}{\rho c^2} + \frac{\partial v(x,t)}{\partial x} = q(x,t). \quad \textbf{4-12}$$

If porous sound absorption material is added to the cavity, Gösele (1977) showed that the resistance to the force acting on the air within the cavity can be found from the product of the material's flow resistivity (Ξ) and the air velocity such that Equation 4-5 becomes

$$\rho_0 \frac{\partial v(x,t)}{\partial t} + \Xi v(x,t) + \frac{\partial P(x,t)}{\partial x} = 0. \quad \textbf{4-13}$$

From Equation 4-6 $\frac{\partial v(x,t)}{\partial t} = j\omega v(x)e^{j\omega t}$. Substituting this rate of change of velocity with respect to time into Equation 4-13 and utilizing the relationship for $v(x,t)$ given by Equation 4-6 gives

$$j\omega\rho_0 v(x)e^{j\omega t} + \Xi v(x)e^{j\omega t} + \frac{\partial P(x,t)}{\partial x} = 0. \quad \textbf{4-14}$$

Assuming stationary conditions Equation 4-14 can be written as

$$j\omega\rho_0 v(x) + v(x)\Xi = -\frac{dP(x)}{dx} \quad . \tag{4-15}$$

Rearranging Equation 4-15 in terms of the velocity along the length of the cavity gives

$$v(x) = -\frac{1}{\Xi + j\omega\rho_0}\frac{dP(x)}{dx}. \tag{4-16}$$

Inserting $v(x)$ from Equation 4-16 into Equation 4-12 gives the wave equation for the wall cavity

$$-\frac{1}{\Xi + j\omega\rho_0}\frac{d^2P(x)}{dx^2} + \frac{j\omega P(x)}{\rho_0 c^2} = q(x). \tag{4-17}$$

Multiplying both sides of Equation 4-17 by $-j\omega\rho$ makes Equation 4-17 into the standard inhomogeneous Helmholtz wave equation form as follows

$$\frac{j\omega\rho}{\Xi + j\omega\rho_0}\frac{d^2P(x)}{dx^2} + k^2P(x) = -j\omega\rho_0 q(x). \tag{4-18}$$

Equation 4-18 shows the inhomogeneous wave equation for the wall cavity of the system under consideration. The derivation above, showed how both the flow resistivity and particle velocity can be included into this equation based on the assumptions of having stationary conditions and a uniform pressure distribution within the wall cavity.

4.3 Solution to governing equations

In order to find the solution for the wave equation given by Equation 4-18 an analytical method based on the extension of the Linearity Principle given by Blanchard (1998) is used to solve both the homogeneous and forced situations. The derived solutions describe both the

forced and reflected waves within the cavity and will be used in the derivation of the radiation efficiency for these respective waves. These solutions will also be used in the derivation of the STL and directivity of the transmitted sound through double glazed window systems.

Starting from Equation 4-18 , if the stationary form of the volume addition per unit volume q from Equation 4-10 is substituted into this equation it becomes

$$\frac{j\omega\rho}{\Xi + j\omega\rho_0}\frac{d^2P(x)}{dx^2} + k^2P(x) = -j\omega\rho_0\frac{1}{d}\left(\frac{2P_i - P(x)}{Z_1} - \frac{P(x)}{Z_2}\right). \quad \textbf{4-19}$$

Equation 4-19 can be re-written as

$$\frac{d}{\Xi + j\omega\rho_0}\frac{d^2P}{dx^2} + \left(\frac{dk^2}{j\omega\rho_0} - \frac{Z_2 + Z_1}{Z_1Z_2}\right)P(x) = -\frac{2P_i}{Z_1}, \quad \textbf{4-20}$$

with the general solution being in the form

$$P(x) = P_{particular}(x) + P_{homogenous}(x).$$

The **homogenous** solution for the system can be found from the homogenous equation given by

$$\frac{d}{\Xi + j\omega\rho_0}\frac{d^2P}{dx^2} + \left(\frac{dk^2}{j\omega\rho_0} - \frac{Z_2 + Z_1}{Z_1Z_2}\right)P(x) = 0. \quad \textbf{4-21}$$

Equation 4-21 can be re-arranged to give

$$\frac{d^2P}{dx^2} + \frac{\left(\frac{dk^2}{j\omega\rho_0} - \frac{Z_2 + Z_1}{Z_1Z_2}\right)}{\left(\frac{d}{\Xi + j\omega\rho_0}\right)}P(x) = 0. \quad \textbf{4-22}$$

Using the substitution method as described in (Blanchard *et al.*, 1998) Equation 4-22 can be broken down into a linear system such that

$$S = \frac{dP(x)}{dx}, \tag{4-23}$$

and

$$\frac{dS}{dx} = -\frac{\left(\frac{dk^2}{j\omega\rho_0} - \frac{Z_2 + Z_1}{Z_1 Z_2}\right)}{\left(\frac{d}{\Xi + j\omega\rho_0}\right)} P(x). \tag{4-24}$$

This linear system can be written in matrix form as

$$\frac{d\boldsymbol{Q}}{dx} = \boldsymbol{AQ}. \tag{4-25}$$

Consequently

$$\frac{d\boldsymbol{Q}}{dx} = \begin{bmatrix} \frac{dP(x)}{dx} \\ \frac{dS}{dx} \end{bmatrix} = \begin{bmatrix} 0 & 1 \\ -\frac{\left(\frac{dk^2}{j\omega\rho_0} - \frac{Z_2 + Z_1}{Z_1 Z_2}\right)}{\left(\frac{d}{\Xi + j\omega\rho_0}\right)} & 0 \end{bmatrix} \begin{bmatrix} P(x) \\ S \end{bmatrix}. \tag{4-26}$$

The eigenvector for this linear system of matrix A is a nonzero vector U such that $\mathbf{AU} = \lambda\mathbf{U}$. Where λ is the eigenvalue for U such that

$$\begin{bmatrix} 0 & 1 \\ -\frac{\left(\frac{dk^2}{j\omega\rho_0} - \frac{Z_2 + Z_1}{Z_1 Z_2}\right)}{\left(\frac{d}{\Xi + j\omega\rho_0}\right)} & 0 \end{bmatrix} \begin{bmatrix} P(x) \\ S \end{bmatrix} = \lambda \begin{bmatrix} P(x) \\ S \end{bmatrix}. \tag{4-27}$$

From Equation 4-27 λ can be found from the determinant, which results in

$$\lambda = \pm\sqrt{-\frac{\left(\frac{dk^2}{j\omega\rho_0} - \frac{Z_2 + Z_1}{Z_1 Z_2}\right)}{\left(\frac{d}{\Xi + j\omega\rho_0}\right)}} = \pm j\sqrt{\frac{\left(\frac{dk^2}{j\omega\rho_0} - \frac{Z_2 + Z_1}{Z_1 Z_2}\right)}{\left(\frac{d}{\Xi + j\omega\rho_0}\right)}}. \quad \textbf{4-28}$$

Equation 4-28 can be expanded and simplified to give

$$\lambda = \pm\left[\frac{Z_2 + Z_1}{Z_2 Z_1}\frac{\Xi}{d} - k^2 + \frac{j\Xi k^2}{\omega\rho_0} + \frac{Z_2 + Z_1}{Z_2 Z_1}\frac{j\omega\rho_0}{d}\right]^{\frac{1}{2}}. \quad \textbf{4-29}$$

Let $\acute{a}$ and $\acute{b}$ be the real and imaginary part of the portion of Equation 4-29 enclosed within the parentheses such that

$$a' = \frac{Z_2 + Z_1}{Z_2 Z_1}\frac{\Xi}{d} - k^2 \quad \textbf{4-30}$$

and

$$b' = \frac{Ek^2}{\omega\rho_0} + \frac{Z_2 + Z_1}{Z_2 Z_1}\frac{\omega\rho_0}{d} \quad \textbf{4-31}$$

λ can be written as

$$\lambda = \pm\sqrt{a' + jb'} \quad \textbf{4-32}$$

Using DeMoivre's theorem, Rabinowitz (1993) showed that the real (α) and imaginary (β) parts of the square root of a complex number can be found from

$$\alpha = \frac{1}{\sqrt{2}}\sqrt{\sqrt{a'^2 + b'^2} + \acute{a}^2}$$

and

$$\beta = \frac{1}{\sqrt{2}}\sqrt{\sqrt{a'^2 + b'^2} - \acute{a}^2}.$$

Letting $\gamma = \alpha + j\beta$ then $\lambda = \pm\gamma$, the solution for the homogenous equation becomes

$$P(x) = k_1 e^{\gamma x} + k_2 e^{-\gamma x}. \qquad \textbf{4-33}$$

For the **particular** solution, the sound wave incident on panel 1 at an angle θ to the normal can be written as $\hat{P}_i e^{jk_b x}$, where

$$k_b = k_x = ksin\theta. \qquad \textbf{4-34}$$

Consequently Equation 4-20 becomes

$$\frac{d}{\Xi + j\omega\rho_0}\frac{d^2P(x)}{dx^2} + \left(\frac{dk^2}{j\omega\rho_0} - \frac{Z_2 + Z_1}{Z_1 Z_2}\right)P(x) = -\frac{2P_i e^{jk_b x}}{Z_1}. \qquad \textbf{4-35}$$

Assuming that $y_p = Ne^{jk_b x}$ is a particular solution for the cavity pressure, the forced wave amplitude can be found by substituting this particular solution into Equation 4-35 to give

$$\left(\frac{j\omega\rho_0}{\Xi + j\omega\rho_0}\right)(-k_b^2)Ne^{jk_b x} + \left(k^2 - \frac{j\omega\rho_0}{d}\left(\frac{Z_2 + Z_1}{Z_1 Z_2}\right)\right)N^{jk_b x} = -\frac{2j\omega\rho_0 P_i}{Z_1 d}e^{jk_b x}. \qquad \textbf{4-36}$$

Multiplying both sides of Equation 4-36 by minus one and re-arranging it in terms of the amplitude of the forced wave N gives

$$N = \frac{j\omega\rho_0 2P_i}{Z_1 d}\left(\frac{1}{\left[k_b^2\frac{j\omega\rho_0}{\Xi + j\omega\rho_0} - k^2 + \frac{j\omega\rho_0}{d}\frac{Z_2 + Z_1}{Z_1 Z_2}\right]}\right). \qquad \textbf{4-37}$$

As a result the full solution to the wave equation given by Equation 4-18 can be written in the following form

$$P(x) = Ne^{jk_b x} + k_1 e^{\gamma x} + k_2 e^{-\gamma x}. \quad \text{4-38}$$

The coefficients k_1 and k_2 can be found by assuming rigid boundary conditions such that $v(0) = v(l) = 0$; this implies that $dP(x)/dx = 0$ at $x = 0$ and $x = l$. At $x = 0$ $dP(x)/dx$ is

$$Njk_b + k_1\gamma - k_2\gamma = 0, \quad \text{4-39}$$

and at $x = l$, $dP(x)/dx$ becomes

$$jk_b Ne^{jk_b l} + k_1\gamma e^{\gamma l} - k_2\gamma e^{-\gamma l} = 0. \quad \text{4-40}$$

Solving Equations 4-39 and 4-40 gives the amplitude of the reflected waves k_1 and k_2 as follows

$$k_1 = \frac{jk_b N\left(e^{-\gamma l} - e^{ik_b l}\right)}{\gamma(e^{\gamma l} - e^{-\gamma l})}, \quad \text{4-41}$$

$$k_2 = \frac{jk_b N\left(e^{\gamma l} - e^{ik_b l}\right)}{\gamma(e^{\gamma l} - e^{-\gamma l})}. \quad \text{4-42}$$

4.4 Summary and conclusions

The wave equation and the relevant solutions for the wall cavity have been derived within this chapter. These derivations improve on Gösele's (1977) theory by including:

- Pressure doubling on the wall panel
- Wall impedance
- Fluid loading effect on the wall panel
- Radiation efficiency of the wall panel

With the following assumptions being made:

- Uniform sound pressure within the wall cavity in the y-direction
- Stationary conditions

- Rigid boundary conditions
- Limp panels
- The model is valid for the frequency range below half the critical frequency of the wall panels

Although Gösele (1977) indicated that the solution for the sound pressure within the wall cavity is in the form shown in Equation 4-38, he did not give the solution for k_1 and k_2 as given by Equations 4-41 and 4-42 respectively. Instead Gösele combined the effect of the reflected waves into one equation. Consequently the solutions presented here for k_1 and k_2 provide an alternative approach to Gösele's which will be critical in analysing the radiation efficiency of these waves as derived in Chapter 6.

The improvements to Gösele's (1977) theory can now be used to study of the effect of the mass air mass resonance frequency on the STL of the entire wall system. This effect is crucial in understanding why the infinite model under-predicts the STL as explained in Chapter 5.

5 Physical explanation for the under-prediction of London's model

London (1949; 1950) utilized the wave approach and developed the infinite model for the sound transmission loss through both single and double leaf walls. The theoretical basis for the double leaf model was first established from the single wall panel model. Continuity of particle velocity was used in order to find the transmitted pressure and STL of the wall system within London's (1949) single wall panel model. When applied to double leaf wall systems, London's (1950) model underestimated the STL; as a result an empirical correction factor based on measurements had to be used to obtain reliable predictions. The use of this correction factor was criticised by Mulholland *et al.* (1967) and White and Powell (1965) as no physical explanation for the use of this correction factor was given (Smith, 1997). Consequently, in this chapter the proposed model is applied to the infinite cavity situation and compared to London's model in order to validate the developed equations. This model will then be modified to compensate for the finite size of the wall cavity in order to give the physical explanation as to why London's model under-predicts the STL through double leaf wall systems.

5.1 Sound transmission loss model for the infinite double leaf wall system

The STL is defined simply as the logarithm of the incident energy upon the wall to the energy transmitted through it. Written in terms of the interaction of the incident (P_i) and transmitted sound pressure (P_t) the sound transmission coefficient (τ) can be found from

$$\tau = \frac{W_t}{W_i} = \left|\frac{P_t}{P_i}\right|^2, \qquad 5\text{-}1$$

where W_t and W_i are the transmitted and incident sound power respectively; with the corresponding sound transmission loss found from

$$STL = 10\log\left(\frac{1}{\tau}\right). \qquad 5\text{-}2$$

By assuming continuity of the particle velocity, London showed the relationship between the transmitted pressure of the infinite wall system $(P_{\infty,trans})$ and particle velocity is

$$P_{\infty,trans} = \left|\frac{\rho_o c v_2}{\cos(\theta)}\right|, \quad \text{5-3}$$

where v_2 is the particle velocity on the panel 2. v_2 is dependent on the pressure within the wall cavity and the specific acoustic impedance as shown in Equation 4-4. As a result

$$P_{\infty,trans} = \frac{\rho_o c}{\cos(\theta)}\left|\frac{P_{\infty,cavity}}{Z_2}\right| \quad , \quad \text{5-4}$$

where

$$P_{\infty,cavity} = \left|N e^{jk_b x}\right| = |N|. \quad \text{5-5}$$

and N is the amplitude of the forced wave given by Equation 4-37.

Beranek (1971) showed that the forced radiation efficiency of an infinite plate (σ_∞) due to airborne excitation is given by

$$\sigma_\infty = \frac{1}{\sqrt{1 - sin^2(\theta)}} = \frac{1}{cos(\theta)}. \quad \text{5-6}$$

Consequently Equation 5-4 can be written in terms of σ_∞ as

$$P_{\infty,trans} = \rho_o c\, \sigma_\infty \left|\frac{P_{\infty,cavity}}{Z_2}\right|. \quad \text{5-7}$$

From Equation 5-7 it can be seen that for the infinite model, the transmitted pressure squared is dependent only on the amplitude of the forced waves. This is due to the underlying assumption within the infinite model that the panels and by extension the wall cavity is infinitely long such that waves excited within the system keep travelling without any reflections. Consequently from Equation 4-38 the sound pressure within the cavity for the infinite model is only dependent on the forced waves as shown in Equation 5-7.

The STL for the infinite model (STL_{∞}) can be found by assuming that the incident pressure in Equation 5-1 is equal to one. This assumption can be made as the transmitted pressure is also dependent on the incident pressure; since the STL involves the ratio of these two sound pressures any value can be assumed for the incident sound pressure. As a result, the sound transmission loss for the infinite model can be found from

$$STL_{\infty} = 10\log_{10}\left(\frac{1}{P^2{}_{\infty,trans}}\right). \qquad \textbf{5-8}$$

The STL prediction obtained from Equation 5-8 compared to London's model for an empty double leaf infinite wall system with equal mass of 12.3 kg/m^2 for both wall panels and a cavity depth of 90 mm can be seen in Figure 17.The results in Figure 17 show that the prediction produced from the developed model directly match the results obtained from London's work. This figure also shows that the mass air mass resonance frequency varies with angles of incidence, with the lowest of these occurring at the normal mass air mass resonance frequency. London (1950) ascertained that the diminution of the STL at frequencies above the normal mass air mass resonance frequency to the point where total transmission occurs is due to this variation. In reality a diminution to such an extent does not occur. Consequently, London explained that this lack of total diminution is due to incidence energy from all directions within a reverberant sound field. The interaction of sound waves from all directions will ensure that at least some attenuation occurs above the normal mass air mass frequency and will prevent total sound transmission. However, this interaction between the waves from different angles of incidence alone does not explain the reason why London's model under-predicts the STL, since London's diffuse field approximation which takes into account the summation of the components from all angles of incidence also under-predicts the STL (see Figure 21). An alternative explanation for why total transmission does not occur can be found by considering the finite size of the wall system as outlined in Section 5.2.

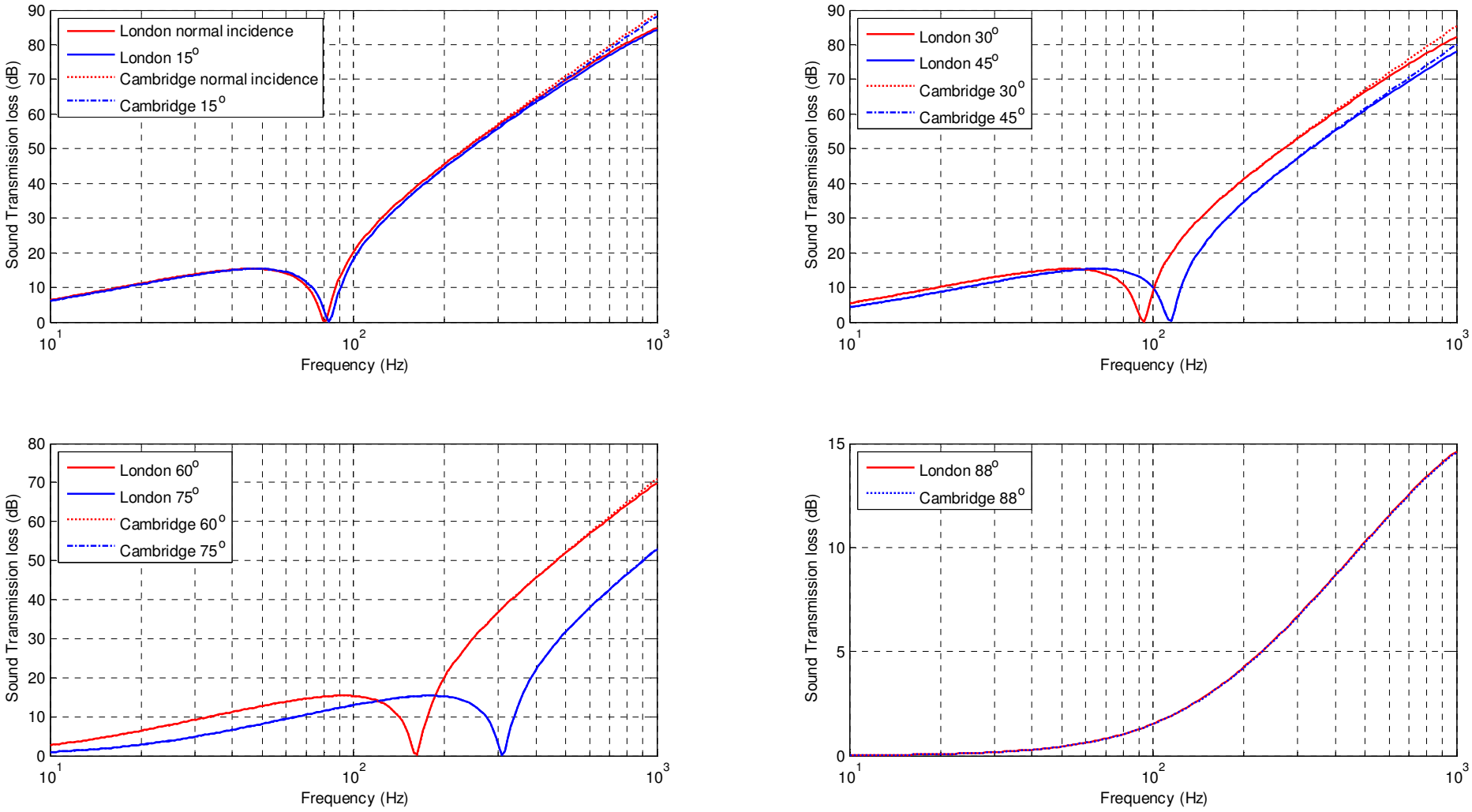

Figure 17 Comparison between the current theory and London's model for an infinite double leaf wall at different angles of incidence

London (1950) showed that the mass air mass resonance frequency ($f_{o,\theta}$) for an infinite double leaf wall system with equal masses for both panels varied based on the angle of incidence (θ) as

$$f_{o,\theta} = \frac{1}{2\pi cos\theta}\left(\frac{2\rho c^2}{md}\right)^{\frac{1}{2}}, \quad \text{5-9}$$

with the corresponding normal mass air mass resonance frequency when both panels are of the same mass being

$$f_o = \frac{1}{2\pi}\left(\frac{2\rho c^2}{md}\right)^{\frac{1}{2}}. \quad \text{5-10}$$

The calculated mass air mass resonance frequency for different angles of incidence using Equation 5-9 for the wall system used to obtain the prediction results shown in Figure 17 can be seen in Table 5.

Table 5 Mass air mass resonance frequency at different angles of incidence for an empty double leaf infinite wall system with both wall panels of equal mass 12.3 kg/m^2 and a cavity depth of was 90 mm

Angle of incidence (degrees)	Mass air mass resonance frequency (Hz)
0	80.6
15	83.5
30	93.1
45	114.1
60	163.3
75	311.6
88	2310.9

The results shown in Table 5 correspond to the frequencies where the mass air mass resonance frequencies occur in Figure 17.

5.2 The effect of the reflected waves on the STL

In Section 5.1 it was shown that an accurate infinite model compared to London's model can be obtained by considering only the magnitude of the forced wave within the cavity. However, for the finite wall system the interaction between the forced and reflected waves within the cavity dictates the response of the entire system.

One major problem associated with the infinite model, is that it predicts that no sound will be transmitted at grazing incidence due to the radiation efficiency of the infinite panels. As a result some researchers utilize a finite radiation efficiency as a substitute for the $1/\cos(\theta)$ when modelling finite wall systems. For example, Rindel (1975) utilized such a substitution and commented that this was similar to the way in which it was employed by Heckl (1964). Rindel stated that the use of the radiation efficiency in this manner also implies that the incident power per unit area is small when kl is large and increases when kl decreases; the deformation of the sound field by diffraction effects was given as the explanation for the reason why this occurs. The use of the finite radiation efficiency in this manner is similar to spatial windowing technique developed by Villot et al. (2001). In this initial introduction of the theory, the spatial window was applied to both the sound pressure field and the vibration before calculating the radiated field. According to Vigran (2009) this technique was modified by Villot and Guigou-Carter (2005) by only taking the spatial window into account on the sound pressure field; a technique which he employed when developing his simplified version of the technique.

However, despite Rindel's (1975) and Villot *et al*'s (2001) successful substitution of the finite radiation efficiency in the manner described, this approximation cannot be done on both the transmitted power and the incident power. This was the reason for Villot and Guigou-Carter's (2005) correction. Furthermore if this approximation is done for the incident power, it should only be utilized when finding the angular dependent sound transmission loss and not when finding the diffuse sound field sound transmission loss. This is because the $\cos(\theta)$ term used when calculating the diffuse sound field transmission coefficient (as shown in Equation 5-18) represents the projected area of the sound field onto the wall panel. Consequently a further substitution of the finite radiation efficiency for this $\cos(\theta)$ term cannot be done.

In finite wall systems an asymptotic increase in the forced radiation efficiency does not occur at grazing angles of incidence; the radiation efficiency is also frequency dependent. As a result, the transmitted pressure of the finite system due to the average mean square pressure within the cavity can be found from Equation 5-11 by considering the forced radiation efficiency of the finite system and the interaction of the force and reflected waves such that

$$P^2_{trans-finite} = (\rho_0 c)^2 \left| \frac{P^2_{cavity-finite}}{Z_2^2} \right| \sigma^2{}_{finite}\,, \qquad \textbf{5-11}$$

with

$$P^2{}_{cavity-finite} = \frac{1}{L}\int_{x=0}^{x=L} \left| N e^{ik_b} + k_1 e^{\gamma x} + k_2 e^{-\gamma x} \right|^2 dx, \qquad \textbf{5-12}$$

where, σ_{finite} is the forced radiation efficiency of a finite panel taken from Davy (2009b), k_1 and k_2 are the pressure amplitudes due to the reflected waves as defined in Equations 4-41, and 4-42 respectively. The STL through the system can then be found by replacing the infinite transmitted pressure in Equation 5-8 by the finite one.

Equation 5-11 represents the full equation required to find the transmitted pressure from the finite wall system. In order to determine the difference between London's infinite model and the finite one due to the interaction between the forced and reflected waves, the infinite radiation efficiency was initially used within this equation. The effect of this interaction on the STL of a 3.05 by 2.44 m gypsum double wall system with a 90 mm cavity can be seen in Figure 18, while the results for the full finite model (given by Equation 5-11) can be seen in Figure 19. A cavity length of 2.44 m was utilized when calculating the results shown in both these figures.

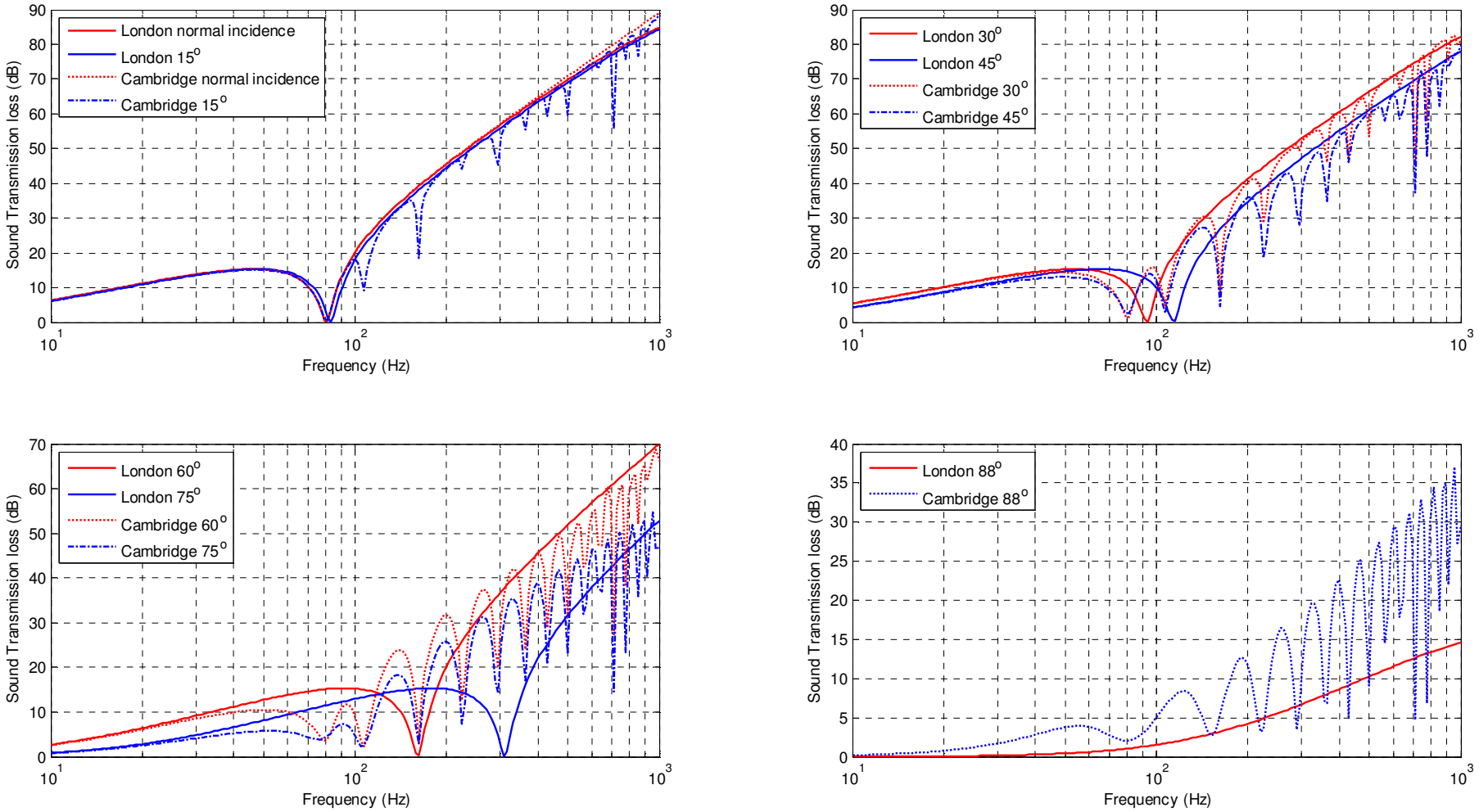

Figure 18 Difference between London's infinite model and the semi- infinite model due to the interaction between the forced and reflected waves only at different angles of incidence

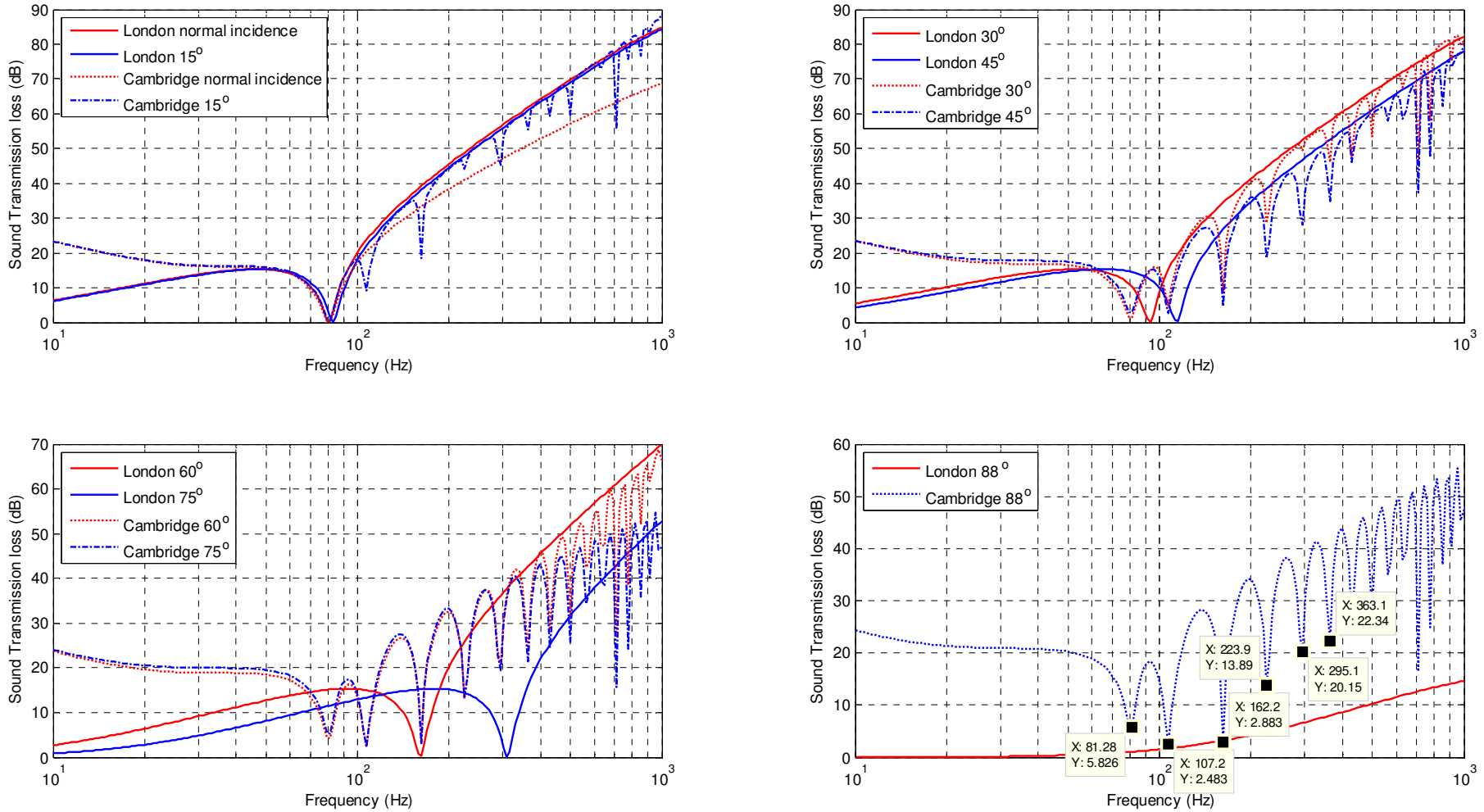

Figure 19 Difference between London's infinite model and the proposed finite model using Davy's forced radiation efficiency at different angles of incidence

The results in Figure 18 and Figure 19 show that the oblique mass air mass resonance frequency for both the semi-infinite and finite model does not vary with the angle of incidence as in London's model. Instead, for all angles of incidence the oblique mass air mass resonance frequency occurs at the normal mass air mass frequency. The presence of the reflected waves within the wall cavity is responsible for the mass air mass frequency being independent of the angle of incidence. Evidence of this can be seen by studying the results obtained for the total average particle velocity (v_{total}) on the boundary of the second panel and by analysing the contribution of the forced (v_{forced}) and reflected waves ($v_{reflected}$). These velocities can be found by considering the impedance of the wall panel and the sound pressure caused by each wave within the wall cavity (see Equation 4-4) such that

$$v^2{}_{forced} = \frac{\frac{1}{L}\int_{x=0}^{x=L}\left|Ne^{jk_b}\right|^2\,dx}{Z_2^2}, \qquad \textbf{5-13}$$

$$v^2{}_{reflected} = \frac{\frac{1}{L}\int_{x=0}^{x=L}\left|k_1e^{\gamma x}+k_2e^{-\gamma x}\right|^2\,dx}{Z_2^2}, \qquad \textbf{5-14}$$

$$v^2{}_{total} = \frac{\frac{1}{L}\int_{x=0}^{x=L}\left|Ne^{jk_b}+k_1e^{\gamma x}+k_2e^{-\gamma x}\right|^2\,dx}{Z_2^2}. \qquad \textbf{5-15}$$

The results for the average particle velocity for the wall system used to obtain the results shown in Figure 19 can be seen in Figure 20.

The results shown in Figure 20 clearly show that the resonance peak at the mass air mass resonance frequency of the total average particle velocity does not vary with the angle of incidence but remains at the normal mass air mass resonance frequency. The results obtained for the forced reflected waves and forced wave indicate that the reason why this resonance peak does not vary with the angle of incidence is due to the interaction of the reflected waves. This can be seen as the resonance peak due to the interaction of the forced reflected waves does not vary with the angle of incidence as opposed to the angular dependent shift which occurs with the forced wave.

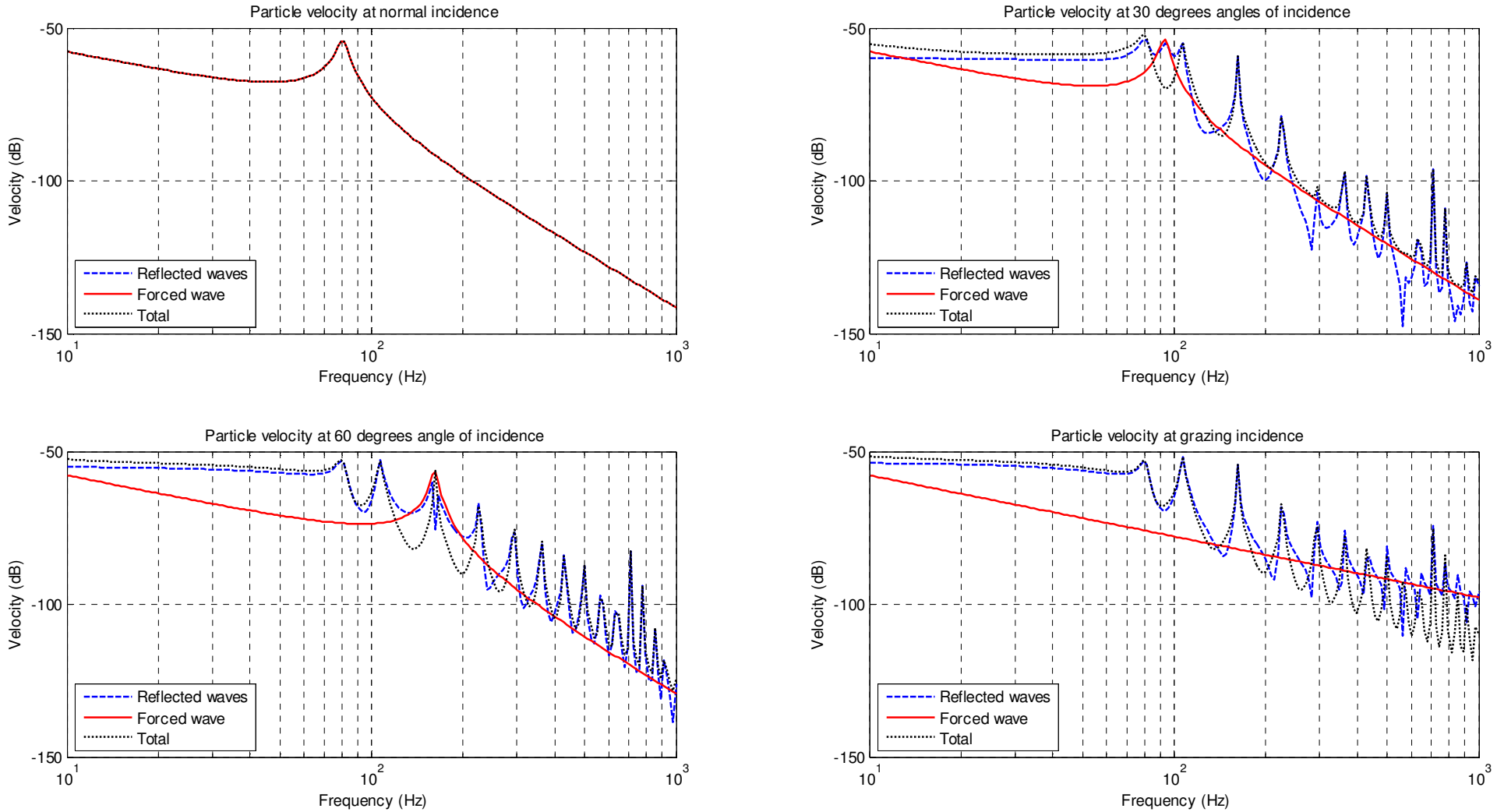

Figure 20 Particle velocity on the boundary of panel 2 at different angles of incidence

The resonance peaks above the mass air mass resonance shown in Figure 20 or the dips in the STL shown in and Figure 19, are due to the cavity resonances associated with the finite size of the wall cavity. The results shown indicate that these resonance frequencies do not vary with the angle of incidence. The frequencies at which these dips in the STL occur can be found by considering the resonances along the length of the cavity and the mass air mass resonance frequency. The resonance frequency along the length of the cavity (f_{n_x}) can be found from Bies and Hansen (2009) such that

$$f_{n_x} = \frac{c}{2}\sqrt{\left(\frac{n_x}{L}\right)^2}, \qquad \text{5-16}$$

where n_x is the mode number along the length of the cavity in the x direction. While the corresponding total resultant resonance due to the mass air mass resonance frequency and the resonances along the length of the cavity can be found from

$$f_{total} = \sqrt{f_{n_x}^2 + (f_o)^2}. \qquad \text{5-17}$$

Prasetiyo and Thompson (2012) also used an identical formula to Equation 5-17. The total resultant resonance frequencies of the first few modes along the length of the cavity which correspond to the dips in the STL can be seen in Table 6. The position of these calculated frequencies are also shown in Figure 19.

Table 6 Resonance frequencies which correspond to dips in the STL

n_x	f_{n_x}(Hz)	f_{total}(Hz)
0	0	80.6
1	70.3	106.4
2	140.6	161.7
3	210.9	225.5
4	281.9	292.3
5	351.4	360.4

In order to determine how the prediction results shown in Figure 18 and Figure 19 compare to measurements reported by Warnock (2010), the diffuse sound field sound transmission coefficient (τ_d) was calculated used using Equation 5-18 and averaged into 1/3 octave band centre frequencies.

$$\tau_d = 2\int_0^{\pi/2} \tau \sin(\theta)\cos(\theta)\, d\theta. \qquad 5\text{-}18$$

The results of this comparison can be seen in Figure 21 while the description of the wall systems can be found in Appendix A.

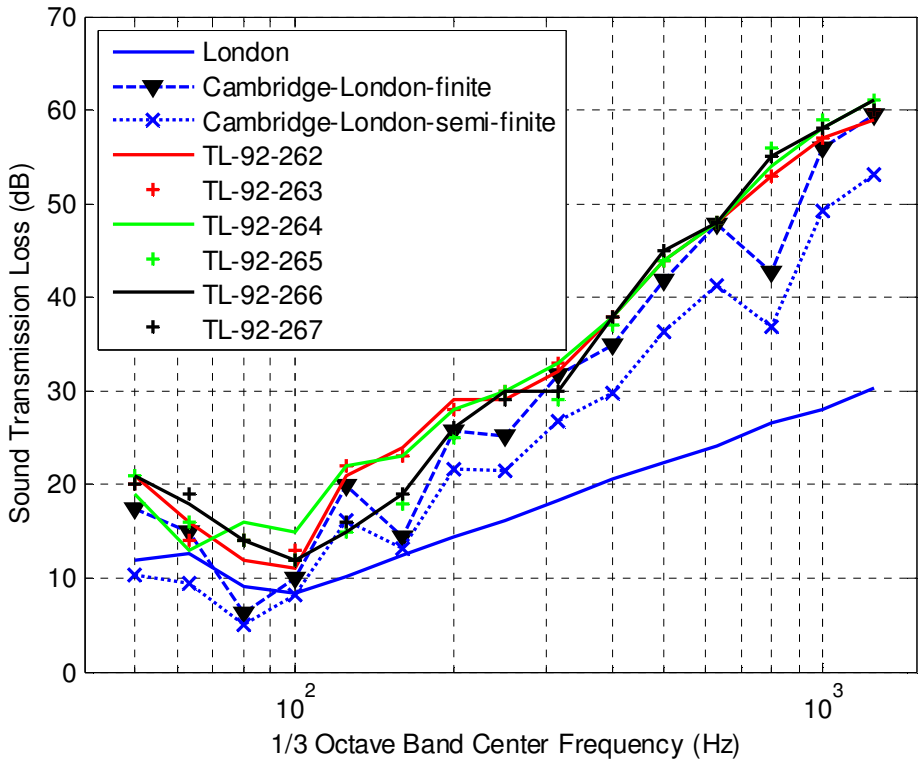

Figure 21 Measured and calculated sound transmission loss in 1/3 octave bands

The results in Figure 21 clearly show the extent by which London's model underestimates the STL through double leaf wall systems due to the angular dependent mass air mass resonance. Once this effect is removed by taking into account the interaction of the reflected forced waves within the wall cavity due to its finite size in the semi-infinite model and accounting

for the effect of the finite forced radiation efficiency in the finite model, more realistic predictions are obtained. Therefore the physical explanation for the reason why London's model under-predicts the STL comes from the effect of the angular dependent mass air mass resonance frequency.

The link between the angular dependent mass air mass resonance frequency and London's under-prediction of the STL has not been reported within the literature (even though the presence of the angular dependent mass air mass was discussed by Wilson (1992)). Although Prasetiyo and Thompson's (2012) recent publication which is based on the coupled Waveguide Finite Element-Wavedomain Boundary Element method to predict the STL showed that the oblique resonance does not vary with the angle of incidence (an observation which agrees with the results presented here); they could not use their results to explain the reason why London's model under-predicted the STL since they were not able to predict the normal mass air mass resonance frequency with their model. Instead, their first resonance occurred at the point where the first cavity resonance (i.e $n_x = 1$) combined with the normal mass air mass resonance frequency. Despite this fact, even though the technique presented here is different from Prasetiyo and Thompson's (2012), the results obtained from both models indicate that the lateral cavity modes do have a significant impact on the prediction results obtained for the STL through double leaf wall systems. Consequently, understanding the impact of the forced and reflected forced waves within the cavity is crucial for the development of accurate prediction models.

5.3 Summary and conclusions

In this chapter, it was shown that it is possible to determine the STL through both the infinite and finite double leaf wall system by studying the propagation of the forced and reflected forced waves. The infinite model's prediction compared well with London's model, while the behaviour of the mass air mass resonance frequency within the finite model gave insight as to why London's model under-predicts the STL. From this investigation the influence of the radiation efficiency became apparent. Consequently the following conclusions can be drawn:

- The sound transmission of an infinite double leaf wall system is due to the forced excitation

- The interaction between the forced and reflected waves is responsible for the mass air mass resonance frequency being independent of the angle of incidence
- The physical explanation for the reason why London's model under-predicts the STL is due to both the forced waves interaction within the wall cavity and the radiation efficiency of the finite panel.

In this chapter it was assumed that the same radiation efficiency could be used for both the forced and reflected forced waves. This assumption is not entirely valid as the radiation efficiencies of both waves are different since their wavelength and rates of attenuation are not the same. A numerical vibrating strip model for the radiation efficiency for both waves will be developed in the following chapter in-order to improve the accuracy of the model. Furthermore, in order to improve the method of calculating the STL, the sound pressure radiated over angles of radiation instead of an average sound pressure from within the wall cavity as in London's model will be utilized. These improvements will provide additional insight and understanding into the role played by the cavity in the sound transmission through double leaf wall systems.

6 Radiation efficiency

The radiation efficiency of a plate was first calculated by Lord Rayleigh by finding the solution to each normal mode and summing their contributions within the frequency band of interest (Leppington *et al.*, 1982). This method works well in the low frequency range where there are few modes within each frequency band of interest. At higher frequencies, these calculations can become tedious with the higher number of modes. Consequently, Maidanik (1962) utilized the Statistical Energy Analysis (SEA) method in order to find the radiation efficiency/resistance of a panel. Maidaniks's formulation is an extension of Smith's (1962) single mode model and is based on the power flow between linearly coupled systems as described by Lyon (1962). Leppington (1982) re-examined Maidaniks's solution in great detail. Leppington's solution corresponds well to Maidanik's above the coincidence frequency. However below the coincidence region Leppington showed that the $g1$ term in Madanik's formulation is negligible and does not appear to be correct. Leppington also showed that near to coincidence Maidanik overestimated the radiation resistance by a factor of 2.

It must be noted that Leppington (1982), Maidanik (1962) and Smith's (1962) formulations are all for the free bending waves on the plate; below the critical frequency these waves are inefficient radiators. However, the forced bending waves are efficient radiators in this frequency range and as a result should be used in the prediction of the STL.

Beranek (1971) showed that the radiation efficiency of the forced bending waves on an infinite plate is $1/\cos(\theta)$: While according to Davy (2009b), Sato developed the radiation efficiency of a forced wave on a square panel for the case where the panel wavelength is longer than the wavelength of sound in air. Rindel (1975) utilized Sato's (1973) work as the fundamental basis of his thesis and commented on the fact that Sato didn't make the link between the radiation resistance and radiation efficiency so Sato thought that his expression was not valid in the case of grazing incidence.

In this chapter a two-dimensional vibrating strip model is derived for the radiation efficiency of the forced bending waves: A correction to Davy's (2009b) analytical radiation efficiency model to account for radiation into a two-dimensional space is also given.

6.1 Approximation for the radiation efficiency of the forced wave

The approximation for the radiation efficiency of the forced bending wave will be derived within this section. This derivation will be based on the calculation of the radiated power in the far field and the velocity of the vibrating panel. Assuming that the wall panel can be modelled as a thin infinite vibrating strip within an infinite baffle, the radiated sound pressure at a distance (r) in the far field can be obtained.

The derived theory is based on the assumption that any spatially continuous vibrating surface may be represented acoustically by an array of elementary volumetric sources of appropriate amplitude and phase (Fahy, 1995). As a result, in the context of the current investigation it can be assumed that the wall panel is composed of an array of point monopole sources having sources and strengths in phase corresponding to a sinusoidal distribution in one direction.

Davy (2004; 2009b) utilized the radiation from discrete sound sources in a line in order to determine the radiation from a continuous line source while deriving his analytical vibrating strip model for the radiation efficiency. The approach used here begins by utilizing Davy's approach of considering discrete sound sources, however instead of finding an analytical approximation, the solution for the radiated power of the vibrating strip is found while deriving the two dimensional model for the radiation efficiency. This approach is also different from Ljunggren's (1991) two-dimensional model which utilized Green's function in order to determine the response of the plate and from the three-dimensional models developed by authors such as Sato (1973) and Sewell (1970) for the radiation efficiency of the forced wave.

Consider the model of a vibrating strip placed within an infinite baffle as shown in Figure 22. The radiated sound power subtended over angles of radiation (φ) between $\pi/2$ and $-\pi/2$ is required in order to determine the forced radiation efficiency. The radiation efficiency is defined as the ratio of the average acoustic power radiated per unit area of a vibrating surface to the average acoustic power radiated per unit area of a piston vibrating with the same average mean square velocity (Fahy, 1995). The magnitude of the average mean square velocity is equivalent to the rms velocity. Since rms values will be used within all of the proceeding equations and measurements are usually conducted with rms values, the radiation efficiency will be defined in terms of its rms equivalent such that

$$\sigma = \frac{W_{rad}}{\rho c S |v_n|^2} \qquad \textbf{6-1}$$

where W_{rad} is the radiated sound power, S is the area of unit length of the strip and v_n is the normal velocity.

The radiated sound power can be determined from the radiated sound pressure for an observer at a distance (r) away from the vibrating strip. The distance (r) is considered to be much greater than the distance (x) between the two discrete sound sources on the wall panel modelled as a vibrating strip shown in Figure 22; while the distance (R) is the distance from the centre of the strip to an observer in the far field.

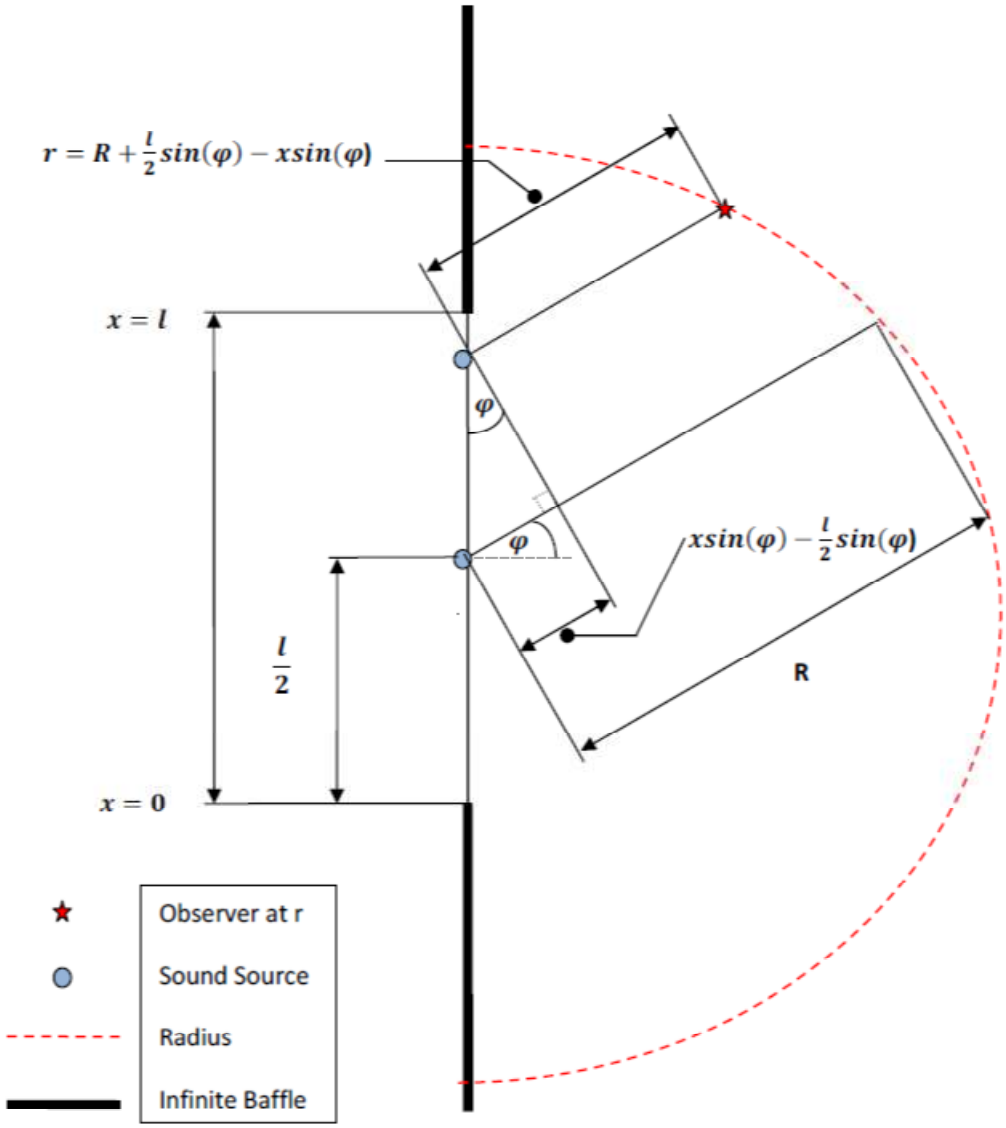

Figure 22 Two discrete sound sources on a vibrating strip in an infinite baffle

The **radiated sound pressure** from the strip can be found as follows.

For small values of kl (i.e. the wave number of sound in air k multiplied by the length of the strip, l) the directivity of a vibrating strip is almost omni-directional. As a result, the radiated sound pressure is approximately equal to the radiated sound pressure of a zero order cylindrical source of the same strength (Jacobsen and Juhl, 2010). Jacobsen showed that the radiated sound pressure from a zero order cylindrical source at a distance (r) corresponds to

$$p(r,t) = A_0 H_0^2(kr) e^{j\omega t}, \qquad 6\text{-}2$$

where A_0 is the amplitude of the pressure wave, H_0^2 is the zero order Hankel function of the second kind and k is the wave number of sound in air. In order to determine radiated pressure in the far field expressions for both $H_0^2(kr)$ and A_0 are needed.

The Hankel function of the second kind for asymptotic expansion of large arguments (i.e. in the far field) is given by formula 9.2.4 in page 364 of Abramowitz and Stegun (1965)

$$\lim_{z\to\infty} H_v^2(z) \sim \sqrt{\frac{2}{\pi z}} e^{-j\left(z - v\frac{\pi}{2} - \frac{\pi}{4}\right)}, \qquad 6\text{-}3$$

where v is the order of the Hankel function and z is the argument which is equal to kr as r goes to infinity (i.e. corresponding to the far field). Consequently the zero order Hankel function of the second kind in the far field is

$$H_0^2(kr) = \sqrt{\frac{2}{\pi kr}} e^{-j\left(kr - \frac{\pi}{4}\right)}. \qquad 6\text{-}4$$

With regards to the amplitude A_0 in Equation 6-2, if it is assumed that the radial velocity (U_0) of the zero ordered cylindrical source at the surface is $U_0 e^{j\omega t}$, Jacobsen (2010) showed that

$$A_0 = \frac{U_0 j \rho_0 c}{H_1^2(kl)}, \qquad 6\text{-}5$$

where H_1^2 is the first order Hankel function of the second kind. For the low frequency range (i.e. when kl is small) the first order Hankel function of the second kind is given by formula 9.1.9 in page 360 of Abramowitz and Stegun (1965)

$$Y_v(z) \sim -iH_v^1(z) \sim iH_v^2(z) \sim \frac{1}{\pi}\Gamma(v)\left(\frac{1}{2}z\right)^{-v}, \qquad 6\text{-}6$$

where Y_z is the Bessel function of the second kind, $\Gamma(v)$ is the gamma function and v is the order of either the Hankel or Bessel function.

According to Table 6.1 on page 267 of Abramowitz and Stegun (1965), the gamma function $\Gamma(1)$ =1. As a result the first order Hankel function of the second kind for small arguments is

$$\lim_{kl\to 0} H_1^2(kl) = \frac{2j}{\pi kl}. \qquad \textbf{6-7}$$

Substituting Equation 6-7 into Equation 6-5 gives

$$A_0 = \frac{U_0 \rho c\, \pi kl}{2}. \qquad \textbf{6-8}$$

Consequently the sound pressure at a distance (r) away from the surface of the vibrating strip can be found by substituting Equations 6-4 and 6-8 into Equation 6-2 such that

$$p(r,t) = \frac{U_0 \rho c\, \pi kl}{2}\sqrt{\frac{2}{\pi kr}}\, e^{j\left(\omega t - kr + \frac{\pi}{4}\right)}. \qquad \textbf{6-9}$$

The volume velocity q_0 of a cylinder per unit length is equal to $2\pi l U_0$. Since the radiation into the half space is of interest, $q_0 = \pi l U_0$. Substituting the half space volume velocity into Equation 6-9 gives

$$p(r,t) = \frac{q_0 \rho c\, k}{2}\sqrt{\frac{2}{\pi kr}}\, e^{j\left(\omega t - kr + \frac{\pi}{4}\right)}. \qquad \textbf{6-10}$$

Fahy (1985) stated that it can be assumed that the sound field produced by a small volume velocity source is independent of the detailed form of distribution of velocity over the source surface. The normal volume velocity and normal velocities (v_n) are related by

$$q_0 = v_n \delta S. \qquad \textbf{6-11}$$

For an element δx of the infinitely long narrow vibrating strip, $q_0 = v_n \delta x$. Therefore Equation 6-10 can be re-arranged to give

$$p(x,r,t) = \rho c \sqrt{\frac{k}{2\pi r}} e^{j\left(\omega t - kr + \frac{\pi}{4}\right)} v_n \delta x. \qquad \textbf{6-12}$$

From Figure 22 if the observer is at a distance $r = R + \frac{l}{2}\sin(\varphi) - x sin(\varphi)$, Equation 6-12 can be written as

$$p(x,\varphi,t) = \rho c \sqrt{\frac{k}{2\pi\left(R + \frac{l}{2}\sin(\varphi) - x sin(\varphi)\right)}} e^{j\left(\omega t - k\left(R + \frac{l}{2}\sin(\varphi) - x sin(\varphi)\right) + \frac{\pi}{4}\right)} v_n \delta x. \qquad \textbf{6-13}$$

Assuming that the distance from the centre of the cylinder/strip (R) is significantly greater than $\frac{l}{2} sin(\varphi) - x sin(\varphi)$ it can be assumed that $\sqrt{R + \frac{l}{2}\sin(\varphi) - x sin(\varphi)} = \sqrt{R}$. Consequently Equation 6-12 can be written as

$$p(x,\varphi,t) = \rho c \sqrt{\frac{k}{2\pi R}} e^{j\left(\omega t - k\left(R + \frac{l}{2}\sin(\varphi) - x sin(\varphi)\right) + \frac{\pi}{4}\right)} v_n \delta x. \qquad \textbf{6-14}$$

The sound pressure radiated from the finite strip can be found by integrating over the length of the strip such that

$$p(x,\varphi,t) = \rho c \sqrt{\frac{k}{2\pi R}} \int_0^l e^{j\left(\omega t - k\left(R + \frac{l}{2}\sin(\varphi) - x sin(\varphi)\right) + \frac{\pi}{4}\right)} v_n dx\,. \qquad \textbf{6-15}$$

For the forced wave

$$v_n = v_{forced} e^{j k_b x}, \qquad \textbf{6-16}$$

where v_{forced} is the amplitude of the normal velocity of the forced wave and $k_b = k sin(\theta)$ is the wave number of the forced bending wave on the strip. Consequently the radiated sound

pressure due to the forced bending wave can be found by substituting Equation 6-16 into Equation 6-15 such that

$$p_{forced}(x,\varphi,\theta,t) = \rho c \sqrt{\frac{k}{2\pi R}}\, e^{j\left(\omega t - k\left(R+\frac{l}{2}\sin(\varphi)\right)+\frac{\pi}{4}\right)} v_{forced} \int_0^l e^{jx(ksin(\varphi)+k_b)}\, dx. \qquad \textbf{6-17}$$

Solving the integral in Equation 6-17 gives

$$p_{forced}(\varphi,\theta,t) = \rho c \sqrt{\frac{k}{2\pi R}}\, e^{j\left(\omega t - k\left(R+\frac{l}{2}\sin(\varphi)\right)+\frac{\pi}{4}\right)} v_{forced} \left[\frac{(e^{jl(ksin(\varphi)+k_b)}-1}{j(ksin(\varphi)+k_b)}\right]. \qquad \textbf{6-18}$$

Jacobsen and Juhl (2010) showed that in the far field both the sound pressure and particle velocity are in phase. As a result the radiated sound power per unit length over angles of radiation is

$$W_{rad} = R\int_{-\frac{\pi}{2}}^{\frac{\pi}{2}} I d\varphi = R\int_{-\frac{\pi}{2}}^{\frac{\pi}{2}} \frac{|p|^2}{\rho c} d\varphi\,. \qquad \textbf{6-19}$$

The pressure modulus of Equation 6-18 can be written as

$$|p(\varphi,\theta)| = \rho c \sqrt{\frac{k}{2\pi R}}\, v_{forced} \frac{\left|e^{(il(ksin(\varphi)+k_b)}-1\right|}{|i(ksin(\varphi)+k_b)|}. \qquad \textbf{6-20}$$

Utilizing Euler's formula the corresponding pressure modulus squared is

$$|p(\varphi,\theta)|^2 = \rho^2 c^2 \frac{k}{\pi R} v_{forced}^2 \frac{1-\cos\left(l(ksin(\varphi)+k_b)\right)}{(ksin(\varphi)+k_b)^2}. \qquad \textbf{6-21}$$

Substituting the pressure magnitude squared from Equation 6-21 into Equation 6-19 gives the radiated power per unit length due to the forced wave as

$$W_{rad,forced}(\varphi,\theta) = \rho c \frac{k}{\pi} v_{forced}^2 \int_{-\frac{\pi}{2}}^{\frac{\pi}{2}} \frac{1-\cos\left(l(ksin(\varphi)+k_b)\right)}{(ksin(\varphi)+k_b)^2} d\varphi. \quad \text{6-22}$$

The radiated sound power per unit length of the forced wave shown in Equation 6-22 was obtained by integrating over the length of the strip from 0 to l (see Equation 6-17). This integration from 0 to l was done in accordance with the boundary conditions established in Section 4.3 while deriving the k_1 and k_2 terms in Equation 4-40 and Equation 4-41 respectively. As a result the same co-ordinate system is required to be maintained. Integrating from 0 to l means that the integration is conducted asymmetrically to the $x = 0$ co-ordinate line. However in the literature this integration has mostly been performed symmetric to the $x = 0$ co-ordinate line with the limits of integration being from $l/2$ to $-l/2$ or from l to $-l$ if l is defined as twice the length of the strip (see Figure 23 below). Lyon (1962) and Midanek (1962) used configuration B when integrating over the lengths of their panels, while Swell (1970), Sato (1973), Ljunggren (1991) and Davy (2009b) all used configuration C shown in Figure 23.

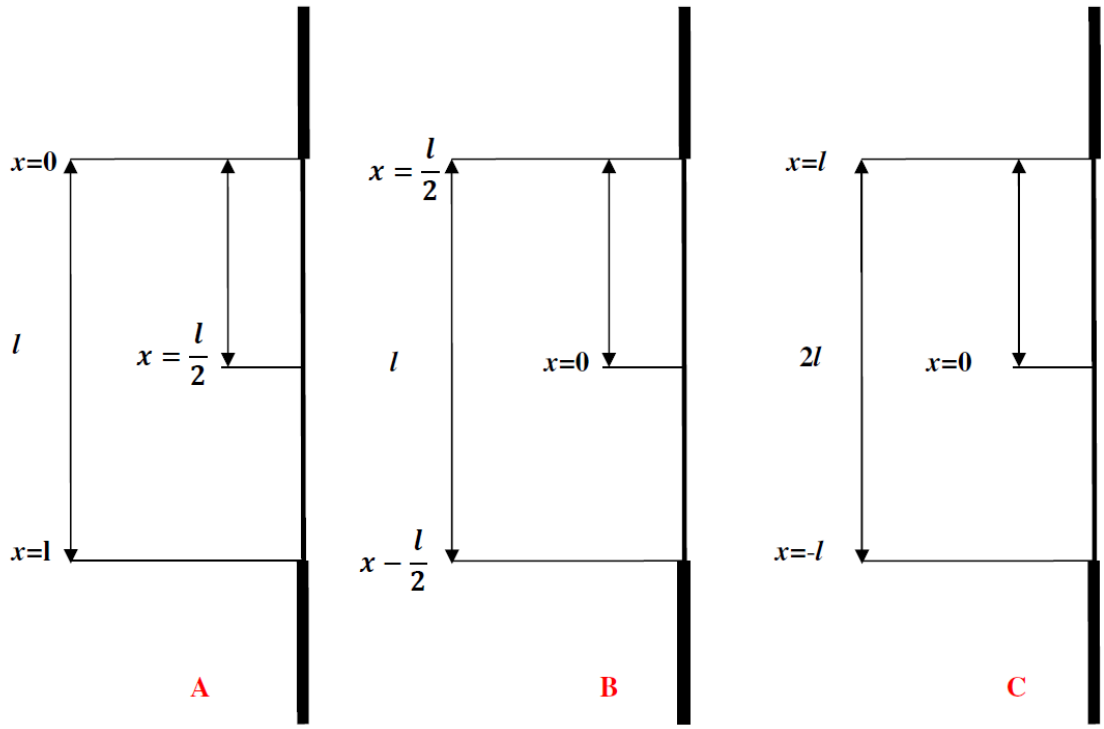

Figure 23 Asymmetric (A) and symmetric (B and C) configurations used in determining the radiated power over the length of a vibrating strip or wall panel

The integration in Equation 6-22 can be written in terms of the sine function. Gradshteyn and Ryzhik (1980) on Page 25 Section 1.317 showed the following half angle relationship

$$\sin\left(\frac{x}{2}\right) = \pm\sqrt{\frac{1}{2}(1-\cos(x))}. \qquad 6\text{-}23$$

Applying this half angle relationship to Equation 6-22 gives

$$W_{rad,forced}(\varphi,\theta) = \rho c \frac{k}{\pi} v_{forced}^2 \int_{-\frac{\pi}{2}}^{\frac{\pi}{2}} \frac{2\sin^2\left(\frac{l}{2}(ksin(\varphi)+k_b)\right)}{(ksin(\varphi)+k_b)^2} d\varphi. \qquad 6\text{-}24$$

This expression for the radiated power per unit length due to the forced wave can be used for the radiation efficiency of the strip. Assuming that the area (S) of unit length of the infinite strip is l and substituting the Equation 6-24 into Equation 6-1, gives the radiation efficiency of the forced wave as

$$\sigma_{forced}(\varphi,\theta) = \frac{k}{\pi l}\frac{(v_{forced}^2)}{|v_n|^2} \int_{-\frac{\pi}{2}}^{\frac{\pi}{2}} \frac{2\sin^2(\frac{l}{2}(ksin(\varphi)+k_b))}{(ksin(\varphi)+k_b)^2} d\varphi. \qquad 6\text{-}25$$

The normal velocity due to the forced wave (v_n) was defined in Equation 6-16, the magnitude of which is

$$|v_n| = v_{forced}. \qquad 6\text{-}26$$

Also, since $k_b = ksin(\theta)$ Equation 6-25 can be written as

$$\sigma_{forced}(\varphi,\theta) = \frac{k}{\pi l}\int_{-\frac{\pi}{2}}^{\frac{\pi}{2}} \frac{2\sin^2(\frac{kl}{2}(sin(\varphi)+\sin(\theta)))}{k^2(sin(\varphi)+\sin(\theta))^2} d\varphi. \qquad 6\text{-}27$$

The integration in Equation 6-27 cannot be solved analytically, as a result in order to foster the required numerical integration, this equation will be written in terms of the sinc function. Spanier (1987) defined the sinc function as

$$sinc(x) = \frac{\sin(x)}{x}. \qquad \textbf{6-28}$$

The properties, use and implementation of the sinc function within the developed model are discussed within Chapter 8.

Equation 6-27 can be simplified multiplying it by $\frac{l^2}{2}/(\frac{l^2}{2})$ to give

$$\sigma_{forced}(\varphi,\theta) = \frac{kl}{\pi}\int_{-\frac{\pi}{2}}^{\frac{\pi}{2}} \frac{\sin^2(\frac{kl}{2}(sin(\varphi)+\sin(\theta)))}{\frac{(kl)^2}{2}(sin(\varphi)+\sin(\theta))^2} d\varphi. \qquad \textbf{6-29}$$

As a result Equation 6-29 can be written in terms of the sinc function as

$$\sigma_{forced}(\varphi,\theta) = \frac{kl}{2\pi}\int_{-\frac{\pi}{2}}^{\frac{\pi}{2}} sinc^2\left(\frac{kl}{2}(\sin(\varphi)+\sin(\theta))\right) d\varphi. \qquad \textbf{6-30}$$

The forced radiation efficiency (in dB) while utilizing the two-dimensional vibrating strip model can be seen in Figure 24. The results shown are similar to that obtained by both Davy (2009b) and Sato (1973) with the corresponding finite radiation efficiency at grazing incidence (i.e. 90°) being observed. This finite radiation efficiency at grazing incidence is responsible for ensuring the STL does not go to zero at this angle of incidence for finite wall systems.

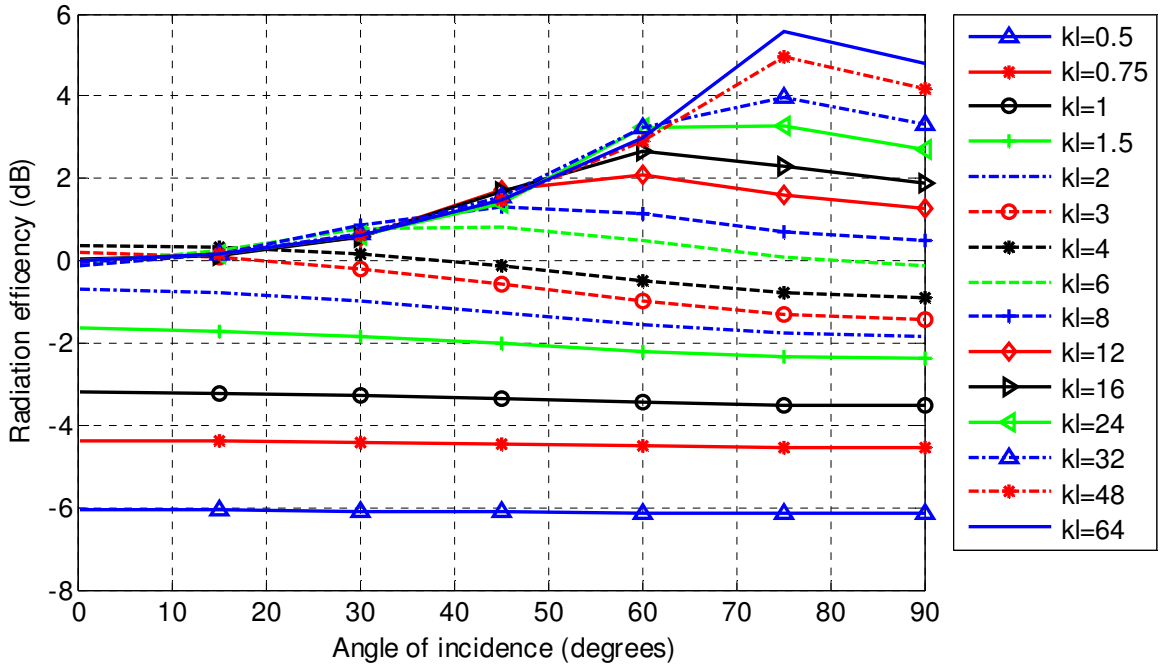

Figure 24 Forced radiation efficiency of a 2.44 m vibrating strip

In order to verify the results shown in Figure 24, these results were compared to the Davy's (2009b) forced radiation efficiency model. This comparison shown in Table 7 shows the discrepancies between the derived theory and Davy's in the low frequency region; with the highest discrepancy of 2.55 dB being highlighted in red. Close inspection of Davy's (2009b) model shows that although it was developed as a two-dimensional model, Davy considered the sound radiation of a vibrating hemisphere into a three-dimensional space. Accounting for sound radiation into a three-dimensional space would explain the discrepancies in the results shown in Table 7.

Ljunggren (1991) obtained similar discrepancies when he compared his two-dimensional model to Sato's (1973) three-dimensional model and stated that the difference obtained was due to the difference in the dimensions of both models. Ljunggren showed that for *kl* equal to 8 and 64 the difference between Sato's and his theory was within 0.5 dB, but stated that larger discrepancies can be expected for smaller *kl* numbers. In the situation when diffuse incidence was considered, Ljunngren found that the difference between his two-dimensional theory and both Sato's and Sewell was within 0.5 dB. Consequently, based on the similarities obtained between the two and three-dimensional radiation efficiency, there is a strong argument which supports the use of the two dimensional model.

Table 7 The differences (dB) between the proposed theory and Davy's radiation efficiency

Difference							
Angle of incidence	**0°**	**15°**	**30°**	**45°**	**60°**	**75°**	**90°**
kl							
0.5	1.97	1.98	2.00	2.06	2.16	2.33	2.55
0.75	0.36	0.38	0.45	0.60	0.84	1.16	1.54
1	-0.49	-0.45	-0.32	-0.10	0.23	0.64	1.11
1.5	-0.79	-0.75	-0.62	-0.42	-0.13	0.24	0.69
2	-0.40	-0.40	-0.39	-0.34	-0.24	-0.03	0.31
3	0.27	0.02	-0.27	-0.44	-0.57	-0.58	-0.39
4	0.40	0.21	-0.42	-0.80	-0.86	-0.83	-0.62
6	-0.07	0.12	0.15	-0.66	-0.97	-1.01	-0.81
8	-0.10	0.01	0.24	-0.19	-1.10	-1.11	-0.92
12	-0.01	0.01	-0.04	0.24	-0.92	-1.23	-1.07
16	0.05	-0.01	-0.06	0.17	-0.33	-1.28	-1.15
24	0.01	0.01	0.00	-0.11	0.21	-1.31	-1.22
32	-0.02	0.01	0.03	0.05	0.24	-1.34	-1.27
48	0.01	0.01	0.01	-0.04	-0.10	-0.92	-1.32
64	-0.01	0.01	-0.01	-0.02	-0.02	-0.31	-1.35

6.2 Analytical approximation for the radiation efficiency of the forced waves

Davy (2009b) developed an analytical two-dimensional strip model for the forced radiation efficiency which produced results which were similar to Sato's (1973) three-dimensional numerical model. Although Davy's model is a two-dimensional model, it accounts for radiation into a three-dimensional space at low frequencies. In this section Davy's model is modified to account for sound radiation into a two-dimensional space, as it is believed that such a modification would be useful when applied to the transmission of sound which is often modelled as a two-dimensional problem. All of the symbols used within this section correspond to those used within Davy's (2009b) paper.

Davy's (2009b) model can be summarized by the following equations

$$\sigma(g) = \begin{cases} \dfrac{1}{\sqrt[n]{g^n + q^n}} & if\ 1 \geq |g| \geq f \\ \dfrac{1}{\sqrt[n]{[h - \alpha g]^n + q^n}} & if\ f > |g| \geq 0 \end{cases} \qquad \text{6-31}$$

where σ is the radiation efficiency, n is an empirical constant, and f, g, h, q and α are defined by the following equations

$$g = \cos(\theta) \geq f = \begin{cases} wg_l = w\sqrt{\dfrac{\pi}{2ka}} & if\ wg_l \leq 1 \\ 1 & if\ wg_l > 1 \end{cases} \qquad \textbf{6-32}$$

where, θ is the angle of incidence, w is an empirical correction factor, k is the wave number.

$$h = \frac{1}{\frac{2}{3g_l} - \beta} = \frac{1}{\frac{2}{3}\sqrt{\frac{2ka}{\pi}} - \beta} \qquad \textbf{6-33}$$

where β is an empirical factor needed because the developed theory was developed for an infinite strip but applied to a square panel, while

$$\alpha = \frac{h}{f} - 1. \qquad \textbf{6-34}$$

The parameter q in Equation 6-31 is the inverse radiation efficiency of a finite panel at low frequencies. Davy determined this parameter from the real part of the fluid wave impedance (Z_{wf}) of a pulsating hemisphere such that

$$\sigma = \frac{Re(Z_{wf})}{\rho_o c} = k^2 r^2 = \frac{k^2 S}{2\pi} = \frac{1}{q} = \frac{2k^2 a^2}{\pi}, \qquad \textbf{6-35}$$

where r is the radius of the hemisphere and S is the area of the panel (such that the results obtained for a pulsating hemisphere also applies to a panel set in an infinite rigid baffle provided that the area of the panel is equal to the surface area of the hemisphere i.e. $2\pi r^2 = S$, Davy (2009b)). For a square panel of side length 2a (see configuration C in Figure 23) the area of the panel is $S = 4a^2$. The use of the fluid wave impedance of a pulsating hemisphere

implies that the radiation into a three-dimensional space is being taken into account. As a result Davy's analytical model is actually a two dimensional model which considers the radiation into a three dimensional space. To account for radiation into a two dimensional space the fluid wave impedance of a vibrating strip (i.e. a cylinder) must be considered.

Jacobsen (2010) showed that the radiation impedance of a small cylinder at low frequencies is

$$Z_{cylinder} = \rho_o c \left[\frac{\pi}{2} kr - jkrln(kr)\right]. \quad \textbf{6-36}$$

While the surface area of a cylinder is

$$S_{cylinder} = 2\pi r^2 + 2\pi rh, \quad \textbf{6-37}$$

where h is the height of the cylinder or the length of the vibrating strip (l). Assuming that $r \ll h$, the surface area of the cylinder is approximately equal to that of the vibrating strip such that

$$S_{cylinder} \cong S_{strip} = 2\pi rl. \quad \textbf{6-38}$$

Substituting r from Equation 6-38 into the real part of Equation 6-36 and equating the length of the half circle to the length of the strip of length 2a, the radiation efficiency for the finite strip at low frequencies can be found from

$$\sigma_{strip} = \frac{Re(Z_{cylinder})}{\rho_o c} = \frac{\pi kr}{2} = ka = \frac{1}{q_{strip}} \quad \textbf{6-39}$$

Consequently

$$q_{strip} = \frac{1}{ka}. \quad \textbf{6-40}$$

With regard to the empirical constants β and n, Davy (2009b) used $\beta = 0.124$ and $n = 2$ which were determined by comparison with Sato's numerical prediction. Similarly, by comparison with the developed two-dimensional model in Section 6.2, $\beta = 0$ and $n = 3$ are utilized. The results obtained by implementing these changes to the empirical constants as well as accounting for the wave impedance of the vibrating strip can be seen in Figure 25.

The results shown in Figure 25 were similar to those obtained in Figure 24, the comparison of which is shown in Table 8. The results shown in Table 8 indicate that the modified version of Davy's model and the developed numerical predictions were within 0.58 dB, which is of the same order of magnitude as Davy obtained when he compared his model to Sato's. In order to further verify the modifications made to Davy's model, a comparison was made between Davy's original model and the modified version for the diffuse field forced radiation efficiency. The modified version of this radiation efficiency can be found from

$$\sigma_{diffuse} = ln\left(\frac{1+\sqrt{1+{q_{strip}}^2}}{f+\sqrt{f^2+{q_{strip}}^2}}\right)+\frac{1}{\alpha}ln\left(\frac{h+\sqrt{h^2+{q_{strip}}^2}}{f+\sqrt{f^2+{q_{strip}}^2}}\right), \qquad \text{6-41}$$

where, f, q_{strip}, h and α were defined above. The results from this comparison can be seen in Figure 26 and shows that the modified version was within 0.5 dB of the original. A result which is similar to that obtained by Ljunggren (1991) when he compared his two-dimensional model to Sewell's (1970) three-dimensional model for diffuse incidence.

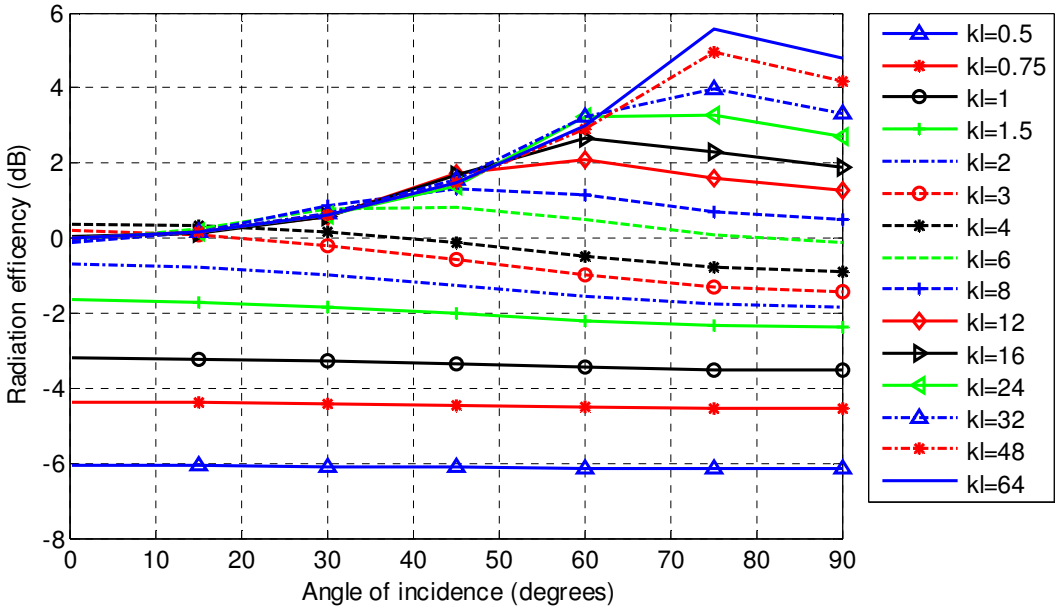

Figure 25 Modified version of Davy's analytical radiation efficiency for a 2.44 m vibrating strip

Table 8 The differences between the numerical two-dimensional radiation efficiency and the modifications to Davy's radiation efficiency

	Difference						
Angle of incidence	**0°**	**15°**	**30°**	**45°**	**60°**	**75°**	**90°**
kl							
0.5	-0.02	-0.03	-0.04	-0.06	-0.07	-0.07	-0.06
0.75	-0.03	-0.04	-0.06	-0.09	-0.11	-0.10	-0.06
1	-0.01	-0.02	-0.06	-0.10	-0.12	-0.10	-0.01
1.5	0.11	0.08	0.02	-0.05	-0.07	-0.01	0.16
2	0.29	0.26	0.16	0.06	0.02	0.08	0.30
3	0.58	0.53	0.41	0.27	0.18	0.23	0.47
4	0.55	0.55	0.52	0.42	0.29	0.25	0.40
6	-0.02	0.18	0.22	0.32	0.27	0.16	0.29
8	-0.08	0.04	0.27	-0.03	0.16	0.09	0.24
12	0.00	0.02	-0.03	0.26	0.01	0.01	0.15
16	0.05	-0.01	-0.06	0.18	-0.20	-0.03	0.10
24	0.01	0.01	0.00	-0.11	0.21	-0.06	0.07
32	-0.02	0.01	0.03	0.05	0.24	-0.09	0.05
48	0.01	0.01	0.01	-0.04	-0.10	-0.20	0.04
64	-0.01	0.01	-0.01	-0.02	-0.02	-0.31	0.03

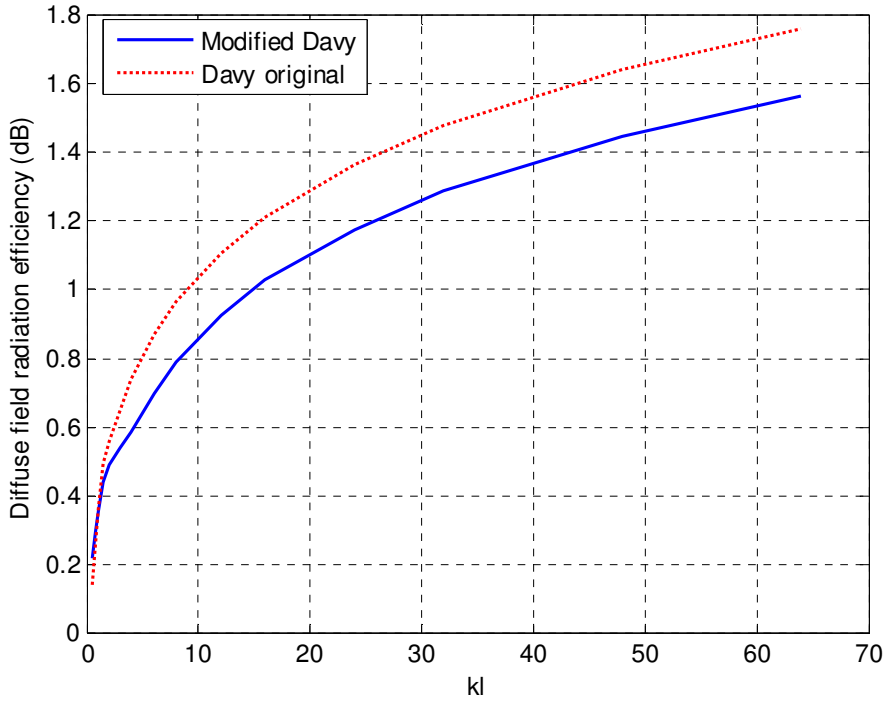

Figure 26 Comparison between Davy's original model and the modified version for diffuse field incidence

6.3 Radiation efficiency of the reflected waves

The efficiency of the forced wave was derived in the previous section. The forced wave which is radiated into the wall cavity would produce reflected waves with different wavelengths and rate of attenuation. As a result the radiation efficiency of the reflected waves will be different from that of the forced wave. Consequently, in this section an iterative numerical approximation is derived for the radiation efficiency of the reflected waves within the wall cavity. An iterative approach is needed because the radiation efficiency of the reflected waves is dependent on its rate of attenuation ($Re(\gamma)$), which is dependent on the impedance of the wall panels, depth and airflow resistivity of the wall cavity (see Equation 4-29). The wall panel impedance (see Equation 4-1) is dependent on the fluid loading effect which is determined by the radiation efficiency of the reflected waves. Therefore, in order to determine the radiation efficiency of these waves, initial approximations must be made for both γ and their radiation efficiencies. A flow chart which summaries the steps taken within the iterative model is shown in Figure 28 after all the required equations are derived.

The radiated sound pressure in the far field due to the reflected waves within the wall cavity exciting the wall panels can be solved by substituting the normal velocity due to the reflected waves into Equation 6-15. The normal velocity due to the reflected waves is

$$v_{n,\pm} = v_{o\pm} e^{\pm \gamma x}\,, \tag{6-42}$$

where the $\pm$ corresponds to the signs used for γ shown in Equation 4-38 and $v_{o\pm}$ is the amplitude of the two reflected waves.

Substituting Equation 6-42 into Equation 6-15 gives

$$p_{\gamma\pm}(x,\varphi,t) = \rho c \sqrt{\frac{k}{2\pi R}}\, e^{j\left(\omega t - k\left(R+\frac{l}{2}\sin(\varphi)\right)+\frac{\pi}{4}\right)} v_{o\pm} \int_0^l e^{jx(k\sin(\varphi))} e^{\pm\gamma x}\, dx. \tag{6-43}$$

For the first approximation of the radiation efficiency due to the reflected waves within the wall cavity, it can be assumed that $\gamma = 0$. Consequently, the radiated sound pressure in the far field when $\gamma = 0$ is

$$p_{\gamma=0}(x,\varphi,t) = \rho c \sqrt{\frac{k}{2\pi R}}\, e^{j\left(\omega t - k\left(R+\frac{l}{2}\sin(\varphi)\right)+\frac{\pi}{4}\right)} v_{o\pm} \int_0^l e^{jx(k\sin(\varphi))}\, \delta x. \tag{6-44}$$

Solving this integral gives

$$p_{\gamma=0}(\varphi,t) = \rho c \sqrt{\frac{k}{2\pi R}}\, e^{j\left(\omega t - k\left(R+\frac{l}{2}\sin(\varphi)\right)+\frac{\pi}{4}\right)} v_{o\pm} \left(\frac{e^{jkl\sin\varphi}-1}{jk\sin\varphi}\right) \delta\varphi. \tag{6-45}$$

The resulting pressure magnitude squared of Equation 6-45 is

$$\left|p_{\gamma=0}(\varphi)\right|^2 = \rho^2 c^2\, \frac{k}{2\pi R}\, v_{o\pm}^2 \frac{1-\cos\left(kl\sin(\varphi)\right)}{\sin^2\varphi} d\varphi. \tag{6-46}$$

The radiated sound power due to each reflected wave can be found by utilizing Equation 6-19. Substituting Equation 6-46 into Equation 6-19 gives, the radiated sound power for the first approximation when $\gamma = 0$ such that

$$W_{\gamma=0}(\varphi) = \rho c \frac{k}{\pi l} v_{o\pm}^2 \int_{-\frac{\pi}{2}}^{\frac{\pi}{2}} \frac{1 - \cos\left(klsin(\varphi)\right)}{\sin^2 \varphi} d\varphi. \qquad \textbf{6-47}$$

Utilizing the half angle relationship given by Equation 6-23 and $W_{\gamma=0}$ from Equation 6-47 the radiation efficiency for the first approximation can be found

$$\sigma_{\gamma=0}(\varphi) = \frac{k}{\pi l} \int_{-\frac{\pi}{2}}^{\frac{\pi}{2}} \frac{2\sin^2\left(\frac{kl}{2}\sin(\varphi)\right)}{k^2 \sin^2(\varphi)} d\varphi. \qquad \textbf{6-48}$$

Equation 6-48 can be simplified and written in terms of the sinc function by multiplying it by $\frac{l^2}{2}/(\frac{l^2}{2})$ to give

$$\sigma_{\gamma=0}(\varphi) = \frac{kl}{2\pi} \int_{-\frac{\pi}{2}}^{\frac{\pi}{2}} sinc^2\left(\frac{kl}{2}\sin(\varphi)\right) d\varphi. \qquad \textbf{6-49}$$

Equation 6-49 gives the first approximation for the radiation efficiency of the reflected waves under the assumption that $\gamma = 0$. Figure 27 shows the results obtained from this first approximation for a 16mm thick gypsum board double leaf wall system with an empty 90 mm cavity. As expected, these results show that the radiation efficiency of the reflected waves is independent of the angle of incidence.

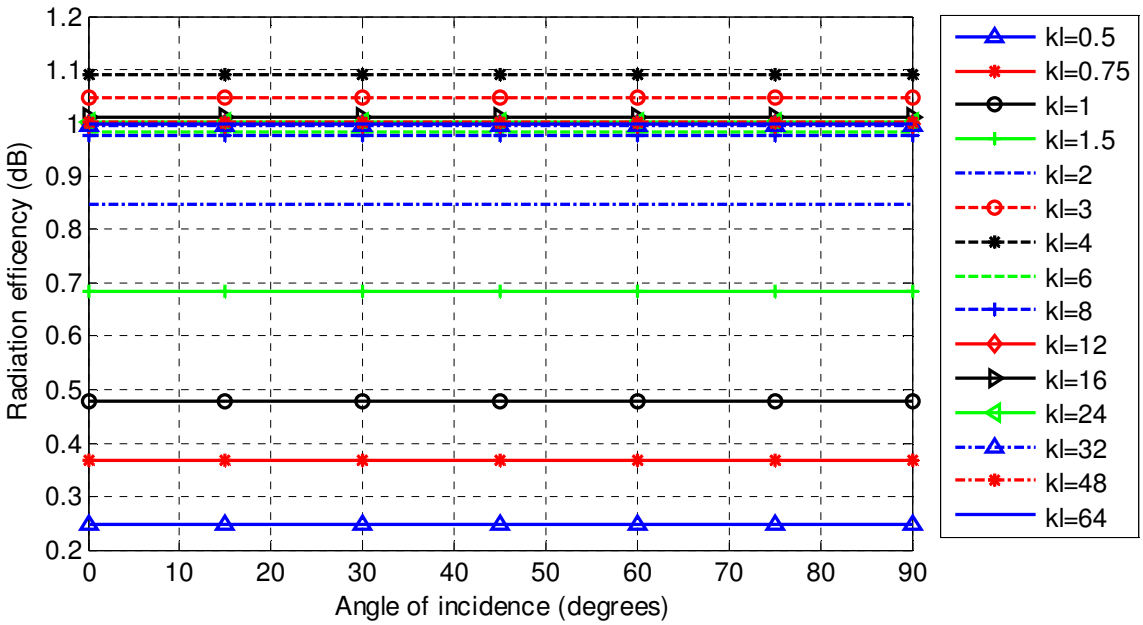

Figure 27 First approximation for radiation efficiency of the reflected waves within a 16 mm double leaf gypsum board wall system with a 90 mm deep cavity

γ can now be determined by substituting this first approximation for the radiation efficiency of the reflected waves into the bending wave impedance of the wall panel (see Equation 4-1).

The radiated sound pressure from the vibrating strip due to the excitation of the wall panel caused by the reflected waves within the wall cavity is given in Equation 6-43. This equation can be factorized and re-written to give

$$p_{\gamma\pm}(x,t,\varphi) = \rho c \sqrt{\frac{k}{2\pi R}}\, e^{j\left(\omega t - k\left(R+\frac{l}{2}\sin(\varphi)\right)+\frac{\pi}{4}\right)} v_{o\pm} \int_0^l e^{jx(k\sin(\varphi)\mp\gamma)}\, dx. \qquad 6\text{-}50$$

The sign change of γ in Equation 6-50 compared to Equation 6-43 due to the factorization should be noted. Solving the integral given in Equation 6-50 gives

$$p_{\gamma\pm}(t,\varphi) = \rho c \sqrt{\frac{k}{2\pi R}}\, e^{j\left(\omega t - k\left(R+\frac{l}{2}\sin(\varphi)\right)+\frac{\pi}{4}\right)} v_{o\pm} \left(\frac{e^{jl(k\sin(\varphi)\mp j\gamma)}-1}{j(k\sin(\varphi)\mp j\gamma)}\right). \qquad 6\text{-}51$$

Utilizing the half angle relationship given by Equation 6-23, the pressure modulus squared of Equation 6-51 becomes

$$\left|p_{\gamma\pm}(\varphi)\right|^2 = \rho^2 c^2 \frac{k}{2\pi R} v_{o\pm}^2 \left(\frac{2\sin^2\left(\frac{l}{2}(ksin(\varphi) \mp j\gamma)\right)}{(ksin(\varphi) \mp j\gamma)^2} \right). \quad \text{6-52}$$

Substituting Equation 6-52 into Equation 6-19 gives the radiated sound power due to the reflected waves within the wall cavity as

$$W_{\gamma\pm}(\varphi) = \rho c \frac{k}{\pi} v_{o\pm}^2 \int_{-\frac{\pi}{2}}^{\frac{\pi}{2}} \left(\frac{2\sin^2\left(\frac{l}{2}(ksin(\varphi) \mp j\gamma)\right)}{(ksin(\varphi) \mp j\gamma)^2} \right) d\varphi. \quad \text{6-53}$$

Substituting the radiated power given by Equation 6-53 into Equation 6-1 gives the radiation efficiency of the reflected waves as

$$\sigma_{\gamma\pm}(\varphi) = \frac{k}{\pi l} \frac{v_{o\pm}^2}{\left|v_{n\pm}^2\right|} \int_{-\frac{\pi}{2}}^{\frac{\pi}{2}} \left(\frac{2\sin^2(\frac{l}{2}(ksin(\varphi) \mp j\gamma)}{(k\,sin\,\varphi \mp j\gamma)^2} \right) d\varphi. \quad \text{6-54}$$

Equation 6-54 can be written in terms of the sinc function by multiplying by $\frac{l^2}{2}/(\frac{l^2}{2})$ to give

$$\sigma_{\gamma\pm}(\varphi) = \frac{kl}{2\pi} \frac{v_{o\pm}^2}{\left|v_{n\pm}^2\right|} \int_{-\frac{\pi}{2}}^{\frac{\pi}{2}} \left(\mathrm{sinc}^2(\frac{l}{2}(ksin(\varphi) \mp j\gamma) \right) d\varphi. \quad \text{6-55}$$

Now since $v_{n\pm} = v_o e^{\pm\gamma x}$ and γ is a complex number, the magnitude of $v_{n\pm}$ can be found from the following

$$\left|v_{n\pm}\right| = v_{o\pm}\left|e^{\pm\gamma x}\right| = v_{o\pm}\left|e^{\pm\gamma_{real} x}\right|\left|e^{\pm\gamma_{imaginary} x}\right| = v_{o\pm}\left|e^{\pm\gamma_{real} x}\right|. \quad \text{6-56}$$

$\left|v_{n\pm}\right|^2$ integrated over the length of the strip can be found from

$$\left|v_{n\pm}\right|^2 = v_{o\pm}^2 \int_0^l \left|e^{\pm 2\gamma_{real} x}\right| = v_{o\pm}^2 \left(\frac{e^{\pm 2\gamma_{real} l} - 1}{2\gamma_{real}} \right). \quad \text{6-57}$$

Substituting Equation 6-57 into Equation 6-55 gives the radiation efficiency due to the excitation of the panel due to the reflected waves within the wall cavity as

$$\sigma_{\gamma\pm}(\varphi) = \frac{kl}{2\pi}\left(\frac{e^{\pm 2\gamma_{real} l} - 1}{2\gamma_{real}}\right)\int_{-\frac{\pi}{2}}^{\frac{\pi}{2}}\left(\mathrm{sinc}^2\left(\frac{l}{2}(ksin(\varphi) \mp j\gamma)\right)\right) d\varphi. \qquad \textbf{6-58}$$

A summary of the steps taken while calculating the radiation efficiency given by Equation 6-58 and the iterative loop used is given in Figure 28 below. In this figure an additional resistance term $r/\rho_o c$ was added to σ_γ within the loop shown. This additional resistance term was included to compensate for the large dip or singularity obtained at the mass air mass resonance frequency while calculating the STL. The effect of the inclusion of this resistance term as well as the number of iterations required for the convergence of the results obtained while implementing the loop shown within Figure 28 is discussed in Chapter 8.

The radiation efficiency given by Equation 6-58 is dependent on the airflow resistivity of any sound absorption material within the cavity, its depth and impedance of the wall panels. Consequently, each of these parameters must be specified when discussing the results obtained for the radiation efficiency of the reflected waves. As a result, in the proceeding discussion the results shown are for a 16 mm double leaf wall system with the airflow resistivity, cavity depth and wall impedance as indicated. The density of each gypsum leaf is taken as 770 kg/m^3, while a length of 3.05 m which represents the largest dimension of the wall panel is utilized as the length of the strip.

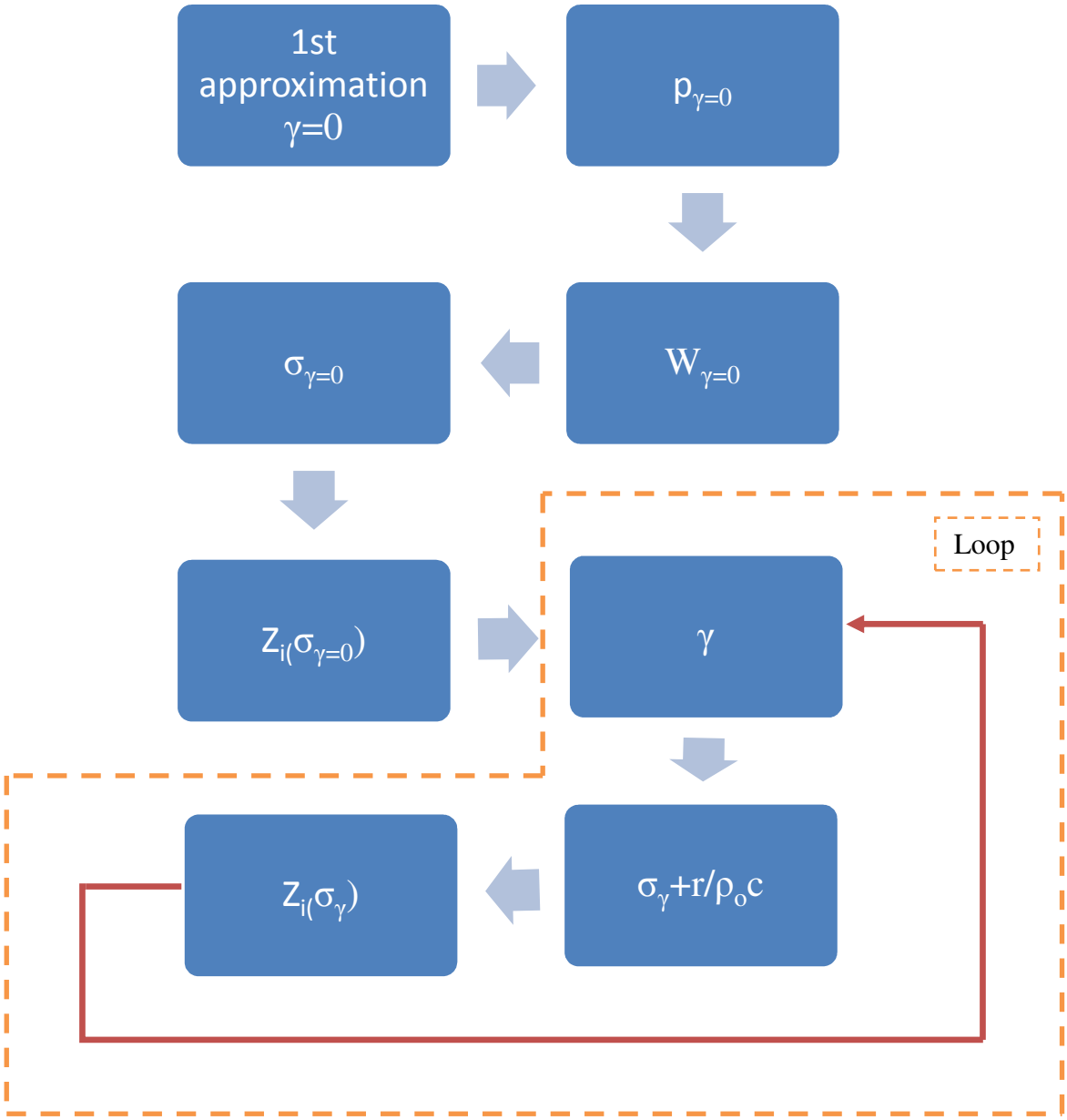

Figure 28 Flow chart outlining how the iterative numerical method is used to determine the radiation efficiency of the reflected waves within the wall cavity

The effect of the airflow resistivity on the radiation efficiency of the reflected waves within a 90 mm deep cavity can be seen in Figure 29. These results indicate that as the airflow resistivity within the wall cavity is increased the radiation efficiency of the reflected waves decreases. Ideally a decrease in the radiation efficiency of the reflected waves will correspond to an increase in the STL only if the initial radiation efficiency of the reflected waves is greater than the radiation efficiency of the forced wave. This can ideally occur because the radiation efficiency of the forced wave is independent of the airflow resistivity of any

material placed within the wall cavity (see Equation 6-30). Consequently, once the radiation due to the forced wave is dominant over the reflected waves no increase in the STL due to increased airflow resistivity within the cavity can ideally occur. Studying the trends associated with the radiation efficiency in this manner may be used to explain some of the experimental trends reported in Chapter 2.

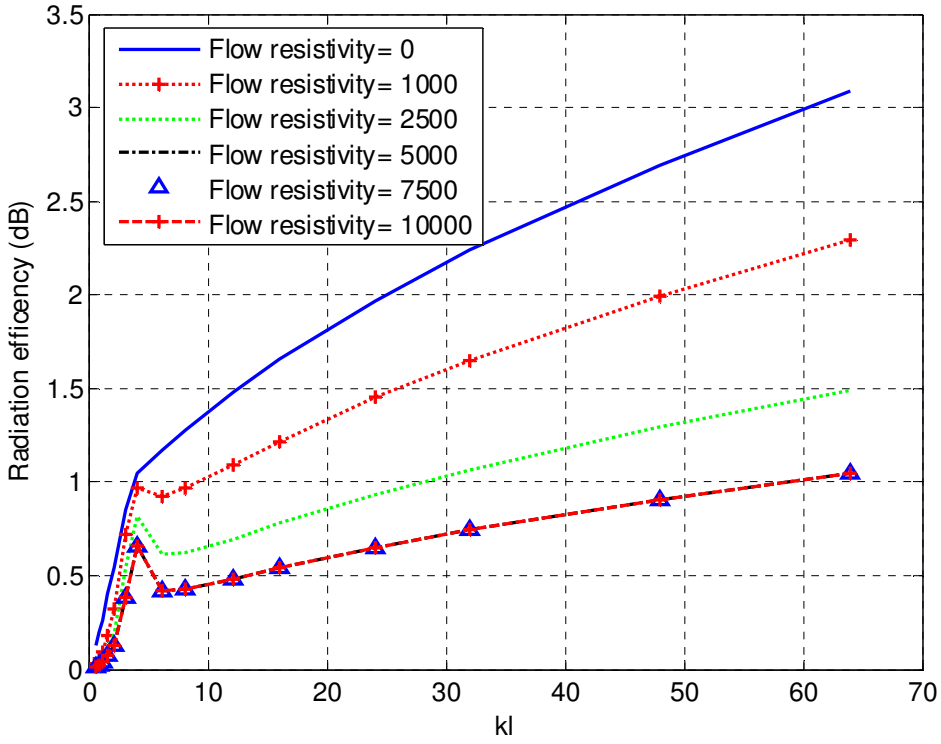

Figure 29 Radiation efficiency of the reflected waves for a 16 mm gypsum double leaf wall system with different airflow resistivity within the cavity

In Chapter 2 it was reported that the airflow resistivity and any associated sound absorption material within the wall cavity had the following influence on the STL:

- The STL increased as the airflow resistivity increased up until an airflow resistivity of approximately 5000 $\mathrm{Ns/m^4}$ was achieved. Little to no improvement occurred in the STL once the airflow resistivity was increased beyond this point
- The first initial amount of sound absorption material had the greatest influence on the STL

These observations could be verified by finding the difference between radiation efficiency of the forced and reflected waves and plotting the regions where the forced waves are dominant as the airflow resistivity is increased. This plot can be seen in Figure 30. In this figure the area in white and red represents the frequencies and angle of incidence where the reflected and forced waves are dominant respectively. Although the results shown cannot give a quantitative estimate of how much improvement will occur it does give a qualitative sense of the frequencies and angles of incidence where improvement can be expected. The quantitative estimate of the wall system is dependent on the normal velocity of the wall panel which is dependent on the amplitudes of the forced and reflected waves as shown in Chapter 7. The amplitude of these waves is dependent on the airflow resistivity within the wall cavity.

The results in Figure 30 show that for the empty cavity situation (i.e. Ξ=0 Ns/m^4) the radiation from the wall system is dominated by the reflected waves for a significant range of frequencies and angles of incidence, the main exception being in the low frequency region below the mass air mass resonance frequency. The dominancy of the forced wave below the mass air mass resonance frequency was expected as the experimental observations reported in Chapter 2 indicated that the wall cavity did not have a major influence on the STL below this frequency. The results in Figure 30 also show that as the airflow resistivity is increased the dominancy of the forced wave increases over the entire range of frequencies and angles of incidence considered. At 5000 Ns/m^4 the radiation from the wall system is almost completely dominated by the forced waves and insignificant improvement in the STL can be expected above this airflow resistivity for this particular wall system, a result which agrees with the reported observation in Chapter 2. Furthermore, the results obtained for an airflow resistivity of 1000 Ns/m^4 explains why the first initial amount of sound absorption material provides the greatest increase or influence on the STL. At 1000 Ns/m^4 a significant region of where the reflected waves are dominant is reduced by this value of airflow resistivity. Therefore as the amount of material or airflow resistivity is increased beyond 1000 Ns/m^4 the region where additional improvement can occur is substantially less; hence the reason why the majority of improvement occurs after the first initial amount of sound absorption material is added to the cavity.

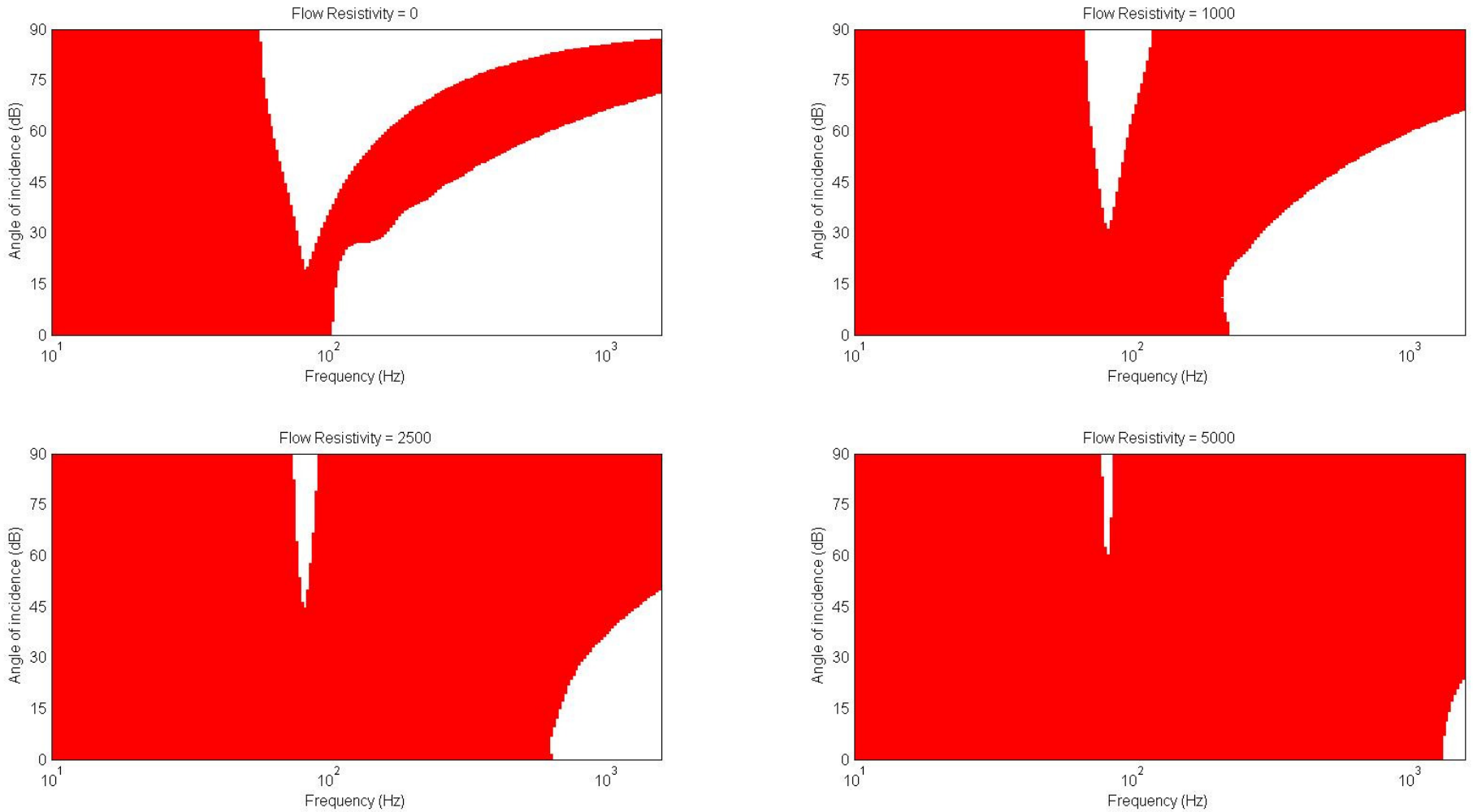

Figure 30 Regions where the radiation efficiency of the forced waves are greater than the reflected waves for different airflow resistivity (Ns/m^4) within the wall cavity

In Chapter 2 it was reported that the STL increased with the depth (d) of the cavity only for the empty cavity. Once sound absorption material was included little to no improvement occurred as the depth was increased. The effect of the depth of the wall cavity on the radiation efficiency of the reflected waves can be seen in Figure 31. This influence of the depth is difficult to see from these results. However, a clearer indication can be seen in the results shown in Figure 32 which relates the regions where the forced and reflected waves are dominant for different depths with no sound absorption material within the wall cavity. In this figure the shift in the mass air mass resonance frequency as well as the increased dominance of the forced wave as the depth of the cavity increased can be seen. The increase in the dominance of the forced wave will translate to an increase in the STL, a result which supports the experimental data. However, for the situation where there is sound absorption material within the cavity (i.e. with $\Xi = 5000$ Ns/m^4) the forced wave is dominant for all the cavity depths shown in Figure 33. This result suggests that little improvement in the STL occurs with increased depth when sound absorption material is included as the region where the reflected waves are dominant remains constant.

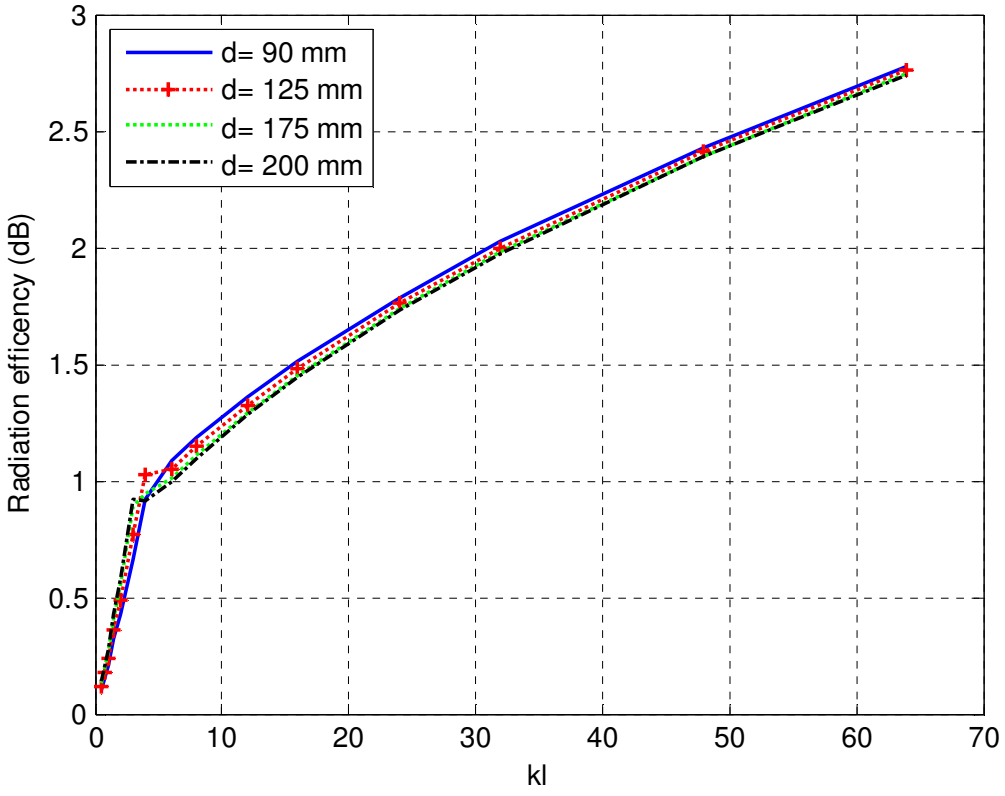

Figure 31 Effect of the depth of the wall cavity on the radiation efficiency of the reflected waves

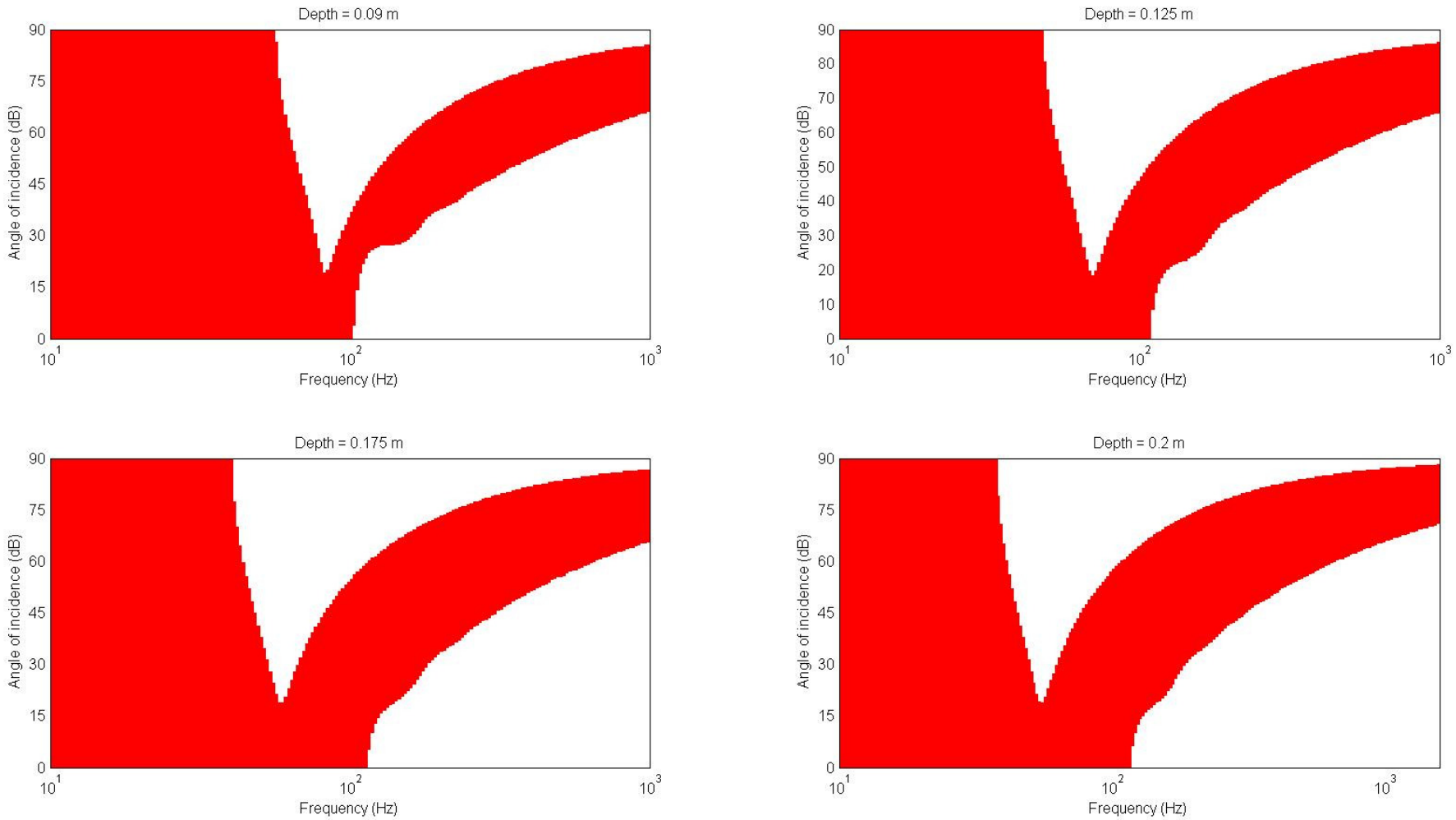

Figure 32 Regions where the radiation efficiency of the forced waves are greater than the reflected waves for different cavity depths within an empty wall cavity

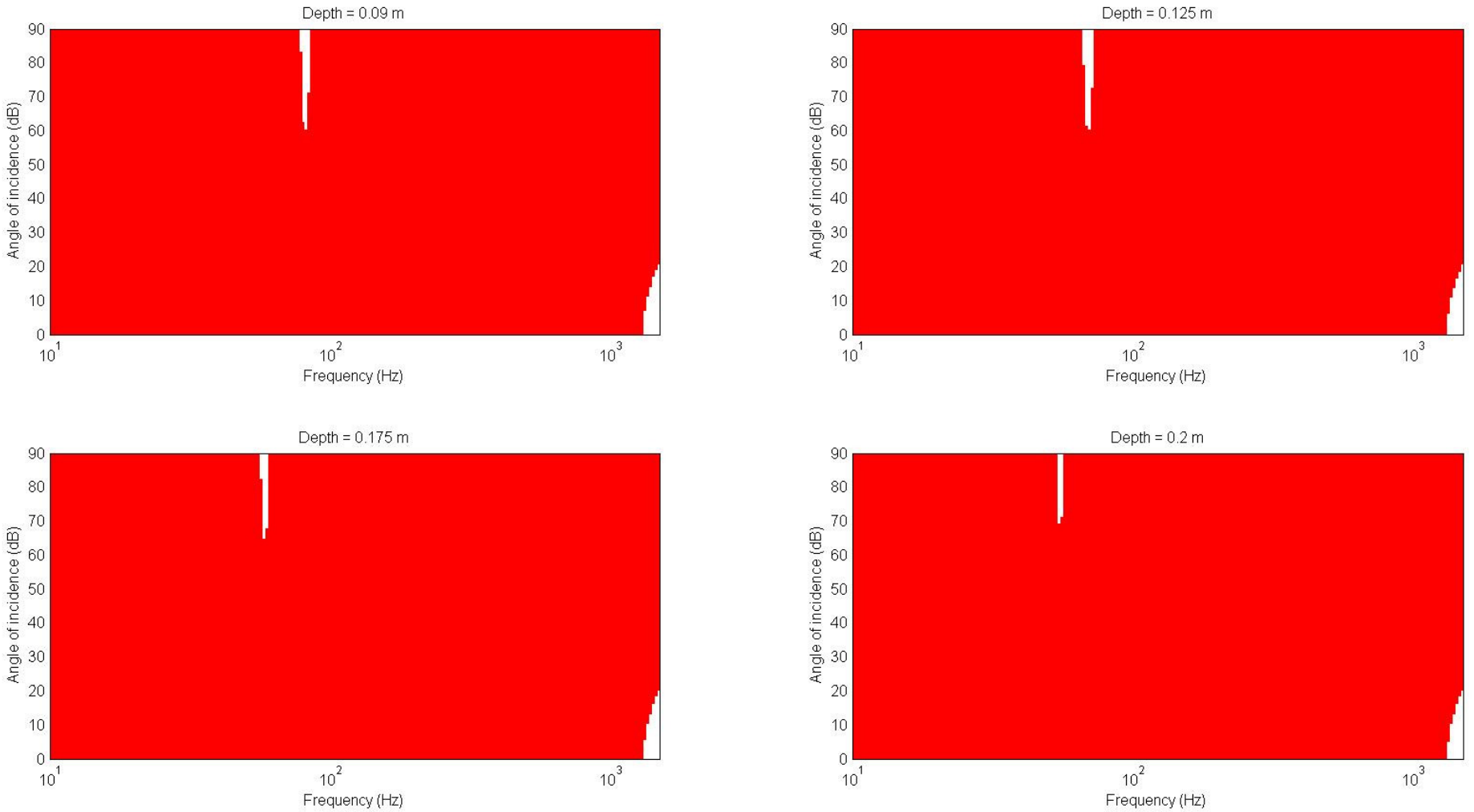

Figure 33 Regions where the radiation efficiency of the forced waves are greater than the reflected waves for different cavity depths with sound absorption within the wall cavity

With regards to the effect of the impedance of the wall panels, in Chapter 2 it was reported that as the mass of the wall panels was increased the influence of the wall cavity decreased even with an empty cavity. As a result with heavy wall panels, placing sound absorption material within the wall cavity didn't lead to a significant increase in the STL. Based on this observation, it would be expected that as the mass of the wall panels is increased the region where the reflected waves are dominant would decrease even with the empty cavity; such a result would indicate that the influence of the cavity is decreasing. The results shown in Figure 34 show this trend around the mass air mass resonance frequency. These results show that as the impedance/mass of the wall panel is increased the mass air mass resonance frequency shifts to the lower frequencies as expected; above this frequency, a slight decrease in the region where the reflected waves are dominant also occurs. However, this decrease is not to the extent where it can be implied that little improvement will occur when sound absorption material is added to the cavity as the mass/impedance is increased as discussed in Chapter 2. This observation does not diminish the validity of the model as it is believed that the reduction in the influence of the wall cavity as the mass of the wall panels are increased is due to the increase in the structure borne sound. This experimental trend is outside the domain of the analysis performed here.

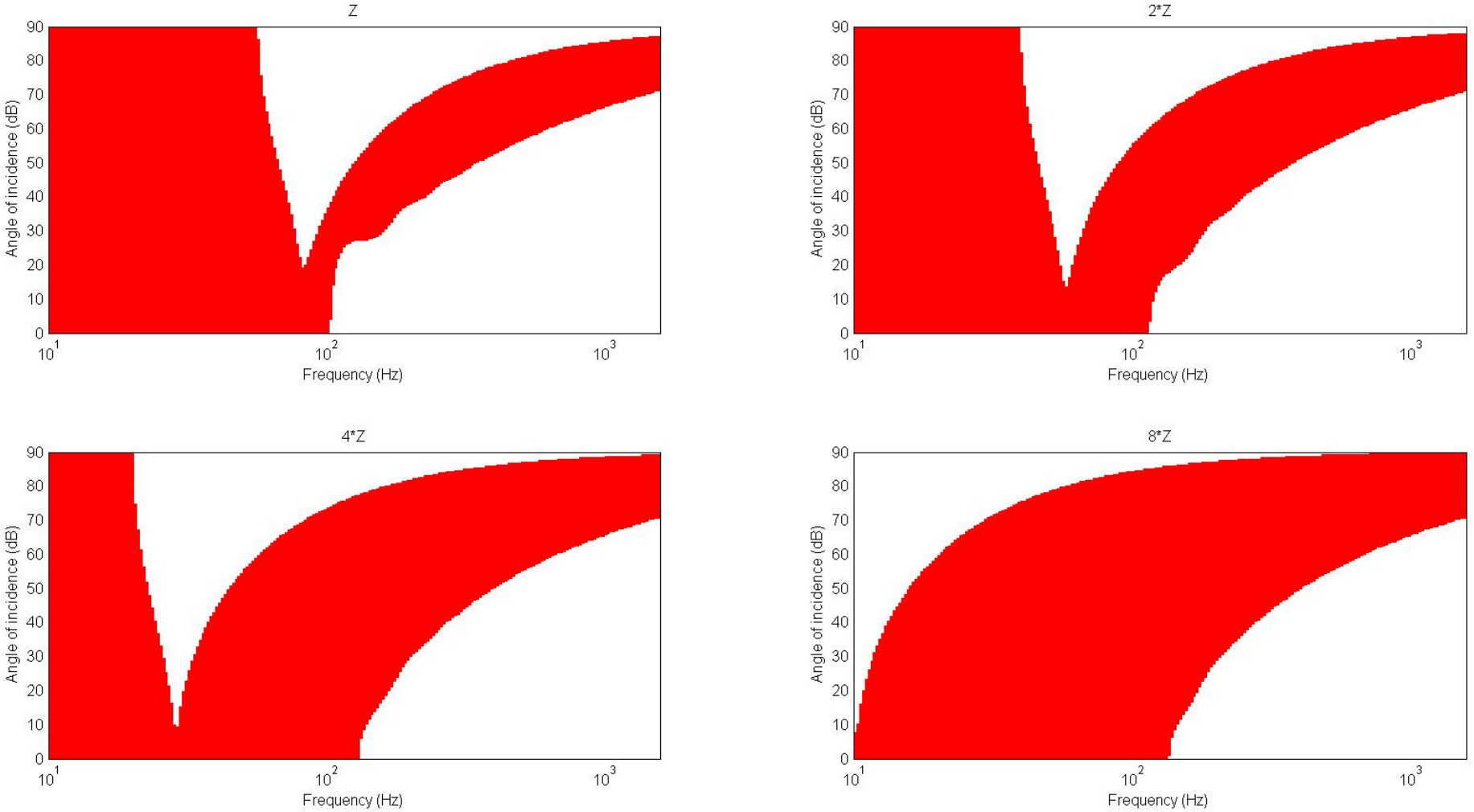

Figure 34 Regions where the radiation efficiency of the forced waves is greater than the reflected waves for different wall impedance with an empty 90 mm cavity

6.4 Summary and conclusions

A two dimensional vibration strip model has been derived and developed for the radiation efficiency of the forced and reflected waves within the wall cavity. The approach presented here is different from that used by Davy (2009b), Ljunngren (1991), Sato (1973) and Sewell (1970) in their models for the forced radiation efficiency. During the development of this model it was assumed that

- The radiated sound pressure from the vibrating strip is approximately equal to the radiated sound pressure of a zero order cylindrical source of the same strength
- The volume velocity is independent of the detailed form of distribution over the surface
- The radiated sound pressure and the particle velocity are in phase

The predictions obtained for the developed two dimensional forced radiation efficiency model when compared to Davy's (2009b) model were similar to Ljunngren's (1991) results when he compared his two dimensional model to Sato's (1973) and Sewell's (1970) three dimensional models. Careful inspection of Davy's (2009b) model revealed that although it was developed as an analytical two-dimensional model, its low frequency correction factor accounted for radiation into a three dimensional space. Consequently a modification of Davy's model to account for the radiation efficiency into a two-dimensional space was also presented within this chapter. Comparisons between the modification of Davy's model and the vibrating strip model were satisfactory.

An iterative model was also developed for the radiation efficiency of the reflected forced waves within the wall cavity which excite the wall panels. The analysis of the results obtained for the radiation efficiency of these waves was conducted in relation to how the airflow resistivity, depth of the cavity and mass of the wall panels affected these results. This was necessary because the rate of attenuation ($Real(\gamma)$) of these waves is dependent on these parameters. As a result, it was possible to verify some of the experimental trends reported in Chapter 2 as it was discovered that:

- A decrease in the radiation efficiency of the reflected waves due to an increase in the airflow resistivity can lead to an increase in the STL only if its initial radiation efficiency was greater than the radiation efficiency of the forced wave
- The reason why little to no improvement of the STL is obtained once an airflow resistivity of 5000 $\mathrm{Ns/m^4}$ achieved is due to the dominance of the forced wave
- The dominance of the forced wave was responsible for the reason why little improvement occurs once the depth of the cavity is increased when sound absorption material of sufficient airflow resistivity is present within the wall cavity
- The analysis performed here does not explain why the influence of the cavity decreases as the mass of the wall panels is increased. The increase in the structure borne sound is believed to be responsible for the reported decrease in the influence of the wall cavity in this situation

The analysis of the influence of the reflected waves within the wall cavity and how it affects different trends associated with the STL is different from other analyses presented within the literature.

In conclusion, from the literature it had been established that below the critical frequency the forced waves were responsible for the STL. The results presented here show that it is the reflection of these forced waves within the cavity which determine the influence of the wall cavity and any associated material placed within it on the STL. This is an important conclusion, as it provides a means of explaining different reported experimental trends. It should be noted that this analysis only gives a qualitative indication of the limits by which the STL can be improved through changing the characteristics of the wall cavity. In the following chapter the STL through double leaf wall systems is presented and the quantitative accuracy of the predictions will be considered.

7 Sound transmission loss for the finite model

The sound transmission from a double leaf wall system occurs due to the movement of the wall panel adjacent to the receiving room as illustrated in Figure 15. The total power transmitted from this wall panel is due to the excitation provided by the forced and reflected waves within the cavity. The attenuation and wavelength of these waves greatly affects this transmitted power. Consequently it is possible to calculate both the total radiated pressure and power of these waves when determining the STL. In this chapter comparisons are made between the predicted and measured STL once the attenuation and wavelength of the forced and reflected waves are considered. Furthermore, the derived model is used to provide a possible explanation for the reason why Sharp's and Davy's theory with a limiting angle of 61° gives the same result for the STL.

7.1 Total transmitted sound power

The radiated sound pressure and sound power due to the forced and reflected waves within the wall cavity were used to determine their respective radiation efficiencies in the previous chapter. In this section the phase relationship between these different waves is taken into account in order to determine the total radiated sound pressure and power from the vibrating strip. All of the symbols used within this section were previously defined within Chapter 6; for numerical integration reasons the total radiated pressure and power from the vibrating strip are written in terms of the sinc function.

The total radiated sound pressure from the vibrating strip can be found by replacing the velocity in Equation 6-17 with the total velocity such that

$$p(x,\varphi,\theta,t) = \rho c \sqrt{\frac{k}{2\pi R}} \int_0^l e^{j\left(\omega t - k\left(R+\frac{l}{2}\sin(\varphi) - x sin(\varphi)\right)+\frac{\pi}{4}\right)} v_{n,total}(x)dx, \qquad 7\text{-}1$$

where,

$$v_{n,total}(x,\theta) = v_{forced} e^{jk_b x} + v_{o+} e^{\gamma x} + v_{o-} e^{-\gamma x}, \qquad 7\text{-}2$$

v_{forced} is the velocity amplitude of the panel due to excitation by forced waves within the wall cavity, while v_{o+} and v_{o-} are the velocity amplitudes of the panel due to the excitation by the reflected waves within the wall cavity.

Substituting the $v_{n,total}$ from Equation 7-2 into Equation 6-15 gives

$$p(x,\varphi,\theta,t) = \rho c\sqrt{\frac{k}{2\pi R}}\int_0^l e^{j\left(\omega t - k\left(R+\frac{l}{2}\sin(\varphi)\right)+\frac{\pi}{4}\right)}\left(v_{forced}e^{jx(\mathrm{ksin}(\varphi)+k_b)} + v_{o+}e^{jx(\mathrm{ksin}(\varphi)-j\gamma)} + v_{o-}e^{-jx(\mathrm{ksin}(\varphi)+j\gamma)}\right)dx. \quad \textbf{7-3}$$

Solving the integral in Equation 7-3 and finding the resulting pressure magnitude squared gives

$$|p(\varphi,\theta)|^2 = \rho^2c^2\left(\frac{k}{2\pi R}\right)\left|v_{forced}\left(\frac{(e^{jl(\mathrm{ksin}(\varphi)+k_b)}-1)}{j(k\sin(\varphi)+k_b)}\right) + v_{o+}\left(\frac{(e^{jl(k\sin(\varphi)-j\gamma)}-1)}{j(\mathrm{ksin}(\varphi)-j\gamma)}\right) + v_{o-}\left(\frac{(e^{jl(k\sin(\varphi)+j\gamma)}-1)}{j(k\sin(\varphi)+j\gamma)}\right)\right|^2. \quad \textbf{7-4}$$

Let,

$$A = kl\sin(\varphi) + lk_b,$$

$$B = kl\sin(\varphi) - j\gamma l,$$

and

$$C = kl\sin(\varphi) + j\gamma l.$$

Substituting A, B and C into Equation 7-4 gives

$$|p(\varphi,\theta)|^2 = \rho^2c^2\left(\frac{k}{2\pi R}\right)\left|lv_{forced}\left(\frac{e^{jA}-1}{jA}\right) + lv_{o+}\left(\frac{e^{jB}-1}{jB}\right) + lv_{o-}\left(\frac{e^{jC}-1}{jC}\right)\right|^2. \quad \textbf{7-5}$$

Equation 7-5 can be written in terms of the sinc function by first re-writing it in the following form

$$|p(\varphi,\theta)|^2 = \rho^2 c^2 \left(\frac{k}{2\pi R}\right) \left| lv_{forced} \left(\frac{e^{\frac{jA}{2}}(e^{\frac{jA}{2}} - e^{-\frac{jA}{2}})}{\frac{2jA}{2}} \right) + lv_{o+} \left(\frac{e^{\frac{jB}{2}}(e^{\frac{jB}{2}} - e^{-\frac{jB}{2}})}{\frac{2jB}{2}} \right) + lv_{o-} \left(\frac{e^{\frac{jC}{2}}(e^{\frac{jC}{2}} - e^{-\frac{jC}{2}})}{\frac{2jC}{2}} \right) \right|^2. \quad \textbf{7-6}$$

Formula 32:3:3 of Spanier (1987) shows

$$\sin(x) = \frac{e^{jx} - e^{-jx}}{2j}. \quad \textbf{7-7}$$

Utilizing the relationship shown in Equation 7-7, Equation 7-6 can be re-written as

$$|p(\varphi,\theta)|^2 = \rho^2 c^2 l \left(\frac{k}{2\pi R}\right) \left| v_{forced} \left(\frac{\sin(\frac{A}{2})}{(\frac{A}{2})} \right) + v_{o+} \left(\frac{\sin(\frac{B}{2})}{\frac{B}{2}} \right) + v_{o-} \left(\frac{\sin(\frac{C}{2})}{(\frac{C}{2})} \right) \right|^2. \quad \textbf{7-8}$$

Equation 7-8 can now be written using the sinc function to give

$$|p(\varphi,\theta)|^2 = \rho^2 c^2 l \left(\frac{k}{2\pi R}\right) \left| v_{forced} sinc(\frac{A}{2}) + v_{o+} sinc(\frac{B}{2}) + v_{o-} sinc(\frac{C}{2}) \right|^2. \quad \textbf{7-9}$$

The radiated sound power can be found from Equation 6-19, as a result the total power radiated from the strip is

$$W_{total}(\varphi,\theta) = \rho c l \left(\frac{k}{2\pi}\right) \int_{-\frac{\pi}{2}}^{\frac{\pi}{2}} \left| v_{forced} sinc\left(\frac{A}{2}\right) + v_{o+} sinc\left(\frac{B}{2}\right) + v_{o-} sinc\left(\frac{C}{2}\right) \right|^2 d\varphi. \quad \textbf{7-10}$$

The velocity amplitude of the panel adjacent to the receiving room due to the forced and reflected waves can be found by considering the impedance of the wall panel and the pressure amplitude of each wave within the wall cavity (see Equation 4-4). As a result the velocity amplitude in Equation 7-10 for the forced and reflected waves can be found from

$$v_{forced} = \frac{N}{Z_2}, \quad \text{7-11}$$

$$v_{o+} = \frac{k_1}{Z_2}, \quad \text{7-12}$$

$$v_{o-} = \frac{k_2}{Z_2}, \quad \text{7-13}$$

where N is the pressure amplitude of due to the forced wave as defined in Equation 4-37, k_1 and k_2 are the pressure amplitudes due to the reflected waves as defined in Equations 4-41, and 4-42 respectively and Z_2 is the impedance of the panel 2 with the appropriate radiation efficiency used for the fluid loading effect as defined in Equation 4-1.

7.2 Incident sound power

The wave impedance on an infinite wall panel is equal to the ratio of the incident sound pressure and the normal particle velocity such that

$$Z_i = \frac{p_i}{u_i \cos(\theta)} = \frac{Z_c}{\cos(\theta)} = \frac{\rho c}{\cos(\theta)}, \quad \text{7-14}$$

where Z_c is the characteristic impedance of air such that $Z_c = p_i/u_i$;

[2]Rindel (1975) showed that the corresponding incident sound power on an infinite panel can be found from

$$W_{i\infty} = \int_S Re(p_i u_{iy}^*) dS = \frac{|p_i|^2 S}{Re(Z_i)} = \frac{|p_i|^2}{\rho c} S \cos(\theta). \quad \text{7-15}$$

[2] Rindel showed $W_{i\infty} = \int_S \frac{1}{2} Re(P_i u_{iy}^*) dS$ which corresponds to the peak power as opposed to the rms power shown in Equation 7-15. Also the subscript *y* corresponds to the coordinate system used in Figure 16.

The area (S) of a unit length of the strip is l; the incident sound power is

$$W_{i\infty} = \frac{|p_i|^2}{\rho c} l cos(\theta). \qquad \textbf{7-16}$$

Equation 7-16 shows that when $\theta = 90°$ the incident power is equal to zero. Rindel (1975) discussed the fact that Equation 7-16 is based on geometrical optics and is only valid for the infinite case and will be insufficient when the diffraction effects occur to a certain extent. The radiation efficiency of an infinite wall panel is $1/\cos(\theta)$ as discussed in Chapter 5. Consequently in order to account for the finite size of the wall panel the $\cos(\theta)$ term in Equation 7-16 can be replaced by the forced radiation efficiency to give

$$W_i = \frac{|p_i|^2 l}{\rho c \sigma_{forced}}. \qquad \textbf{7-17}$$

Rindel (1975) utilized the forced radiation efficiency as shown in Equation 7-17 and commented that this was similar to the way in which it was employed by Heckl (1964). Furthermore, Rindel stated that the use of the radiation efficiency in this manner also implies that the incident power per unit area is small when kl is large and increases when kl decreases; the deformation of the sound field by diffraction effects was given as the explanation for the reason why this occurs. Rindel's comments are also valid for the current model and these trends can be verified by studying the forced radiation efficiency results given in Figure 24 at different kl values.

Furthermore, the use of the finite radiation efficiency in this manner is similar to spatial windowing technique developed by Villot et al. (2001). In this initial introduction of the theory, the spatial window was applied to both the sound pressure field and the vibration before calculating the radiated field. According to Vigran (2009) this technique was modified by Villot and Guigou-Carter (2005) by only taking the spatial window into account on the sound pressure field; a technique which he employed when developing his simplified version of the technique.

However, despite Rindel's (1975) and Villot *et al*'s (2001) successful substitution of the finite radiation efficiency in the manner described, this approximation cannot be done on both the

transmitted power and the incident power. This was the reason for Villot and Guigou-Carter's (2005) correction. Furthermore if this approximation is done for the incident power, it should only be utilized when finding the angular dependent sound transmission loss and not when finding the diffuse sound field sound transmission loss. This is because the $\cos(\theta)$ term used when calculating the diffuse sound field transmission coefficient (as shown in Equation 5-18) represents the projected area of the sound field onto the wall panel. Consequently a further substitution of the finite radiation efficiency for this $\cos(\theta)$ term cannot be done. However, despite this problem the substitution of the finite radiation efficiency does at least provide a solution for what occurs at grazing incidence. Consequently, a choice needs to made about which technique should be employed. As a result for the remaining prediction model results the infinite radiation efficiency will be used when calculating the diffuse field STL while the finite radiation efficiency will be used when calculating the angular dependent STL.

7.3 Sound transmission loss of an empty double leaf wall

The STL can be found from the ratio of the transmitted and incident sound given by Equations 7-10 and 7-17 respectively, while the diffuse sound field STL can be found from Equation 5-18. A comparison between the 1/3 octave band diffuse field prediction obtained from the derived model and measurements conducted by the National Research Institute Canada (Warnock, 2010) for a 16 mm gypsum double leaf walls with a 90 mm cavity without sound absorption material can be seen in Figure 35.

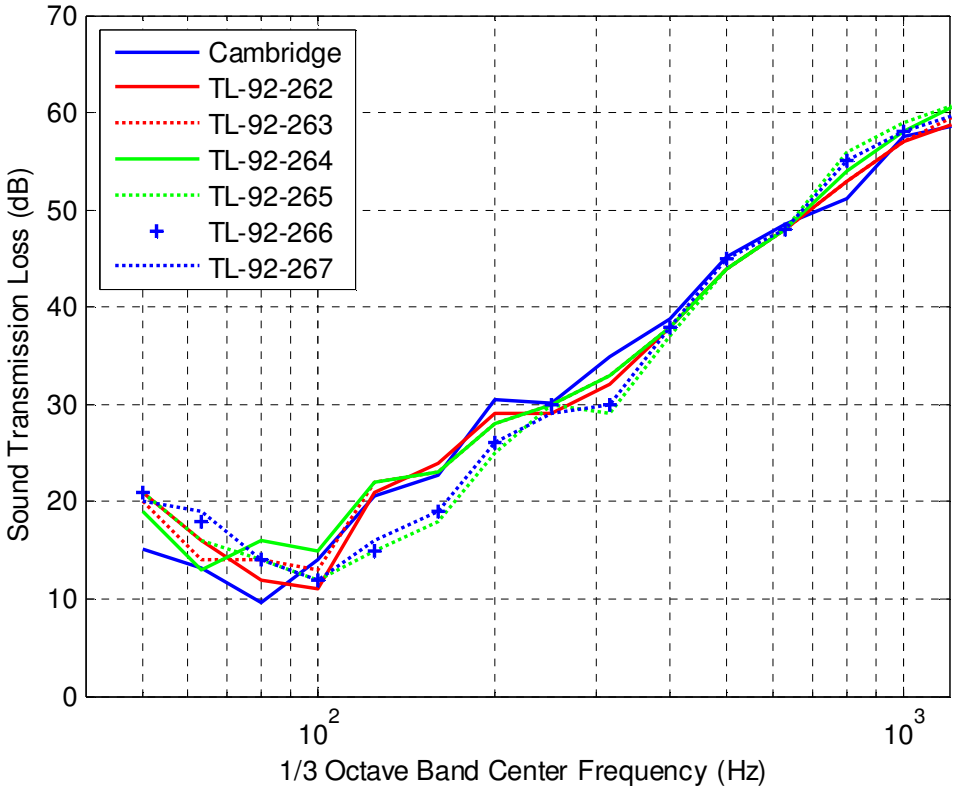

Figure 35 STL of a 16 mm gypsum double leaf wall with a 90 mm cavity without sound absorption material

In order to obtain the results shown in Figure 35 a resistance term $r= 600/\rho_o c$ was included in the model to reduce the extent of the singularity obtained at f_0. The use of this resistance term (r) and the other numerical techniques employed is discussed in Chapter 8. An airflow resistivity of 50 Ns/m^4 was also included for the results shown in Figure 35. This was necessary because it is believed that the air within the empty cavity provides some resistance and absorption of sound. This view is supported by Gosele (1977) whose calculations showed that the empty cavity has a flow resistivity of 1 to 10 Ns/m^4.

The results shown in Figure 35 show that the derived model accurately predicts the STL for the empty double leaf wall system below and above f_0 up until approximately half of the critical frequency of the wall panel. The accuracy of the results obtained below f_o indicates that the developed model accounts for the STL being controlled by the mass of the wall panels. However, the position of f_o predicted by the developed model was lower than obtained from the

measurements even though it corresponded to the calculated f_0 using Fahy's (1985) formula shown in Equation 1-1. Bies and Hansen (2009) considered this discrepancy to be due to the "effective mass" of the wall panel being less than the actual mass. As a result, Bies and Hansen added an empirical constant of 1.8 (as introduced by Sharp) to Fahy's formula when determining f_o such that

$$f_o = \frac{1}{2\pi}\left(\frac{1.8\rho_o c(m_1 + m_2)}{d m_1 m_2}\right)^{\frac{1}{2}}. \qquad \text{7-18}$$

Implementation of this empirical constant as in Equation 7-18 shifts the position of f_o to the point which corresponds to the measurement. Above f_o the prediction results compare well with the experimental data. Consequently it can be concluded that the developed model accurately predicts the STL of empty double leaf wall systems once suitable damping (i.e. Ξ) and resistance (i.e. r) is included within the model.

7.4 Sound transmission loss of a fully filled double leaf wall

The predictions obtained for the STL of the fully filled wall cavity are discussed within this section. In Chapter 6 the analysis of the radiation efficiency of the forced and reflected waves was used to give an explanation for the reason why the STL increase reaches a plateau once an airflow resistivity of approximately 5000 Ns/m^4 is included within the wall cavity. A quantitative assessment could not be obtained from this discussion since the transmitted power is dependent on the velocity amplitude due to the forced and reflected waves (see Equation 7-10) which are affected by the properties of the wall cavity. Consequently, in order to conduct this quantitative assessment the developed model was used to predict the STL for a 16 mm double fully filled leaf wall gypsum board system with various airflow resistivity's within a 90 mm cavity. The results obtained from this prediction can be seen in Figure 36. These results show that as the airflow resistivity is increased the STL steadily increases up until an airflow resistivity of approximately 5000 Ns/m^4 . Above this airflow resistivity little improvement in the STL occurs. These trends shown in Figure 36 correspond well with that reported from experimental

works. However, in order to determine the accuracy of the model, predictions were compared to experimental data.

The prediction for the STL of a 16 mm gypsum double leaf wall system fully filled with glass-fibre (flow resistivity 4800 Ns/m^4) within a 90 mm cavity as measured by Warnock (2010), can be seen in Figure 37. The description of the different configurations of this double leaf wall system is given in Appendix A.

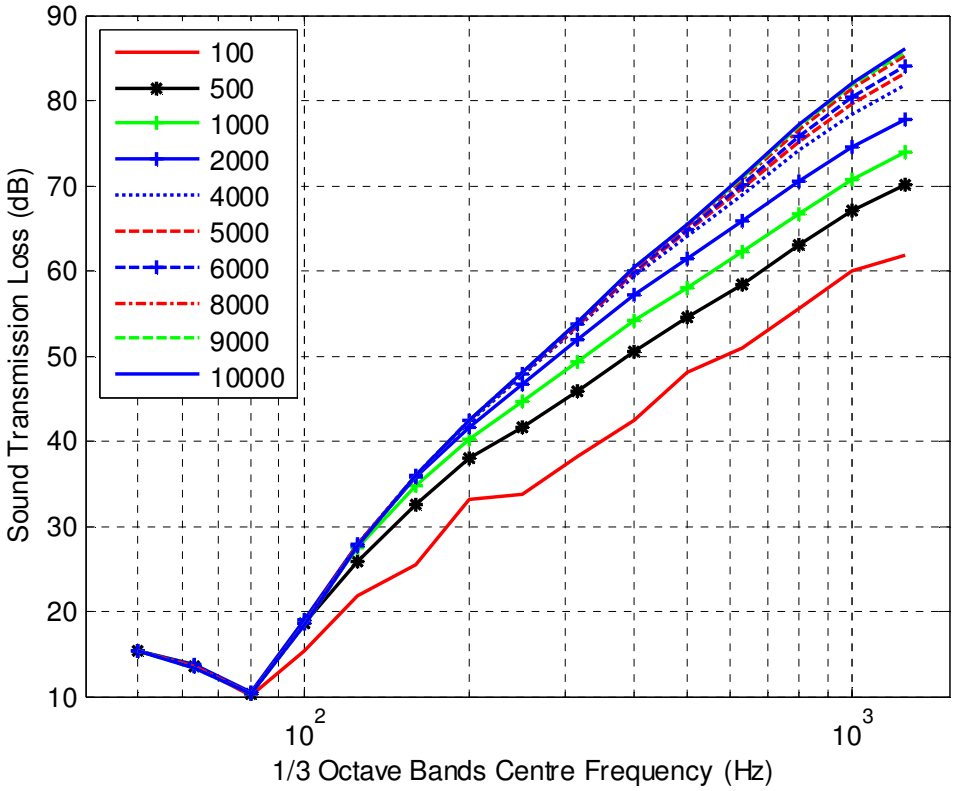

Figure 36 Effect of different airflow resistivity on the predicted STL

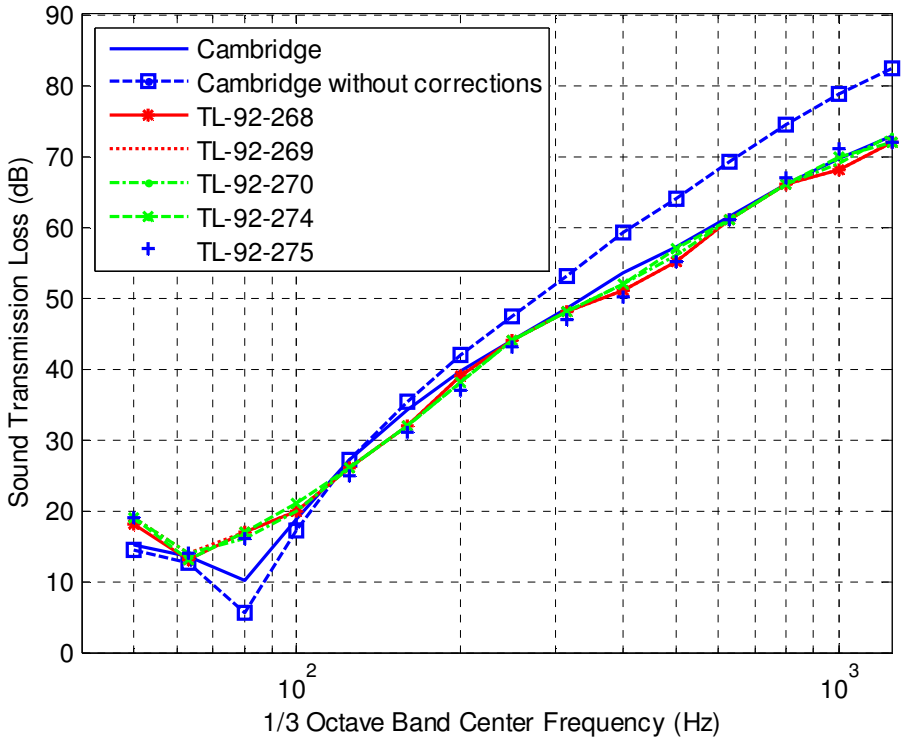

Figure 37 STL of a double leaf wall system with glass-fibre within the 90 mm wall cavity

In order to obtain the predicted result labelled "Cambridge" in Figure 37, an airflow resistivity of 20% of the measured airflow resistivity of the material and a resistance term ($r = 600/\rho_o c$) was utilized. This adjustment to the airflow resistivity was necessary because a higher than expected STL was obtained when the actual airflow resistivity of 4800 Ns/m^4 was used in the developed model. The results labelled "Cambridge without corrections" show the results obtained when the actual airflow resistivity is used without the additional resistance term. The improvement to the prediction at the mass air mass resonance frequency with the addition of the resistance term (r) and the benefit of reducing the airflow resistivity are clearly seen in Figure 37.

The overestimate of the STL when the actual airflow resistivity is used was also observed by Novak (1992) within his transfer matrix model which utilized the airflow resistivity of the material in order to characterise its sound absorption properties. Novak did not give an

explanation for this trend. However, with regard to the proposed model there are three plausible reasons why the overestimate occurs when the actual flow resistivity is used.

The first plausible explanation is related to the fact that the reported airflow resistivity is usually measured normal to the surface of the material and not in a planar direction. Allard (1993) noted that fibrous materials are generally anisotropic and the fibres generally lie in planes parallel to the surface of the material. As a result the normal airflow resistivity (Ξ_n) which is measured perpendicular to the planes of the fibres is different from the planar airflow resistivity (Ξ_p) which is measured parallel to the directions of the planes as illustrated in Figure 38.

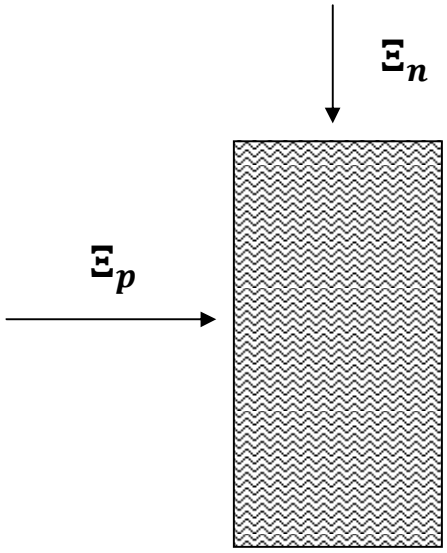

Figure 38 Depiction of a fibrous material showing the direction of the airflow resistivity in the normal and planar directions

Allard (1987) discussed the work of Burke (1983) and Nicholas and Berry (1984) which showed that the ratio of the planar to normal airflow resistivity was approximately 0.5. Consequently since the developed model was derived by integrating along the length of the cavity rather than its depth, the planar airflow resistivity should be utilized within the model rather than the usual reported normal airflow resistivity. This issue relating to direction of the measured airflow

resistivity gives a plausible explanation for the reason why at most 50% of the measured normal airflow resistivity should be used within the developed model.

The second plausible explanation for the over-prediction of the STL is related to the subtle assumption within the developed model that the sound absorption material within the wall cavity does not move when excited by the sound waves. Schultz in Beranek (1971) discussed the sound absorption properties of porous materials when excited by sound waves. In this discussion Schultz noted that for the low frequency region if the material has insufficient inertia to remain motionless it will move as a whole because of the action of the air particles pumped back and forth by the sound pressure through the pores of the blanket. The low frequency region occurs at frequencies where the thickness of the sound absorption material is less than one-tenth of the wavelength of sound within the material. Schultz concluded that under such circumstances the blanket can be treated in terms of lumped constants with no consideration of sound propagation within the blanket (Beranek, 1971). No sound propagation within the blanket means that the sound absorption properties will be drastically reduced. Consequently, if there is any movement of the sound absorption material within the wall cavity for the frequency range considered by the developed model, the airflow resistivity required for these calculations would be significantly lower. Although it can be argued that the movement of the sound absorption material may not significantly affect the predictions from the developed model since the movement of the material in the normal direction will be greater than the planar direction. It must be noted that any movement of the material in any direction will cause some reduction in its sound absorption properties and reduce the required airflow resistivity needed for the model. The extent of this required reduction in airflow resistivity if the sound absorption material moves within the wall cavity is unknown.

The third plausible explanation is related to the sound radiation into the wall cavity. The developed model is based on the assumption that below the critical frequency the forced bending waves are efficient radiators while the free bending waves are inefficient. The hydrodynamic short circuiting of the free bending waves within the finite wall panel is responsible for the inefficiency of these waves. However, although this may be true for radiation into a free space or into an empty wall cavity, Tomlinson *et al.* (2004) showed that the radiation efficiency of the

free bending waves on a plate increases as the airflow resistivity of the porous medium it is radiating into increases. For example, Tomlinson *et al.* calculated the radiation efficiency of a plate at 100 Hz radiating into a 100 Ns/m^4 porous medium as 0.018 and approximately 0.3 into a 5000 Ns/m^4 medium. Clearly the significance of the free bending waves increases as the airflow resistivity increases below the critical frequency. As a result of the assumption used within the developed model that the wall panel is limp, the model cannot accommodate the possible increased influence of the free bending waves due to radiation into a medium with a high airflow resistivity. If this were possible, the prediction obtained would be less than that obtained by the current model. Finally, it should be noted that none of the models within the literature account for the increase in the radiation efficiency of the free bending waves due to the difference in sound radiation into a porous medium as outlined by Tomlinson *et al.* (2004).

Despite the issues discussed relating to the modelling of the sound absorption material within the cavity, the results shown in Figure 37 show that once 20% of the airflow resistivity is used for the 90 mm cavity, the developed model accurately predicts the STL above and below f_0 even though at f_0 the results obtained from the prediction does not account for the shift of f_0 due to the change in the speed of sound through the porous material as discussed within Chapter 2.

Further proof of the accuracy of the model with a reduced airflow resistivity can be seen from the prediction results obtained from over 20 different double stud wall systems measured by Halliwell *et al*. (1998) shown in Appendix B. These wall systems have varying density of the gypsum plasterboard, type and amount of sound absorption material placed within the cavity as well as type and spacing of the studs. The prediction results obtained for the 205 mm deep cavity were derived by using 40 % of the reported airflow resistivity shown in Table 11 when more than 50 % of the cavity was filled with sound absorption material, while 20 % of the reported airflow resistivity was used once less than 50% of the cavity was filled. The reason for the different airflow resistivity for the different cavity depths is unknown. However, in the case of the partially filled cavity not all of the cavity modes will be fully damped, as a result an airflow resistivity different from the fully filled case will be required.

7.5 Davy vs Sharp comparison

Sharp (1973; 1978) and Davy (1990a; 2009c) both produced analytical STL models to predict the STL of double leaf wall systems with sound absorption material within the wall cavity. Sharp used the effective mass for each leaf (as obtained from Josse and Lamure (1964) single leaf theory) and assumed that the normal STL calculated using the effective mass could be used to account for integrating over all angles of incidence. On the other hand, Davy's (1990a; 2009c) model utilized a varying limiting angle of incidence based on Sewell's (1970) forced transmission theory. The predictions obtained from Davy's (1990a) original model were lower than those obtained from Sharp (1973; 1978). Davy's (1990a) model seemed justifiable as it compared well to early STL measurements obtained from the NRCC and supported Rudder's claim that Sharp's model predicted a higher STL than experiments. However, Davy (2009c) discovered that flanking transmission was the reason why early NRCC's measurements were lower than the prediction obtained by Sharp. Consequently, in order to obtain predictions closer to Sharp's (1978) model, Davy (2009c) limited the angle of incidence to a maximum of 61° as follows

$$\cos^2\theta_l = \begin{cases} 0.9 & if\ \dfrac{1}{k\sqrt{A}} > 0.9 \\ \dfrac{1}{k\sqrt{A}} & if\ 0.9 \geq \dfrac{1}{k\sqrt{A}} \geq \cos^2 61° \\ \cos^2 61° & if\ \cos^2 61° > \dfrac{1}{k\sqrt{A}} \end{cases} \qquad \text{7-19}$$

where k is the wave number of sound in air, A is the area of the wall panel and $1/k\sqrt{A}$ is the limiting angle based on Sewell's forced transmission theory (Davy, 2009c). The reason why Davy (2009c) needed to implement a maximum limit of 61° in order to obtain predictions closer to Sharp (1973; 1978) and by extension to measurements unaffected by flanking will be discussed within this section. This understanding is obtained by analysing the gradient of the results obtained from Davy's (2009c) model (i.e. without the maximum limited angle of incidence of 61°) and Sharp's (1978) model, by comparing these results to the developed model presented earlier in this chapter and by utilizing an understanding of the fundamental basis of the

all studied models. However, before explanations are given for the differences which occur between Davy's original model and Sharp's, an analysis of the results obtained from these models must be conducted.

The predictions obtained for a 16mm double leaf gypsum wall system with a 90 mm cavity filled with sound absorption material can be seen in Figure 39. These results indicate that the gradient between f_o and f_l was $18\ \mathrm{dB/octave}$ and $14\ \mathrm{dB/octave}$ for Sharp and Davy's original model respectively. The difference between the gradient obtained between f_0 and f_l is the major reason for the difference obtained between the models. If the angle of incidence is limited to a maximum of 61° (as shown in Equation 7-19) in Davy's model, similar results are obtained to those using Sharp's model.

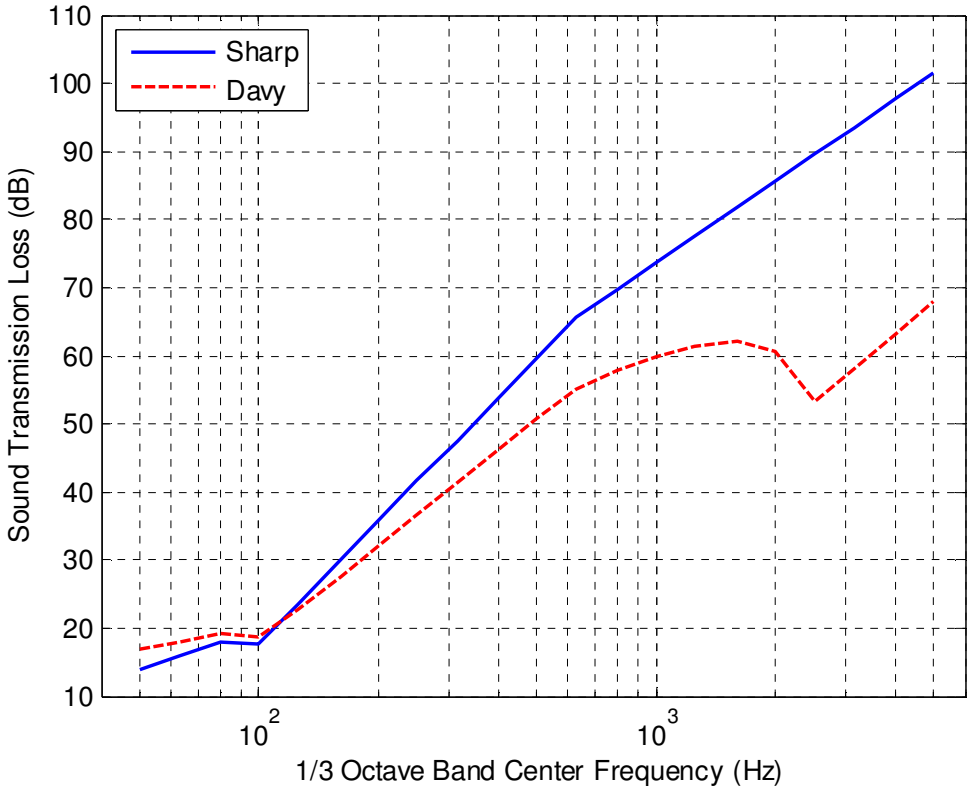

Figure 39 Comparison between Sharp's and Davy's original model

In order to understand why Davy's model needed to be limited by a maximum angle of incidence in addition to the variable limiting angle used, careful attention must be given to the fundamental basis of the theory. Although the varying limiting angle of incidence used within Davy's model is based on Sewell's forced transmission, the core of the model is fundamentally based on the STL model of Rudder (1985) which is derived from the approach of Mulholland (1967).

Mulholland (1967) considered the ray tracing theory which involves multiple reflections of the incident sound waves as they pass through the depth of the wall system as shown in Figure 40. The transmission coefficient is calculated by the reduction in the sound intensity by a fraction x which is based on the mass law theory as the ray is transmitted or reflected through the various paths. The fraction x in Figure 40 is given by

$$x = \frac{1}{1 + \frac{j\omega M cos(\theta)}{2\rho_o c}}, \qquad \textbf{7-20}$$

where M is the mass of the panel.

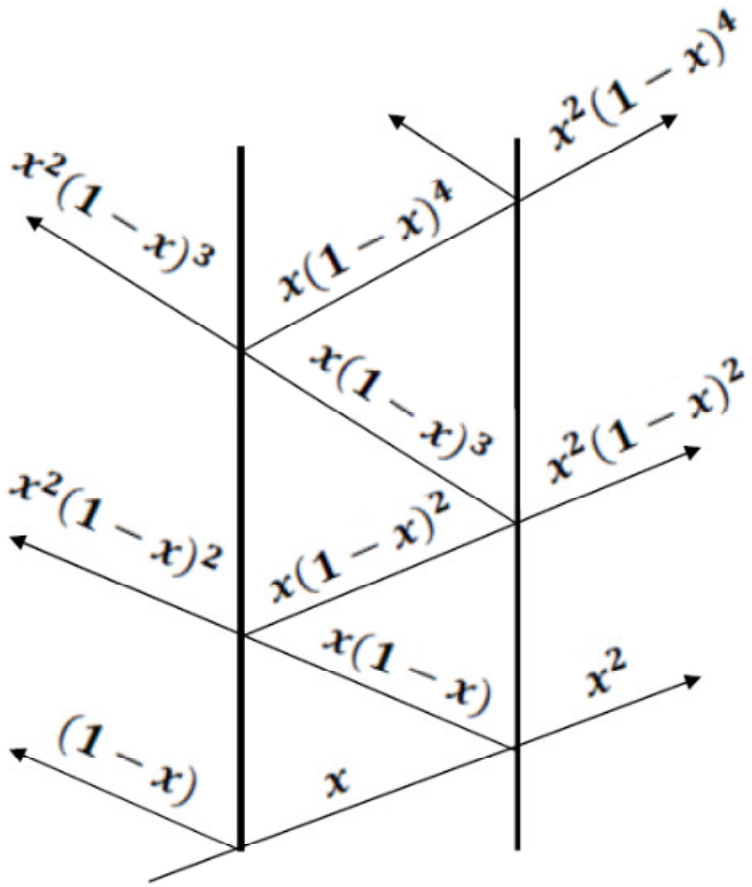

Figure 40 Mulholland's multiple reflection theory

The advantage of the approach of Mulholland (1967) over Beranek (1949) and London (1950) is that it allowed for the inclusion of sound absorption within the wall cavity. However, despite the improvement made, for the empty cavity situation Mulholland's model did not lead to a significant improvement in the prediction of the STL when compared to the results obtained from Beranek's and London's models. This observation provides the first clue to understanding why Davy's original model under-predicts the STL, as Davy simply applied the varying limiting angle of incidence to the theory of Mulholland (1967) as developed by Rudder (1985).

Davy's model for the sound transmission coefficient above f_0 is based on the following equations

$$\tau(\theta) = \frac{1}{R^2(\theta) + I^2(\theta)}, \quad \text{7-21}$$

where,

$$R(\theta) = 1 - A_1 A_2 (1 - {r_{Davy}}^2 \cos(2\beta)), \quad \text{7-22}$$

$$I(\theta) = A_1 + A_2 - {r_{Davy}}^2 A_1 A_2 \sin(2\beta), \quad \text{7-23}$$

while,

$$A_i = a_i \cos(\theta), \quad \text{7-24}$$

$$\beta = kd\cos(\theta), \quad \text{7-25}$$

and

$$a_i = \frac{\omega m_i}{2\rho_0 c}\left[1 - \left(\frac{\omega}{\omega_{ci}}\right)^2\right]. \quad \text{7-26}$$

m_i and ω_{ci} are the mass per unit area and angular critical frequency of the ith leaf of the cavity wall (i =1 or 2), d is the cavity width and r_{Davy} is the reflection factor of the cavity (Davy, 2009c).

The results obtained from Equation 7-21 for an empty (i.e. r_{Davy}= 1) 16 mm double leaf wall system with a 90 mm cavity can be seen in Figure 41. Although the mass air mass resonance frequency at different angles of incidence does not occur at the standing wave frequency as in London's model (as shown in Chapter 5), the angular dependence of the mass air mass resonance frequency is immediately apparent. Furthermore, since the STL does not go to zero at the oblique mass air mass resonances at the higher angles of incidence, the slight improvement over London's model as observed by Mulholland will be evident. However, despite this slight improvement, based on the discussion given in Chapter 5, Davy's model will under-predict the STL as it is the interaction between the forced and reflected waves along the length of the cavity

which is responsible for the mass air mass resonance frequency occurring at the normal air mass resonance frequency for all angles of incidence.

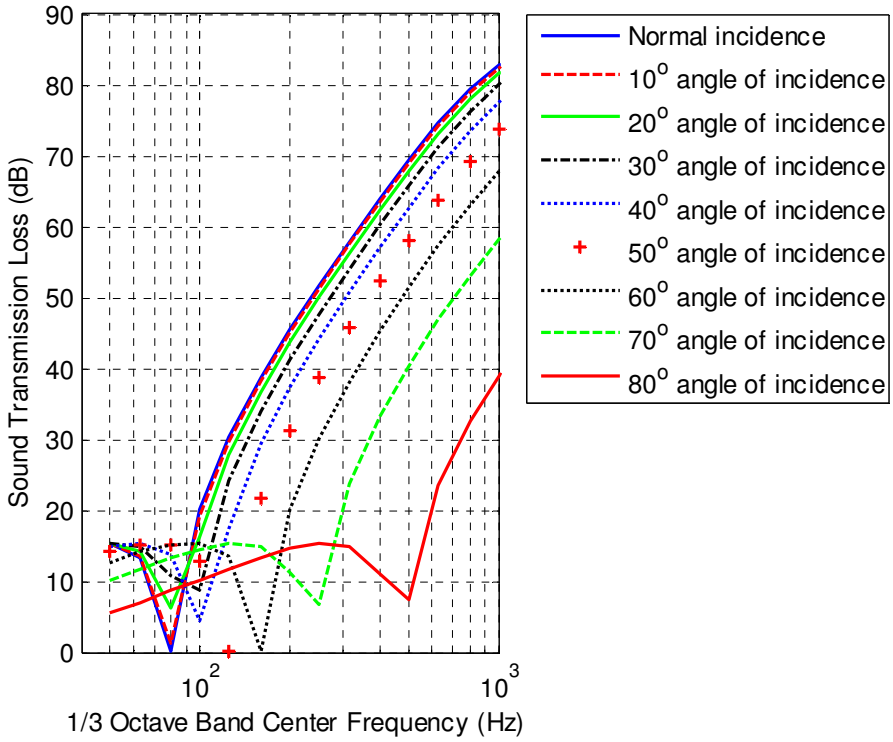

Figure 41 STL for different angles of incidence using Equation 21 from Davy (2009) (i.e. Equation 7-21 above)

The detrimental effects of the angular dependent mass air mass resonance frequency is masked within Davy's model as he considered the case when there is sound absorption within the wall cavity and rearranged Equation 7-21 to give

$$\frac{1}{\tau(\theta)} = \left(\sqrt{(A_1^2+1)(A_2^2+1)} - {r_{Davy}}^2 A_1 A_2\right)^2 + 4{r_{Davy}}^2 A_1 A_2 \sqrt{(A_1+1)(A_2+1)}. \qquad \text{7-27}$$

Davy then assumed that the second term in Equation 7-27 could be ignored since in most cases the bandwidth of the resonance term is broad (i.e. $r_{Davy} \cong 0$ when there is sound absorption

within the cavity) (Davy, 2009c). Also since A_i is usually larger than 1, Davy re-wrote Equation 7-27 as follows

$$\tau(\theta) = \frac{1}{(q + px)^2}, \tag{7-28}$$

where,

$$q = \frac{1}{2}\left(\frac{a_2}{a_1} + \frac{a_1}{a_2}\right), \tag{7-29}$$

$$p = a_1 a_2 \alpha \tag{7-30}$$

$$\alpha = 1 - {r_{Davy}}^2, \tag{7-31}$$

$$x = \cos(\theta) \tag{7-32}$$

with α being the absorption coefficient of the wall cavity (Davy, 2009c). Davy, then integrated Equation 7-28 to give

$$\tau_f = \int_{\cos^2(\theta_l)}^{1} \frac{dx}{(q + px)^2} = \frac{1 - \cos^2(\theta_l)}{\left(q + p\cos^2(\theta_l)\right)(q + p)}, \tag{7-33}$$

which represents the equation used to obtain the results shown in Figure 39, without the maximum limiting angle of incidence of 61°. In order to understand why the results in Figure 39 differ from Sharp's theory and measurements the results obtained from Equation 7-28 must be studied. These results can be seen in Figure 42 below.

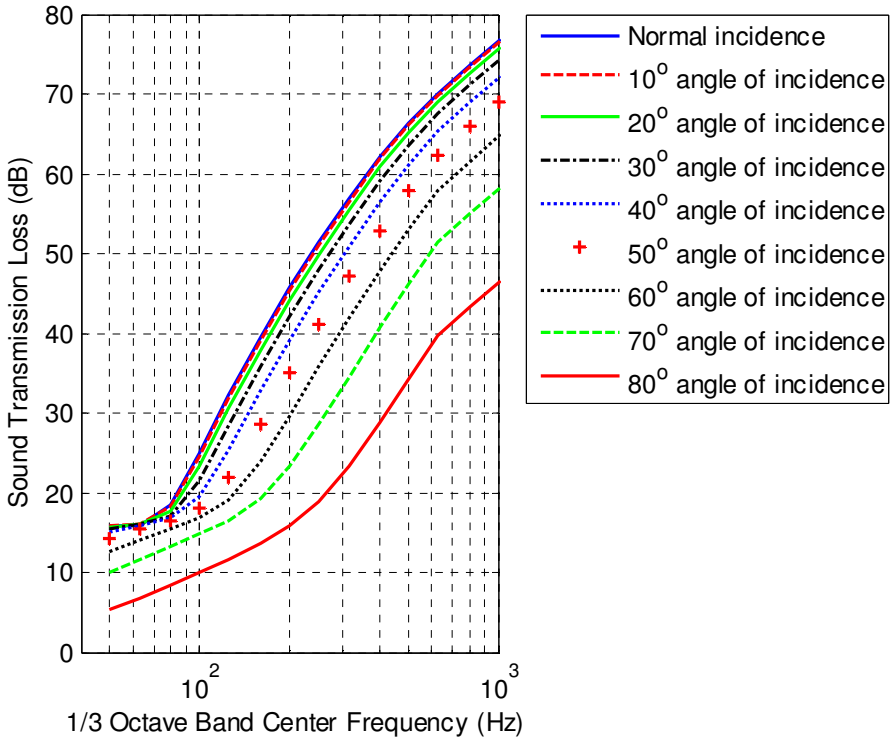

Figure 42 STL for different angles of incidence using Equation 28 from Davy (2009) (i.e. Equation 7-28 above)

Comparing the results obtained from Figure 41 (i.e. without sound absorption) and Figure 42 (i.e. with sound absorption) it can be seen that the effect of the angular dependent mass air mass resonance is masked due to the assumption made in the development of Equation 7-28 that $r_{Davy} \cong 0$. Although this masking occurs, the angular dependent mass air mass resonance still affects the results obtained in Figure 39 as it reduces the gradient of the slope obtained. Consequently a gradient of 18dB/octave as obtained from Sharp's model between the f_0 and f_l cannot be obtained from Davy's model without the additional implementation of the maximum limiting angle of incidence of 61°. In order to give a physical explanation for the reason why this maximum limiting angle is needed, the newly developed model can be used to mirror the results obtained by Davy to justify the use of the terms which he implemented within his model.

Firstly, based on the results shown in Figure 41, Davy's model (for the empty cavity without the maximum limiting angle of 61°) can be considered to be a variant of an infinite model which

utilizes a varying limiting angle of incidence based on Sewell's forced transmission theory. The term "variant" is used because it considers multiple reflections along the depth of the cavity even though along its length it is infinite. Consequently, in terms of the developed model, Davy's model (for this case) is equivalent to integrating the total transmitted power due to the forced waves only (i.e. neglecting the effect of the reflected waves in Equation 7-33) over the angles of radiation and adding a resistance term (r_{forced}) to the radiation efficiency of the forced waves. The resistance term in this case, is equivalent to the multiple reflections included within Davy's model. It should be noted that the addition of this resistance term (r_{forced}) in the infinite cavity situation is similar to London's (1950) use of an additional resistance term within his model. The resistance term (r_{forced}) affects the STL over the entire frequency range and is different from the resistive term (r) used for the finite wall system for the results shown in Figure 35 and Figure 37. Furthermore the resistance term (r) is used to compensate for the extent of the singularity/dip which occurs at the mass air mass resonance frequency and is used in the calculation of the radiation efficiency of the reflected waves only (see Chapter 8).

A comparison between Davy's model and the infinite version of the model developed here with an additional resistance term can be seen in Figure 43 for an empty 16 mm gypsum double leaf wall system with a 90 mm cavity. These results were obtained by using an absorption coefficient of 0.1 as suggested in Davy (2009c) while $\Xi = 1$ and resistance $r = 1150/\rho_o c$ were used for the prediction obtained from the developed model. The similarity in the results obtained from both models suggests that the gradient obtained by both models is as a result of the angular dependent mass air mass resonance frequency.

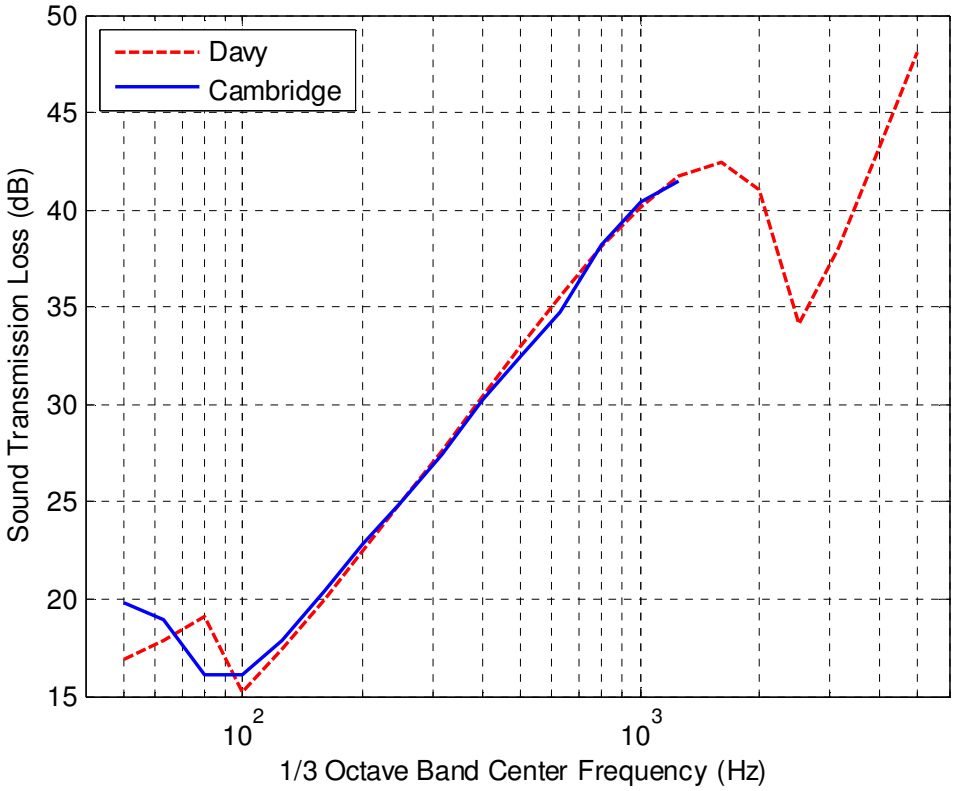

Figure 43 Comparison between Davy and Cambridge STL model for a 16 mm double leaf gypsum board wall system with an empty 90 mm cavity

When sound absorption material is added to the wall cavity, a gradient of 18 dB/octave can be obtained when an airflow resistivity of 4000 $Ns/m\hat{}4$ is utilized within the developed model (i.e. with the reflected waves). A similar slope is obtained in Davy's model once the maximum limiting angle of incidence of 61° is utilized. In Sharp's model the gradient of 18 dB/octave occurs because it was assumed that the normal incidence sound transmission could be used to account for the all angles of incidence. This assumption avoids any possible deterioration of the gradient due to an angular dependent mass air mass resonance. Consequently, the reason why a maximum angle of incidence of 61° had to be imposed on Davy's model is to reduce the effect of the reduction of the STL which occurs due to the angular dependent mass air mass resonance.

7.6 Summary and conclusions

A model for the STL through a double leaf wall system has been develop which takes into account the phase relationship between the forced and reflected forced waves as well as the difference in the radiation efficiency of these waves. In addition to the assumptions already stated in the previous chapters it was assumed that:

- The forced radiation efficiency gave a good approximation for accounting for the finite size of the wall system when calculating the incident sound power
- The total normal velocity of the transmitting wall panel could be found by the summation of the contributions due to excitation caused by the forced and reflected waves within the wall cavity

The predictions obtained for the STL of the different wall systems under these assumptions compared well to experiments for both the empty and full cavity case although an additional resistance term and a reduced airflow resistivity had to be incorporated within the model. The inclusion of the additional resistance term r was needed to reduce the extent of the reduction in the prediction of the STL at the mass air mass resonance frequency. The reduction in the required airflow resistivity was needed because:

- The planar airflow resistivity is approximately 50% of the usually normal airflow resistivity
- There is a possibility that the sound absorption material may move within the cavity at frequencies where the thickness of the sound absorption material is less than one-tenth of the wavelength of sound within the material, therefore reducing its sound absorption properties
- The radiation efficiency of the free bending waves was not included due to the belief that they are inefficient radiators within the investigated frequency range. However, Tomlinson *et al*'s (2004) investigation suggests that the radiation efficiency of these waves actually increase when radiation into a porous medium is considered

The issues encountered while using the airflow resistivity of the material to model its sound absorption characteristics is consistent with that encountered by Novak (1992), although no explanation was given by him for the reason why an over prediction of the STL occurred once the actual normal airflow resistivity was used.

Finally, by evaluating the fundamental basis of Davy's (2009c) model, it was discovered that Davy's model can be considered to be a "variant" of the infinite STL model. Consequently the deteriorating effects of the angular dependent mass air mass resonance were responsible for the difference between Davy's model without a maximum angle of incidence of 61° and Sharp's (1973; 1978) model. This effect was not easily seen while modelling the STL with sound absorption within the cavity. Furthermore, it was explained that Sharp's use of the normal incidence to account for the STL over all angles of incidence was justified as it avoided the deterioration of the gradient caused by the angular dependent mass air mass resonance frequency.

8 Numerical methods

The developed model was implemented within Matlab and the prediction results shown within the previous chapters obtained. The use of the sinc function, an adaptive integration function (quadgk) and the additional resistance term r were the numerical techniques included within the Matlab code. In this chapter the implementation of these techniques are explained and justified. An analysis of the number of iterations required for the radiation efficiency of the reflected waves in order for the calculated STL to converge is also given.

8.1 Sinc function

The sinc function can be defined as

$$\mathrm{sinc}(x) = \frac{\sin(x)}{x}, \tag{8-1}$$

or more commonly in its normalized form with the following properties as

$$\mathrm{sinc}(x) \equiv \begin{cases} \dfrac{\sin(\pi x)}{\pi x}, & x \neq 0 \\ 1 & x = 0 \end{cases} \tag{8-2}$$

(Lund and Bower, 1992). The properties of the sinc function shown in Equation 8-2 could be proven by using a combination of Lauent and Cauchy's theorem as shown in Example 1.10 in Lund (1992). Alternatively these properties could be proven through the use of L'hospital's theorem from calculus. A comparison between the sinc function and the sine and cosine functions can be seen below.

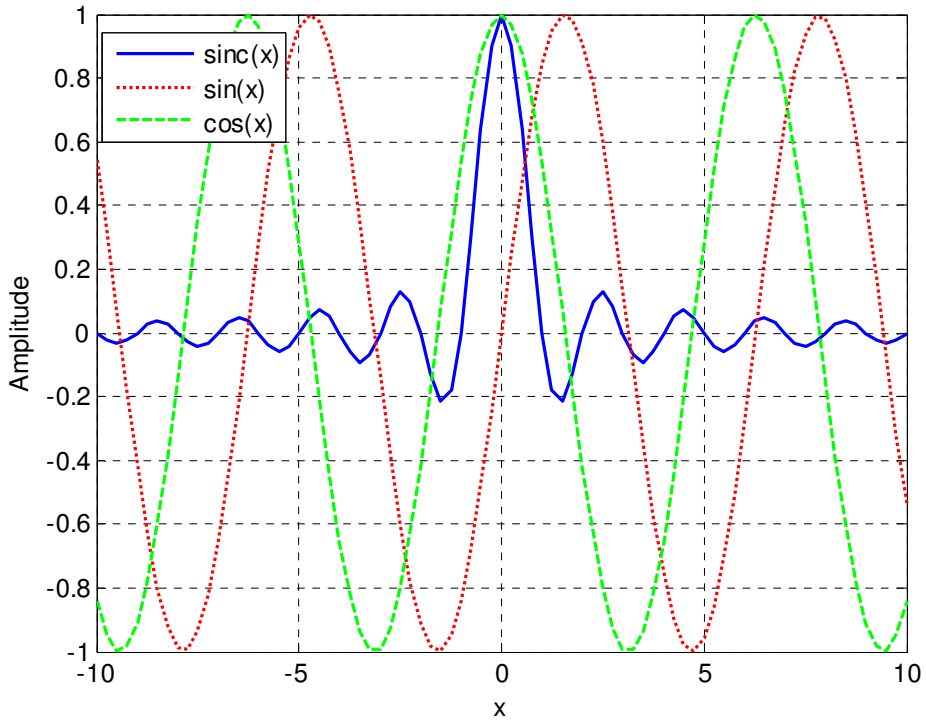

Figure 44 Comparisons between the sinc, sine and cosine functions

Sinc methods excel for problems with singularities, for boundary-layer problems and for problems over infinite and semi-infinite ranges (Stenger, 1993). This makes the sinc function useful for the current study as the resonances which occur along the cavity occur at moderate singularity points. Due to these moderate singularities, the adaptive numerical integration function, quadqk was utilized when integration of the sinc function was required. The quadgk function may be most efficient for high accuracies and oscillatory integrands; it supports infinite intervals and can handle singularities at the endpoints (Matlab, 2012). Matlab's help file suggests that if the singularity occurs at points within the limits of the integral, the integral should be written as the sum of integrals over subintervals with the singular points as endpoints, computed with quadgk and added to find the final result (Matlab, 2012). Consequently this type of summation was implemented within the matlab code.

Consider Equation 6-30 for the forced radiation efficiency re-written below.

$$\sigma_{forced}(\varphi,\theta)=\frac{kl}{2\pi}\int_{-\frac{\pi}{2}}^{\frac{\pi}{2}} sinc^2\left(\frac{kl}{2}(\sin(\varphi)+\sin(\theta))\right). \quad \text{8-3}$$

When implemented in Matlab Equation 8-3 becomes

$$\sigma_{forced}(\varphi,\theta)=\frac{kl}{2\pi}\int_{-\frac{\pi}{2}}^{\frac{\pi}{2}} sinc^2\left(\frac{kl}{2\pi}(\sin(\varphi)+\sin(\theta))\right) \quad \text{8-4}$$

the division by the additional π term within the sinc functions is as a result of Matlab's use of the normalized sinc function as opposed to the original definition.

8.2 Implementation of additional resistance at the mass air mass resonance

The use of the sinc and quadgk function as described above enhances the required integrations at points where moderate singularities occur. However, at the mass air mass resonance frequency, the extent of the dip in the STL obtained was greater than that observed from experiments. Consequently, an additional resistance term (r) (divided by $\rho_o c$) had to be added to the radiation efficiency of the reflected waves (as shown in Figure 28) in order to improve the prediction results. At the mass air mass resonance frequency the sound transmission through the wall system is at its greatest. As a result it is not completely surprising that an additional resistance term is needed to deal with the dip which occurs at this point, since very little resistance has been included into the model otherwise. The effect of different (r) values on the prediction of the STL can be seen in Figure 45.

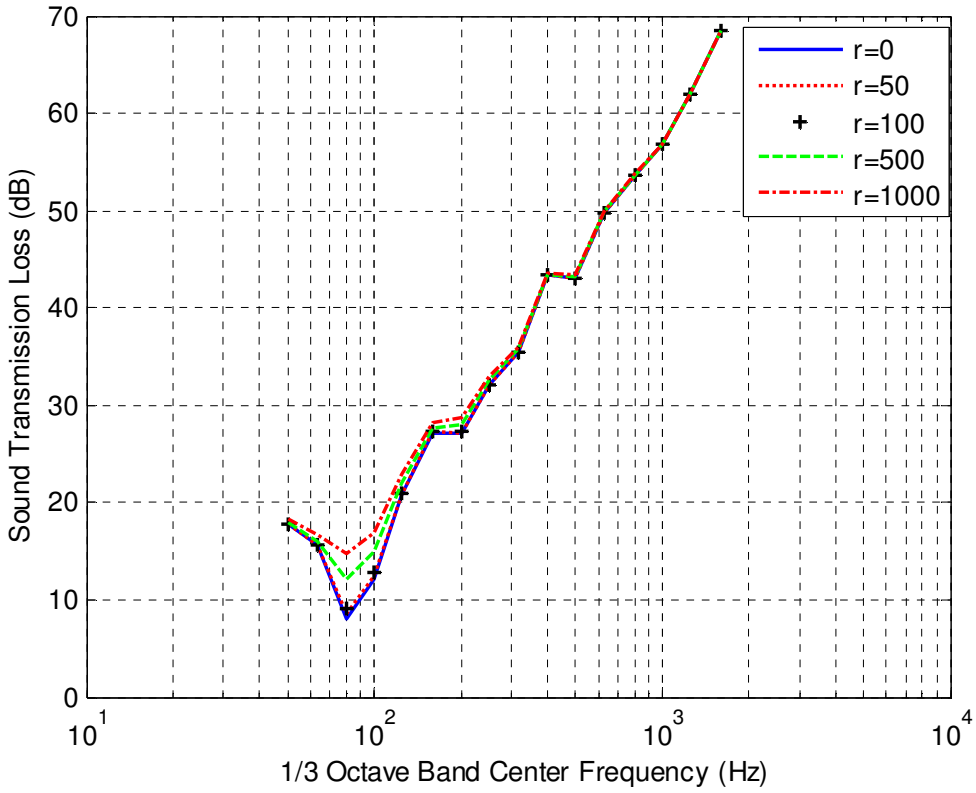

Figure 45 Effect of the resistance term r on the predicted STL for a 16 mm double leaf gypsum wall system without sound absorption material (i.e. airflow resistivity= 50 Ns/ m^4)

The results shown in Figure 45 show that as the resistance r is increased, the extent of the mass air mass resonance dip decreases. The results obtained at approximately $r = 500$ best depict what is observed from experimental results.

8.3 Iterations and convergence of the STL

An iterative model was utilized while finding the radiation efficiency of the reflected waves as discussed in Chapter 6. Consequently, the number of iterations required from this calculation in order for the STL to converge had to be assessed. This assessment was performed by studying the approximate percent relative error (ε_a) given by

$$\varepsilon_a = \frac{present\ approximation - previous\ approximation}{present\ approximation} 100\%, \qquad 8\text{-}5$$

in Chapra and Canale (2002). The greatest ε_a occurred around the mass air mass resonance frequency. The results of this assessment for a 16 mm double leaf gypsum wall system without sound absorption material within the cavity can be seen in Table 9.

Table 9 Approximate percent relative error of the STL for successive iterations of the radiation efficiency of the reflected waves

1/3 Octave Band Centre Frequency (Hz)	Iteration 2	Iteration 3	Iteration 4
80	2.62E-02	-4.56E-04	8.28E-06
100	-1.21E-02	6.52E-05	-3.49E-07
125	-2.02E-03	2.69E-06	1.80E-09
160	5.63E-04	-1.03E-06	1.91E-09
200	-1.21E-03	1.57E-06	-2.05E-09

From the results shown in Table 9 it can be seen that with successive iterations the diffuse sound field STL rapidly converges. Similar rates of conversion were obtained for the STL at discrete frequencies for different angles of incidence as well as for the radiation efficiency of the reflected waves. As a result of the small ε_a which occurs by the 4th iteration, only four iterations were used for all the prediction results obtained throughout the report here.

8.4 Summary

The numerical techniques used within the developed model have been discussed within this chapter. The implementation of the sinc and quadgk functions as well as the additional resistive term all enhanced the quality of the prediction results. An investigation into the number of iterations required for the convergence of the STL loss showed that the ε_a was insignificant after four iterations, consequently only four iterations were used for all of the reported prediction results. Finally, the implementation of the numerical techniques discussed within this chapter is justified by the improvement obtained to the prediction results once these techniques are included.

9 Alternative applications

The developed model has been used to predict the radiation efficiency and STL through double leaf wall systems in the previous chapters. Alternatively, this model can also be used in the prediction of the diffuse field and angular dependent STL through double glazed windows as well as the directivity of the transmitted sound.

9.1 Sound transmission through double pane glass systems

The developed model can be applied directly to the prediction of the airborne STL through double glazed systems. However, based on observations made by Davy (2010) the STL through double glazed systems with wider cavities is significantly affected by the structure borne sound transmission via the window frame. Consequently while investigating the STL through these systems; the airborne, structure borne and total STL are given. In these predictions the structure borne sound transmission coefficient is found from Davy's (2009c) formula given by,

$$\tau_{st} = \frac{64\rho_o c^3 D}{\left[g^2 + \left(4\omega^{\frac{3}{2}} m_1 m_2 c C_m - g\right)^2 b\omega^2\right]}, \qquad 9\text{-}1$$

where

$$g = m_1 \omega_{c2}^{\frac{1}{2}} + m_2 \omega_{c1}^{\frac{1}{2}}, \qquad 9\text{-}2$$

b is the spacing in between the studs, D is a factor to account for resonant transmission and C_m is the mechanical compliance of the stud (Davy, 2009c).

The total sound transmission coefficient is found from the sum of the airborne (τ) and structure borne transmission (τ_{st}) coefficients; since no assumption was made that the walls were coupled below f_0 within the developed airborne model, this sum was found throughout the entire

frequency range as opposed to Davy (2010) where only the airborne transmission coefficient was used below f_0.

Quirt (1981) measured the STL through different window systems mounted within an opening 2.44 m high and 3.05 m wide, with the windows mounted within the a filler wall as shown in Figure 46. The windows were mounted in wooden window frames 620 mm wide and 1760 mm high and 41 mm thick while the glass planes were 560*1680 mm with different thickness (Quirt, 1981). Comparisons between Quirt's measured STL for the 3 mm thick double glazed system with different cavity depths and the prediction results can be seen in Figure 47, while comparisons involving the 4 mm thick double glazed systems can be seen in Appendix C.

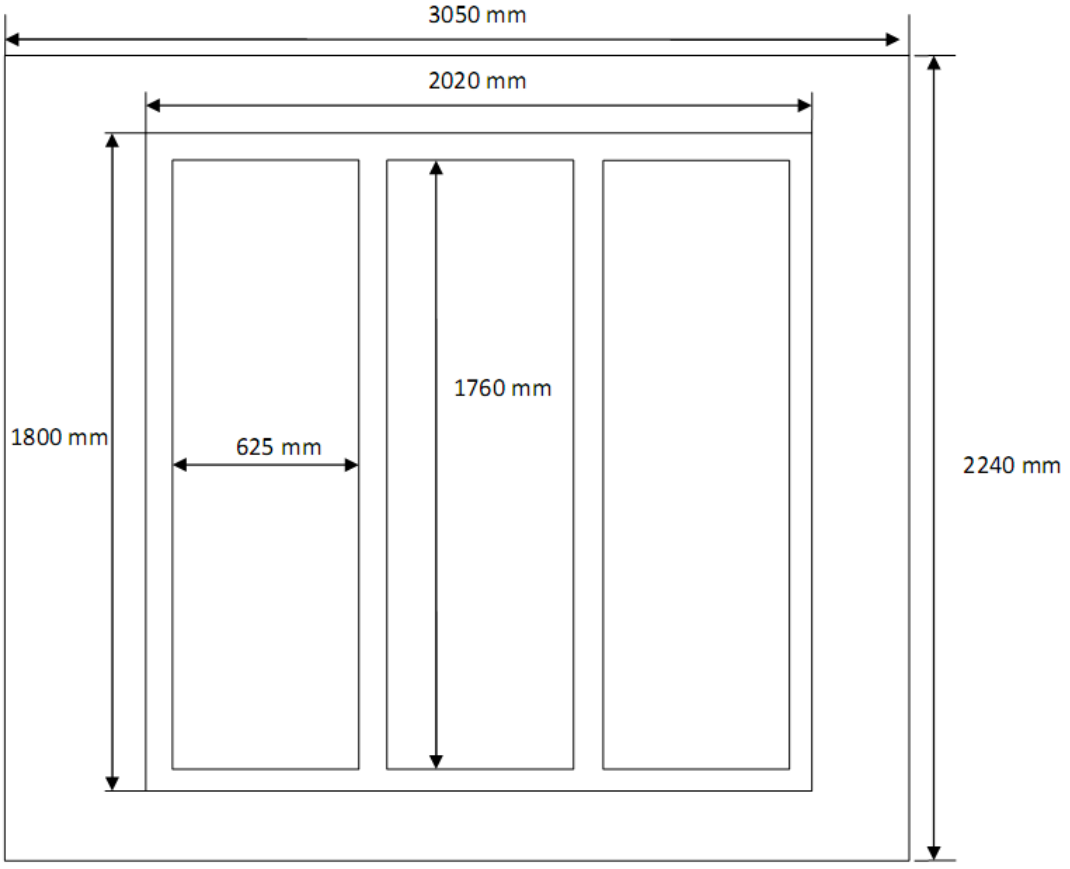

Figure 46 Location and size of the window within the filler wall used by Quirt's (1981) in the measurement of the STL

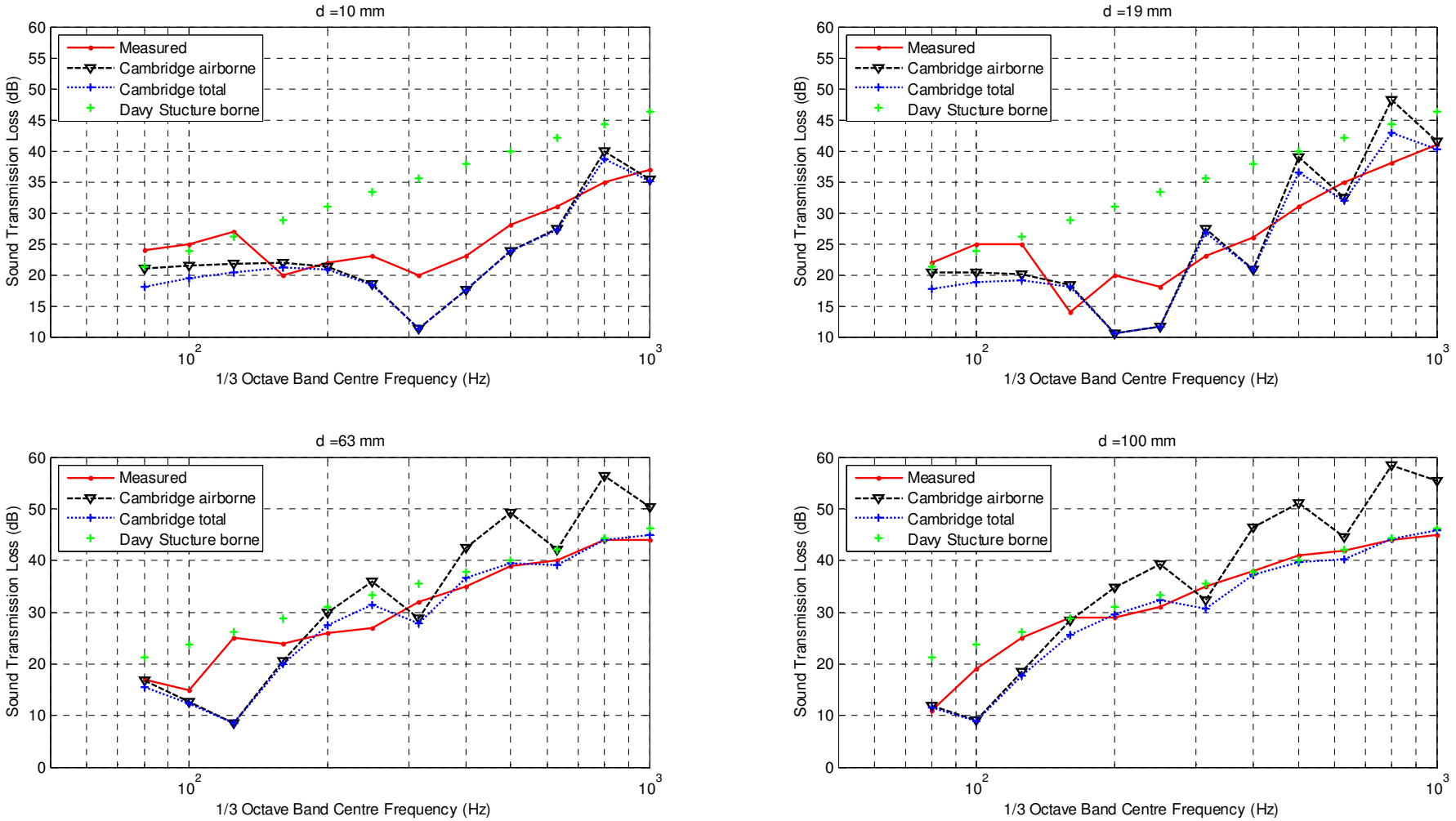

Figure 47 Comparison between NRCC measured STL and predictions for a 3 mm double glazed system with different cavity depths

In order to obtain the prediction results shown in Figure 47 it was assumed that $C_m = 0$ Pa^{-1} and the distance between the window frames was 0.67 m for the structure borne transmission, while $\Xi = 50$ Ns/m^4 , $r = 600/\rho_o c$ and $l = 0.625$ m was used for the airborne sound transmission.

The results shown in Figure 47 and Appendix C correspond well with Davy's observation that the sound transmission through the wider cavity (i.e. 100 mm cavity) is dominated by the structural transmission via the wooden window frame while the airborne sound transmission dominates the sound transmission through the smaller one. Davy (2010) did not give an explanation for this trend. However, One plausible explanation for this trend comes from Gösele's (1977) observation that as the depth of the cavity increases the stiffness of the cavity decreases. When the depth of the cavity is small, the stiffness of the cavity is high and causes the sound transmission to be dominated by the airborne sound. As the depth of the cavity increases the stiffness of the cavity decreases, while little change occurs to the sound transmission via the window frame. Consequently the structure borne sound transmission becomes dominant as the cavity depth is increased.

9.2 Rindel's external traffic STL

Rindel (1975) examined the influence of the angle of incidence on the STL of windows with respect to road traffic noise by creating a new measurement term for the STL called the external STL. This new measure utilized the radiation efficiency of the forced wave for the incident sound power as shown in Equation 7-17 in order to compensate for the problem associated with calculating the STL at grazing angles of incidence when $\cos(\theta)$ is used.

During this investigation Rindel (1975) measured the incident and transmitted pressure through scale model windows for different angles of incidence within an anechoic chamber as depicted in Figure 48. The STL from the measured sound pressures was then calculated and compared to the external STL. Unfortunately, the measurement results did not agree with the prediction obtained from Rindel's theory. Consequently, the model developed here is used to find an explanation for the reason why Rindel's theory did not agree with his measurements.

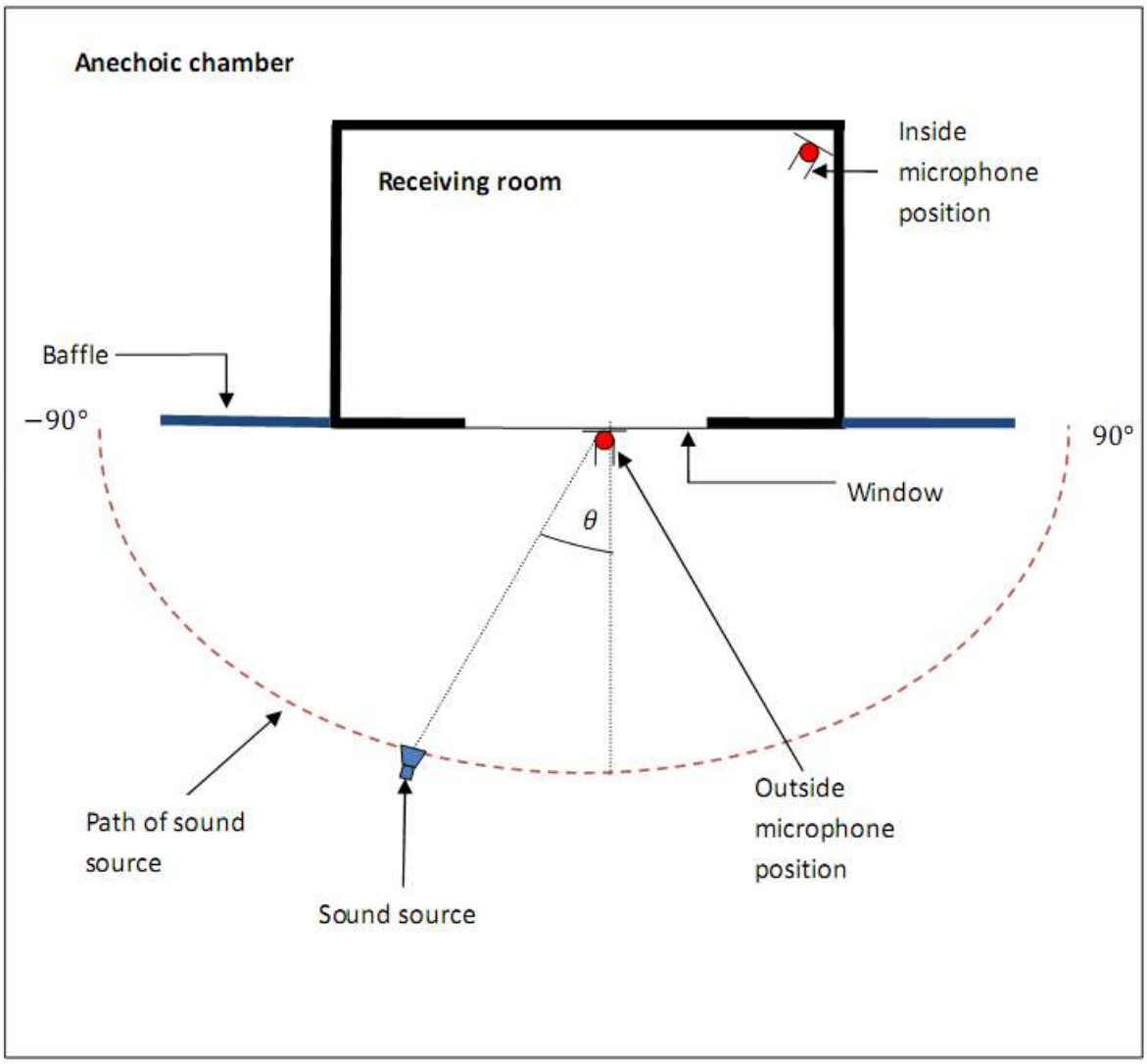

Figure 48 Depiction of Rindel's(1975) measurement setup for the traffic STL through windows

Comparisons between the measured and predicted results for a 1.64*1.2 m double glazed window with a 0.1 m cavity can be seen in Figure 49. The prediction results were obtained by assuming that the length of the vibrating strip was 1.2 m, $\boldsymbol{\Xi} = 50$ Ns/m^4 and the additional resistance term (r) was 600 while the compliance of the window frame (C_m) was assumed to be 0. The results show that for all angles of incidence the prediction obtained from the airborne sound transmission was greater than the measured results. Although the airborne STL predictions

were considerably better than Rindel's model, satisfactory results were only obtained once the structural transmission through the window frame was considered. Consequently, one plausible reason why Rindel did not obtain reasonable predictions was because he didn't consider the structural transmission via the window frame.

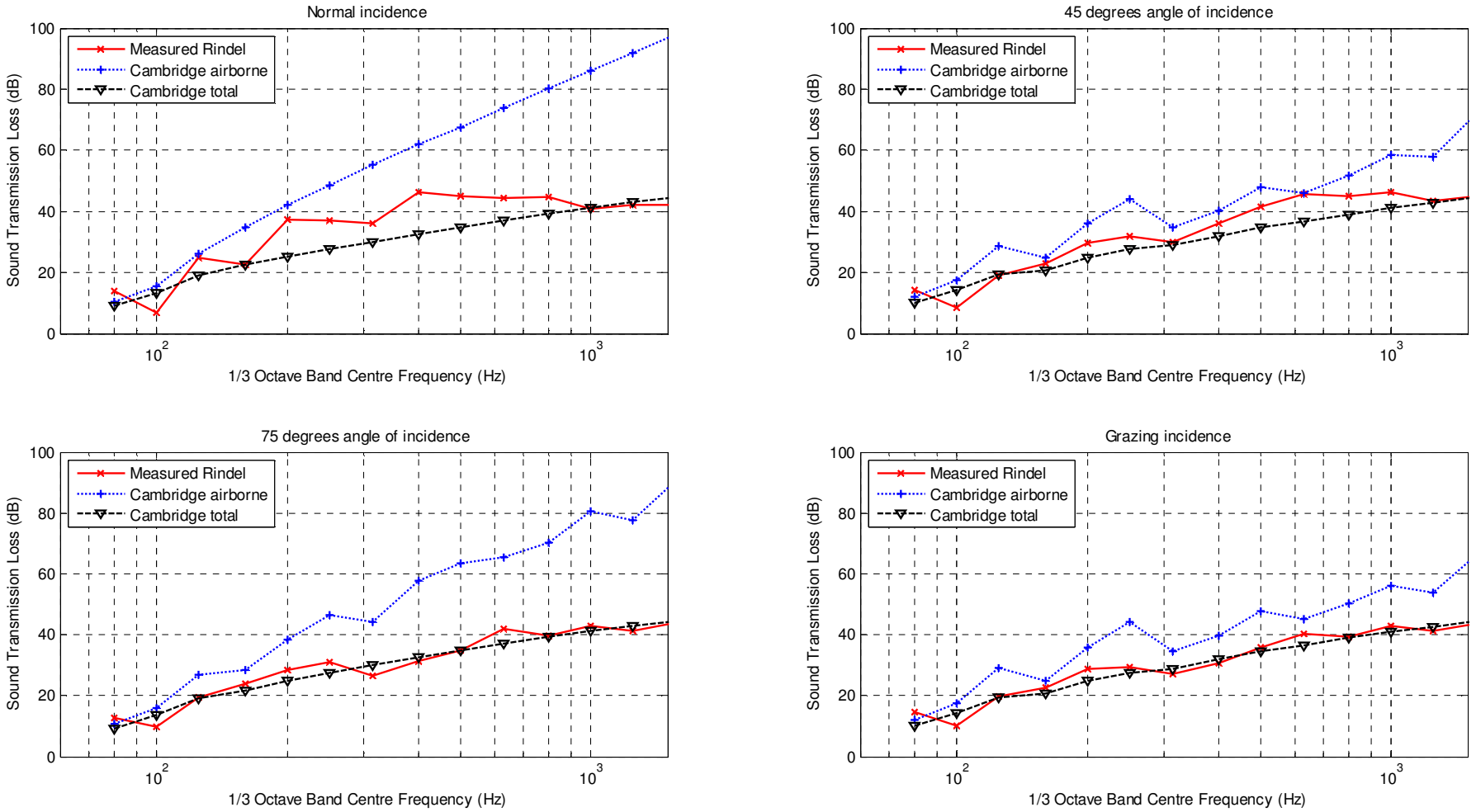

Figure 49 Comparison between Rindel's (1975) measured STL at different angles of incidence for a 1.64*1.2 m double glazed window with a 0.1 m cavity and Cambridge's prediction results

9.3 Directivity of the transmitted sound

Rindel (1975) measured the incident and transmitted sound pressure levels at different angles of incidences using the setup shown in Figure 48. Consequently the directivity of the radiated sound from double glazed windows can be calculated from this measured data. Furthermore the model developed here can be used to predict this radiated directivity.

Davy (2009a) developed a model for predicting the directivity of the sound radiating from an opening or panel excited by a sound source. Davy calculated this directivity for the situation when the sound source was located within a room with the receiver in the free field. Due to the principle of reciprocity, Davy argued that this model could also be applied to the opposite situation (i.e. with the sound source within the free field and the receiver within the room as shown in Figure 48). Consequently, by using some of the principles outlined by Davy's (2009a) model, the model developed here can be used to predict the directivity of the Rindel's (1975) measured results.

Consider the effect of the window and baffle used in Rindel's measurement setup on the sound pressure level at a particular frequency for different angles of incidence shown in Figure 50. At each particular frequency there will be a region where the incident sound pressure will double as it is reflected from the baffle. This region is illustrated in orange in Figure 50. At a particular angle, the upper and lower boundary of this region is determined by the limiting angle (θ_m). Between $\pm\theta_m$ the sound pressure does not vary with angles of incidence (or radiation) as

$$\theta_m = \begin{cases} 0 & if\ kL \leq \frac{\pi}{2} \\ \arccos\left(\sqrt{\frac{\pi}{2kL}}\right) & if\ kL > \frac{\pi}{2} \end{cases} \quad \text{9-3}$$

where θ_m is set equal to zero for values of kl less than $\pi/2$ (Davy, 2009a).

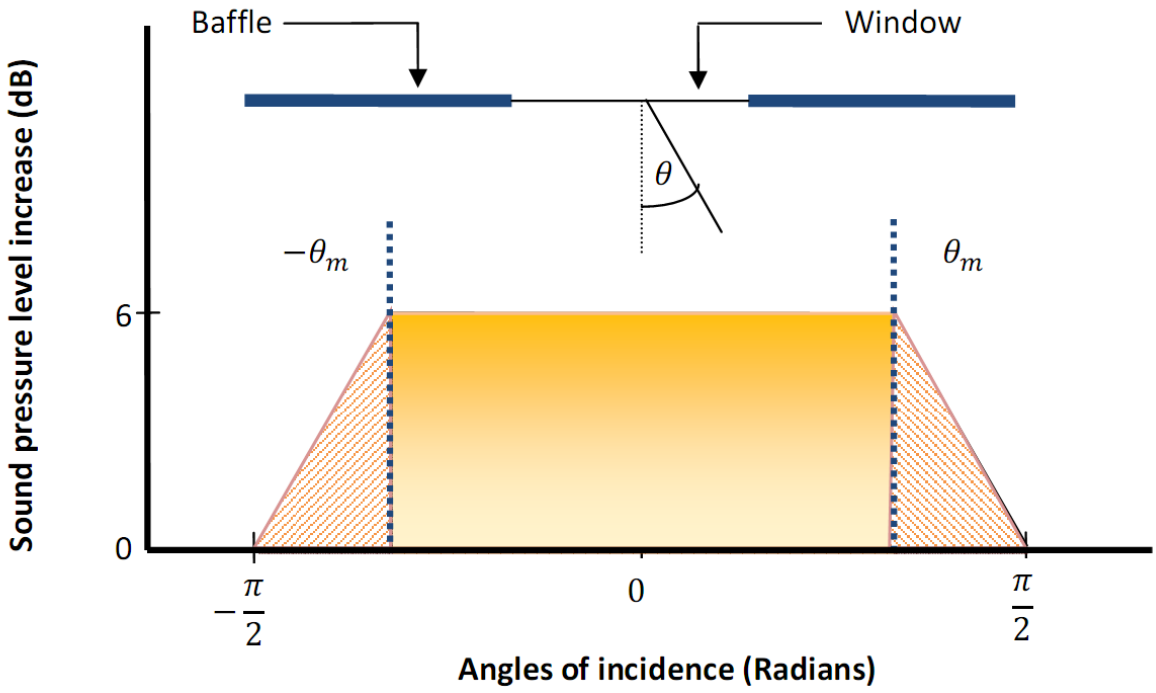

Figure 50 Illustration of the regions where pressure doubling occurs at a particular frequency for different angles of incidence

Figure 50 shows that for angles of incidence greater than θ_m or smaller than $-\theta_m$ the sound pressure level decreases. This decrease is due to the change in the diffraction of the incident sound waves by the baffle due to its finite size. Davy (2009a) used linear interpolation as a function of $\cos(\theta)$ in order to find this decrease in the sound pressure level and showed that the pressure $p(\theta)$ due to the finite size of the baffle could be found from,

$$p(\theta) = \begin{cases} p(0) & if\ \cos(\theta) \geq \cos(\theta_m) \\ \dfrac{p(0)\cos(\theta) + p\left(\frac{\pi}{2}\right)(\cos(\theta_m) - \cos(\theta))}{\cos(\theta_m)} & if\ \cos(\theta_m) > cos(\theta) \geq 0 \end{cases}. \qquad 9\text{-}4$$

$p(0)$ is the sound pressure which occurs at normal incidence and is given by,

$$p(0) = 1 + p_W p_L \qquad 9\text{-}5$$

where,

$$p_W = \begin{cases} \sin(kW) & if\ kW \leq \frac{\pi}{2} \\ 1 & if\ kW > \frac{\pi}{2} \end{cases} \quad \text{9-6}$$

and

$$p_L = \begin{cases} \sin(kL) & if\ kL \leq \frac{\pi}{2} \\ 1 & if\ kL > \frac{\pi}{2} \end{cases} \quad \text{9-7}$$

with L and W being the length and width of the baffle respectively. Equation 9-5 implies that once kL and kW are greater than $\pi/2$ the normal incidence sound pressure doubles and remains constant (i.e. sound pressure level increase plateaus at 6 dB as illustrated in Figure 50). Davy verified this result by comparing his theory to experimental results obtained by Brül and Rasmussen (1959), Muller et al. (1938), Rindel (1975) and Sivian and O'Neil (1932). Davy then showed that the relative sound pressure level ($L(\theta)$) in the direction of the angle of incidence[3] (θ) after consideration of the finite size of the baffle can be found from

$$L(\theta) = 10\log_{10}\left(|p_T(\theta)|^2 p^2(\theta)\right) - 10\log_{10}(|p_T(0)|^2 p^2(0)) \quad \text{9-8}$$

where $|p_T(\theta)|^2$ is the total mean square transmitted pressure. Since this pressure is being transmitted into a room it must be integrated over the angles of radiation because of the reverberant nature of the sound (Davy, 2009a). $|p_T(\theta)|^2$ could be found by converting the transmitted sound power used to find the sound transmission loss at particular angles of incidence in Figure 49 into the sound pressure. This can be done from the following since

[3] In Davy θ was used as the angle of radiation of the radiating sound into the free field, while ϕ was the angle of incidence when the sound source was located within the room. However, since Rindel's sound source was located within the free field, θ represents the angle of incidence while ϕ is the angle of radiation in this case.

$$\tau_{total} = \tau + \tau_{st} \qquad \textbf{9-9}$$

where, τ and τ_{st} are the transmission coefficients due to the airborne and structure borne transmission respectively. Since $\tau = W_t/W_{in}$ the transmitted power due to the structure borne sound can be found by assuming that it has the same input power (W_{in}) as the airborne sound. Therefore,

$$W_{st,t}(\theta) = \tau_{st} * W_{in}(\theta), \qquad \textbf{9-10}$$

where W_{in}could be found from Equation 7-17. Consequently $|p_T(\theta)|^2$ could be found from the developed model by using

$$|p_T(\theta)|^2 = \frac{(W_t(\theta) + W_{st,t}(\theta))\rho_o c}{S}, \qquad \textbf{9-11}$$

where S is the area of the window and W_t is the transmitted power due to airborne sound found from Equation 7-10. Furthermore, since the developed model was derived with the assumption that the window/panel is located within an infinite baffle (i.e. by assuming that pressure doubling occurred at the surface) the $p(\theta)$ correction term in Equation 9-8 is needed in order to compensate for the finite size of the baffle used by Rindel (1975).

Comparisons between the measured relative sound pressure level (SPL) and the predictions obtained from the developed theory can be seen in Figure 51. The "measured" results were obtained by taking the difference between the sound pressure level at normal incidence and the corresponding angle of incidence.

The "relative SPL" also shown in Figure 51 is calculated using Equation 9-8, while the "weighted" results shown were obtained by multiply the predicted sound pressure (i.e. Equation 9-11) by a weighting factor $w(\varphi)$ divided by the effective impedance of a finite panel in an infinite baffle such that

$$Weighted = \int_{-\frac{\pi}{2}}^{\frac{\pi}{2}} \frac{w(\varphi)}{\left|2\rho_o c(\varphi) + Z_{wp}(\varphi)\right|^2} \left|p_T(\theta,\varphi)\right|^2 d\varphi, \quad \textbf{9-12}$$

where, $2\rho_o c(\varphi) + Z_{wp}(\varphi)$ is the effective impedance of a finite panel assuming that the impedance on both the receiving and transmitting sides of the panel are the same and

$$w(\varphi) = (1-\alpha)^n, \quad \textbf{9-13}$$

with α being the sound absorption coefficient of the walls of the room and

$$n = \frac{b}{g}\tan(\varphi), \quad \textbf{9-14}$$

where, b is the distance from the receiver to the nearest point on the surface of the window and g is the length of the room in the plane containing the incident ray (Davy, 2009a). The weighting factor $w(\varphi)$ is needed as the sound waves radiating at grazing angles will have more wall collisions and therefore be more attenuated before reaching the receiving position (Davy, 2009a). Since $w(\varphi)$ is dependent on the angle of radiation (φ), the total pressure/power must be multiplied by $w(\varphi)$ before it is integrated over the angles of radiation.

Finally the original result shown in Figure 51 was found from the difference between the predicted sound pressure level at normal incidence and the corresponding angle of incidence from Equation 9-11 without considering the effect of the finite baffle as done in Equation 9-8.

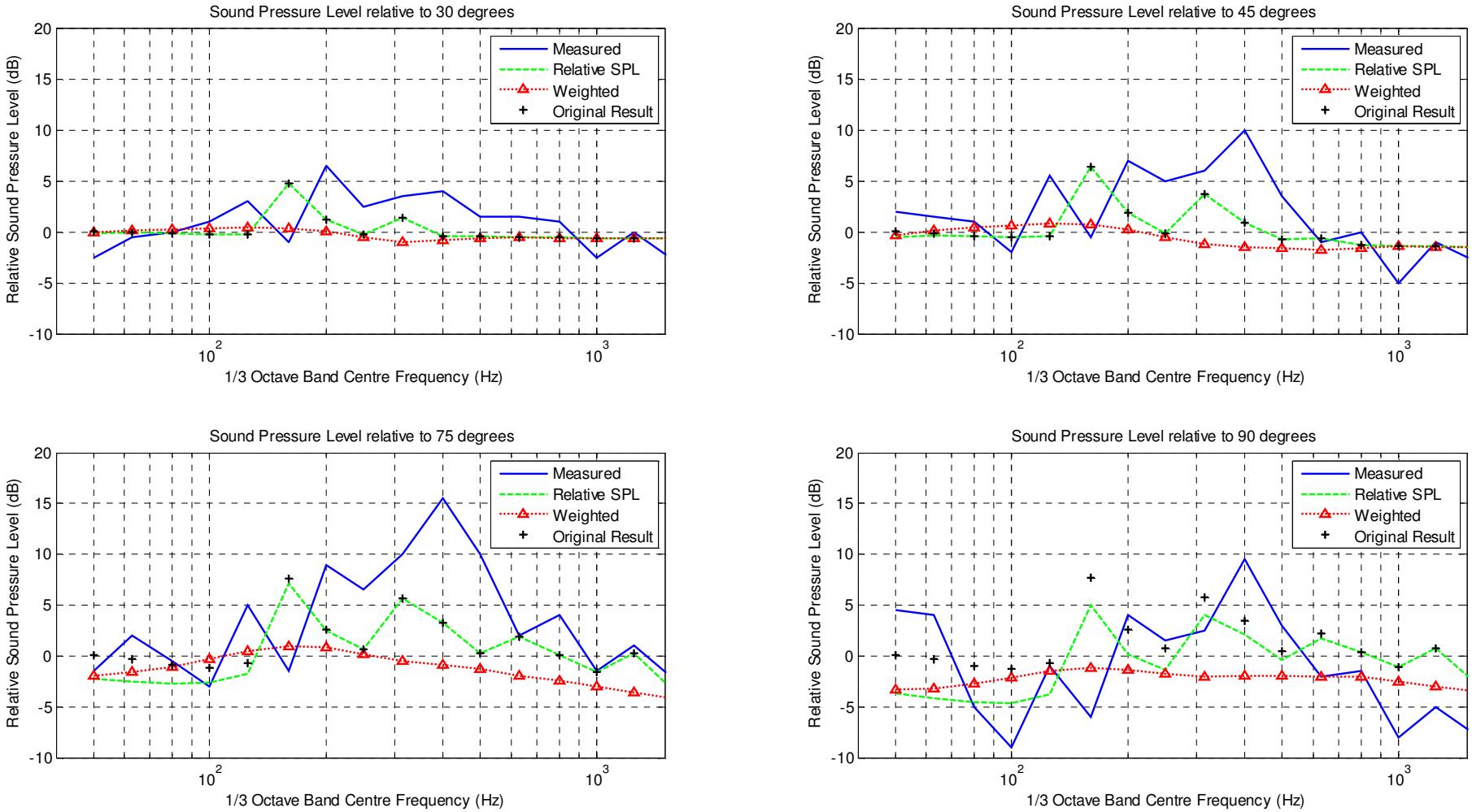

Figure 51 Relative sound pressure level of the transmitted sound from Rindel's (1975) 1.64*1.2 m double glazed window with a 0.1 m cavity

The results shown in Figure 51 show that the prediction obtained from the relative SPL results best compare to the measured values; while the effect of the finite baffle could be seen by comparing the "relative SPL" result to the "original" result. This effect was greatest at grazing incidence, since the results were similar at the other angles of incidence as expected. With regard to the "weighted" results, it would appear that this weighting is not needed for the present model as the inclusion of the effect of the structure borne sound seems to be the dominating feature in the model. Consequently, it can be concluded that the reason why Rindel's measurement results appear to be almost omni-directional is due to the presence of the structure borne transmission.

9.4 Conclusions

The diffuse sound field STL, the angular dependent STL as well as the directivity of the transmitted sound through double glazed windows have been calculated within this chapter. From these predictions the following conclusions can be made:

- The reduction of the stiffness of the cavity with increased depth is responsible for the dominance of the structure borne sound within larger cavities
- The reason why Rindel (1975) was unable to obtain satisfactory prediction results for his directivity and STL calculations was because he didn't take into account the structure borne transmission
- Once the structure borne transmission is taken into account the additional weighting term $w(\varphi)$ is not needed to compensate for the extra wall collisions which the sound experiences when radiated at grazing incidence
- The effect of taking into account the finite size of the baffle can only be seen near to the grazing incidence.
- The reciprocity argument provided by Davy (2009a) for the prediction of the directivity of sound radiating into a room is valid as the calculations performed here were in the opposite direction to the that used within his model

These conclusions provide additional insight into the factors which affect both the STL and directivity of the radiated sound through windows. Their significance comes not only from the fact that they explain the trends associated with Rindel (1975) and

Quirt's (1981) measurements, but also because they are applicable to any baffled system.

10 Conclusions

The influence of the wall cavity and any associated sound absorption material on the STL of double leaf/glazed systems has been investigated. The research was justified by the fact that some of the existing prediction models could not explain some observed experimental trends. Consequently, the reported work gave explanations for some of these discrepancies found within the literature.

The research began by first looking at the influence of the wall cavity on the STL from experimental trends. This investigation revealed that a wide variety of conclusions exists within the literature with regard to how the material's airflow resistivity, density, thickness, amount, location as well as the type of material and size of the cavity affect the STL. The effects of these parameters are highly dependent on the type of structural connections, the properties of wall panels, whether the cavity is filled with sound absorption material or not as well as the frequency range of interest; as a result caution must be taken when alterations are being made. The implications of the latter conclusion is that the potential of the cavity for improving the STL is related to other properties of the wall system and all recommendations given for the appropriate parameters which govern the cavity should be taken with this in mind. The importance of the relationship between the parameters which govern the wall cavity and the rest of the wall system was clearly shown from the literature when it was demonstrated that the effectiveness of the wall cavity on the STL decreases when the mass of the wall panels and rigidity of the wall connection is increased. Furthermore this understanding was instrumental in explaining why the STL was dominated by the structural transmission through double glazed windows as the depth of the cavity is increased.

A major part of the reported work dealt with explaining the reason why London's model under-predicted the STL and why Davy's (2009c) model with a limiting angle of 61° corresponds to Sharp's (1973; 1978). The importance of understanding the interaction between the forced waves within the wall cavity as well as the radiation efficiency of the transmitted waves was made apparent.

With regard to London's (1950) model, it was demonstrated that the effect of the angular dependent mass air mass resonance frequency was responsible for the under-prediction of the STL obtained. The analysis showed that although the resonance peak in the particle velocity of the forced wave varied with the angle of incidence, it is the interaction of the reflected forced waves which is responsible for ensuring that the total resonance peak of the particle velocity remained at the normal mass air mass resonance frequency. The frequencies of the first few modes above the mass air mass resonance frequency were also identified and it was shown that the observations made in the work reported agreed with Prasetiyo and Thompson's (2012) model even though the techniques employed were different. The conclusion made about the effect of the angular dependent mass air mass resonance frequency has implications for all STL models which assume that the length of the panel or cavity is of infinite extent, regardless of the relative techniques (such as the limiting the angle of incidence or spatial windowing technique) used to account for the finite size of the wall system. Evidence of this was demonstrated when explaining the reason why Davy's (2009c) model with a limiting angle of 61° corresponds to Sharp's (1973; 1978).

The reported work showed that although Davy's original model which is based on Rudder's (1985) and Mulholland's (1967) models improved the prediction of the STL through the use of the frequency dependent limiting angle based on Swell's (1970) theory: The detrimental effects of the angular dependent mass air mass resonance frequency was responsible for Davy's original model under-prediction of the STL when compared to Sharp's. Although these detrimental effects were masked in Davy's original model due to the inclusion of sound absorption material within the cavity, its effects were clearly seen when it was demonstrated that the 18 dB/Octave obtained from Sharp's model could not be attained from Davy's without limiting the angle of incidence to 61°. Consequently, it was concluded that the reason why Sharp's model which utilized the normal incident STL accurately predicted the STL was because it avoided the detrimental effects of the angular dependent mass air mass frequency.

The explanations given for the issues associated with London's and Davy's model were obtained by studying the STL results derived from the developed two-

dimensional vibrating strip model. While developing this model, the radiation efficiency of the forced and reflected forced waves within the cavity, as well as the radiated sound pressure and power were found.

The developed STL model took into account the phase relationship between the forced and reflected forced wave as well as the difference in the radiation efficiency of these waves. This was necessary because the rate of attenuation and the wavelength of both waves were different. The predictions obtained for the STL compared well to experiments for both the empty and full cavity case although an additional resistance term and a reduced airflow resistivity had to be incorporated within the model. The inclusion of the additional resistance term r was needed to improve the prediction of the STL at the mass air mass resonance frequency. While the difference between the normal and planar airflow resistivity, the possible movement of the sound absorption material within the cavity and the possible increase in the radiation efficiency of the free bending waves due to the presence of the sound absorption material within the wall cavity were the three possible explanations given for the reason why the reduced airflow resistivity was required.

The development of the model for the radiation efficiency of the forced and reflected waves within the wall cavity as well as the discussion surrounding the use of the forced radiation efficiency as a replacement for $1/\cos(\theta)$ while calculating the incident power was crucial to the presented theory.

The approach presented for the calculation of the forced radiation efficiency was different from that used by Davy (2009b), Ljunngren (1991), Sato (1973) and Sewell (1970) in their models. The results obtained when compared to Davy's (2009b) model were similar to Ljunngren's (1991) results when he compared his two-dimensional to model to Sato and Sewell's three dimensional models. Careful inspection of Davy's (2009b) model revealed that although it was developed as an analytical two-dimensional model, its low frequency correction factor accounted for radiation into a three dimensional space. Consequently a modification of Davy's model to account for the radiation efficiency into a two-dimensional space was presented. Comparisons between the modification of Davy's model and the vibrating strip model were satisfactory.

An iterative model for the radiation efficiency of the reflected forced waves within the wall cavity was also developed and provided a qualitative explanation for various trends associated with the STL. The analysis of these results obtained for the radiation efficiency of these waves was conducted in relation to how the airflow resistivity, depth of the cavity and mass of the wall panels affected these results. This was necessary because the rate of attenuation (Re (γ)) of the reflected waves is dependent on these parameters. This analysis was crucial in improving the understanding of the mechanism through which sound is transmitted through double leaf systems as it was shown that it is the reflection of the forced waves within the cavity which determine the influence of the wall cavity and any associated material placed within it on the STL.

With regard to the use of the finite forced radiation efficiency as a replacement for $1/\cos(\theta)$ while calculating the incident power. It was discussed that although the use of this substitution was done successfully by Rindel (1975), Villot et al (2001) and Vigran (2009) such actions do not correspond to the current measurement technique used to measure the STL. However, this method provided a reasonable solution to what occurs at grazing incidence. Consequently, it was decided that the finite forced radiation efficiency be used when calculating the angular dependent STL while the infinite radiation efficiency was employed for the diffuse sound field STL. This was done to ensure that the prediction model best emulate the measurement technique used.

The developed model was also used to predict the STL and directivity through double glazed windows. Comparisons to measurements showed that as the depth of the cavity was increased the structural transmission via the window frame became dominant. The reduction of the cavity stiffness with increased depth was the explanation given for this trend. Furthermore this trend gave insight into the reason why Rindel's theory could not accurately predict the STL or directivity for his window systems as he didn't take into account the effect of the structural transmission. The predictions obtained for the directivity of the transmitted sound were satisfactory. It was shown that the finite size of the baffle was only needed when considering the sound transmission near to grazing angles of incidence. Furthermore it was shown that the

weighting factor $w(\varphi)$ used by Davy is not needed once the structure borne transmission is taken into account.

Finally the reported work has provided significant insight into some of the unanswered questions posed within the literature. The results and conclusions obtained are applicable to all analytical models which are based on the assumption that the elements of the cavity wall system are of infinite extent. Therefore, the physical explanation why such models (without the limiting angle of incidence or use of the spatial windowing technique) under-predict the STL has now been attained. Furthermore, the work shows that the study of the interaction between the forced and reflected forced waves along the cavity is crucial to our understanding of the sound transmission below the critical frequency. Consequently, the understanding gained from the developed model can be combined with the insights obtained from numerical finite element techniques which only consider the finite size of the cavity. As a result, the contributions provided by this reported work fall directly between the gap created by the infinite and the finite based models and will be useful when future attempts at improving the prediction of the STL through cavity wall systems are made.

Appendix A: Descriptions of NRCC's wall systems

Reported STL measurement results from the NRCC were used to verify the accuracy of the predictions obtained from the developed theory. In this section the gypsum plasterboard, sound absorption material and wall systems are described.

Table 10 and Table 11 give the properties of the gypsum plasterboard and sound absorption respectively, while Figure 52 and Figure 53 show a depiction of the single and double stud wall system respectively. Descriptions of the single and double stud wall systems are given in Tables 13, 14 and 15.

Table 10 Thickness and surface density of the gypsum plasterboard measured by the NRCC (Halliwell *et al.*, 1998)

	Surface Density (kg/m^2)	
Nominal Type	Average Value	Standard Deviation
15.9 mm Type X (A)	11.5	0.1
15.9 mm Type X (B)	10.9	0.1
15.9 mm Type X (C)	11.2	0.3
12.7 mm Type X (A)	10.0	0.2
12.7 mm Type X (B)	9.7	0.2
12.7 mm Type X (C)	8.7	0.1
12.7 mm (A)	7.6	0.2
12.7 mm (B)	8.2	0.1
12.7 mm (B) light weight	7.3	0.1
12.7 mm (C)	8.0	0.2

Table 11 Thickness, density and airflow resistivity of the sound absorption materials used within the wall cavity by the NRCC (Halliwell *et al.*, 1998)

		Density (kg/m^3)		Airflow Resistivity (mks rayls/m)	
		Average Value	Standard Deviation	Average Value	Standard Deviation
glass fibre (G1)	89 mm batt	12.2	0.4	4800	400
glass fibre (G1)	65 mm batt	11.7	1.0	3600	200
glass fibre (G1)	150 mm batt	11.2	0.0	4300	700
glass fibre (G2)	89 mm batt	16.4	0.6	7900	400
mineral fibre (M1)	89 mm batt	32.6	2.1	12700	2300
mineral fibre (M1)	65 mm batt	36.7	2.1	11400	1700
mineral fibre (M2)	75 mm batt	44.2	1.7	16600	900
mineral fibre (M2)	40 mm batt	51.9	2.2	15000	500
mineral fibre (M3)	83 mm batt	98.1	1.3	58800	5200
cellulose (C1)	wet spray	56.3	10.2	N/A	N/A
cellulose (C2)	90 mm blown	49.3	6.0	33000	

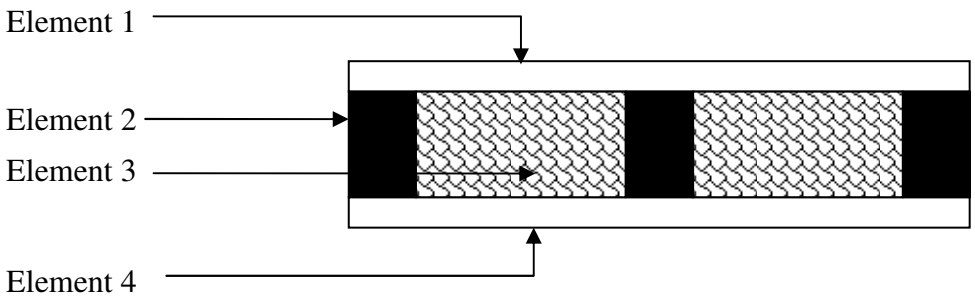

Figure 52 Schematic of the single stud system used by the NRCC (Halliwell *et al.*, 1998)

Table 12 Description of the single stud wall system measured by the NRCC and utilized within the reported work (Warnock, 2010)

NRCC test number	Element 1*	Element 2	Element 3	Element 4*
TL-92-262	16 mm gypsum plasterboard screwed at 203 mm on centre	90 mm steel studs 813 on centre	Air	16 mm gypsum plasterboard screwed at 203 mm on centre
TL-92-263	16 mm gypsum plasterboard screwed at 406 mm on centre	90 mm steel studs 813 on centre	Air	16 mm gypsum plasterboard screwed at 406 mm on centre
TL-92-264	16 mm gypsum plasterboard screwed at 813 mm on centre	90 mm steel studs 813 on centre	Air	16 mm gypsum plasterboard screwed at 813 mm on centre
TL-92-276	16 mm gypsum plasterboard, minimum screws	N/A	Air	16 mm gypsum plasterboard, minimum screws
TL-92-275	16 mm gypsum plasterboard, minimum screws	N/A	90 mm glass-fibre (G1)	16 mm gypsum plasterboard, minimum screws

*A density of 770 kg/m^3 was assumed

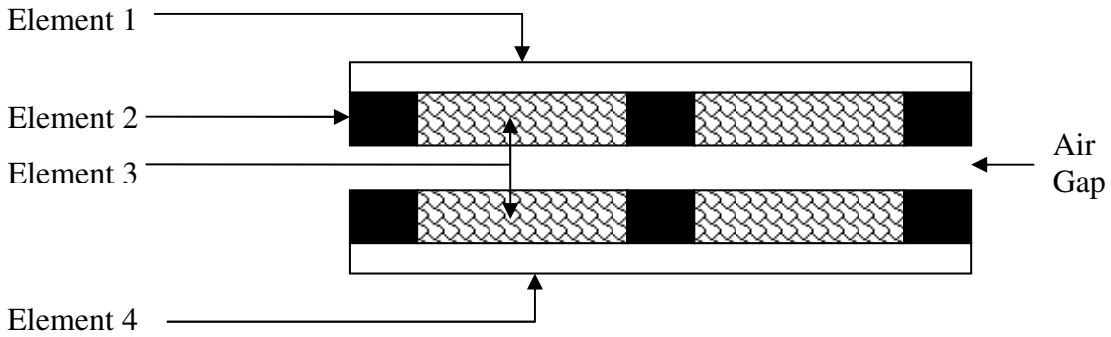

Figure 53 Depiction of the double stud wall system measured by the NRCC (Halliwell et al., 1998)

Table 13 Description of the double stud wall system measured by the NRCC with a 10 mm air gap (Warnock, 2010)

NRCC test number	Element 1*	Element 2**	Element 3	Element 4
TL-92-265	16 mm gypsum plasterboard screwed at 813 mm on centre	40 mm steel studs 813 on centre	Air	16 mm gypsum plasterboard screwed at 813 mm on centre
TL-92-266	16 mm gypsum plasterboard screwed at 406 mm on centre	40 mm steel studs 610 on centre	Air	16 mm gypsum plasterboard screwed at 406 mm on centre
TL-92-267	16 mm gypsum plasterboard screwed at 203 mm on centre	40 mm steel studs 610 on centre	Air	16 mm gypsum plasterboard screwed at 203 mm on centre
TL-92-268	16 mm gypsum plasterboard screwed at 203 mm on centre	40 mm steel studs 610 on centre	90 mm glass-fibre (G1)	16 mm gypsum plasterboard screwed at 203 mm on centre
TL-92-270	16 mm gypsum plasterboard screwed at 406 mm on centre	40 mm steel studs 610 on centre	90 mm glass-fibre (G1)	16 mm gypsum plasterboard screwed at 406 mm on centre
TL-92-274	16 mm gypsum plasterboard screwed at 813 mm on centre	40 mm steel studs 610 on centre	90 mm glass-fibre (G1)	16 mm gypsum plasterboard screwed at 813 mm on centre

*A density of 770 kg/m^3 was assumed

** Studs placed on each side of the double leaf wall

Table 14 Description of the double stud wall system measured by the NRCC (Halliwell *et al.*, 1998) with a 25 mm air gap

NRCC test number	Element 1	Element 2	Element 3	Element 4
TL-93-279*	12.7 mm Type X (A)	90 mm wood studs on 406 centre	90 mm glass-fibre (G1)	12.7 mm Type X (A)
TL-93-277	12.7 mm Type X (A)	90 mm wood studs on 406 centre	65 mm glass-fibre (G1)	12.7 mm Type X (A)
TL-93-273	12.7 mm Type X (B)	90 mm wood studs on 406 centre	90 mm glass-fibre (G1)	12.7 mm Type X (B)
TL-93-278	12.7 mm Type X (A)	90 mm wood studs on 406 centre	90 mm glass-fibre (G2)	12.7 mm Type X (A)
TL-93-296*	12.7 mm Type X (A)	90 mm wood studs on 610 centre	110 mm cellulose (C2)	12.7 mm Type X (A)
TL-93-288	12.7 mm Type X (A)	90 mm wood studs on 610 centre	90 mm glass-fibre (G1)	12.7 mm Type X (A)
TL-93-289	12.7 mm Type X (C)	90 mm wood studs on 610 centre	90 mm glass-fibre (G1)	12.7 mm Type X (C)
TL-93-290	12.7 mm Type X (B)	90 mm wood studs on 610 centre	90 mm glass-fibre (G1)	12.7 mm Type X (B)
TL-93-284	12.7 mm Type B	90 mm wood studs on 610 centre	90 mm glass-fibre (G1)	12.7 mm Type B
TL-93-291	12.7 mm Type A	90 mm wood studs on 610 centre	90 mm glass-fibre (G1)	12.7 mm Type A
TL-93-294	12.7 mm Type C	90 mm wood studs on 610 centre	90 mm glass-fibre (G1)	12.7 mm Type C
TL-93-265*	12.7 mm Type X (C)	90 mm wood studs on 406 centre	90 mm glass-fibre (G1)	12.7 mm Type X (C)
TL-93-262	15.9 mm Type X (C)	90 mm wood studs on 406 centre	65 mm glass-fibre (G1)	15.9 mm Type X (C)
TL-93-263	15.9 mm Type X (C)	90 mm wood studs on 406 centre	90 mm glass-fibre (G2)	15.9 mm Type X (C)
TL-93-266	15.9 mm Type X (C)	90 mm wood studs on 406 centre	90 mm glass-fibre (G1)	15.9 mm Type X (C)
TL-93-264	15.9 mm Type X (C)	90 mm wood studs on 406 centre	90 mm mineral fibre (M1)	15.9 mm Type X (C)
TL-93-295	15.9 mm Type X (C)	90 mm wood studs on 610 centre	90 mm cellulose (C2)	15.9 mm Type X (C)
TL-93-281	15.9 mm Type X (C)	90 mm wood studs on 610 centre	90 mm glass-fibre (G1)	15.9 mm Type X (C)
TL-93-292	15.9 mm Type X (A)	90 mm wood studs on 610 centre	90 mm glass-fibre (G1)	15.9 mm Type X (A)
TL-93-293	15.9 mm Type X (B)	90 mm wood studs on 610 centre	90 mm glass-fibre (G1)	15.9 mm Type X (B)

*Less than 50% of the wall cavity filled with sound absorption material

Appendix B: Predicted and measured STL through double leaf gypsum walls

Comparisons between the measured and predicted results for the double stud wall systems with a 205 mm deep cavity as described in Appendix A are given within this section. The prediction results were obtained by utilizing 40 % of the airflow resistivity when the wall cavity was fully filled and 20% when less than 50% of the cavity was filled. The additional resistance r was taken to be 600 while the length of the strip was 2.44 m.

Generally, the predicted results of the 21 different wall systems compare well with the measurements obtained. In most cases the largest discrepancies occurred below 100 Hz. The results shown within this section illustrate the fact that the model does produce satisfactory results for different densities of the gypsum plasterboard as well as for different types and amount of sound absorption material placed within the cavity.

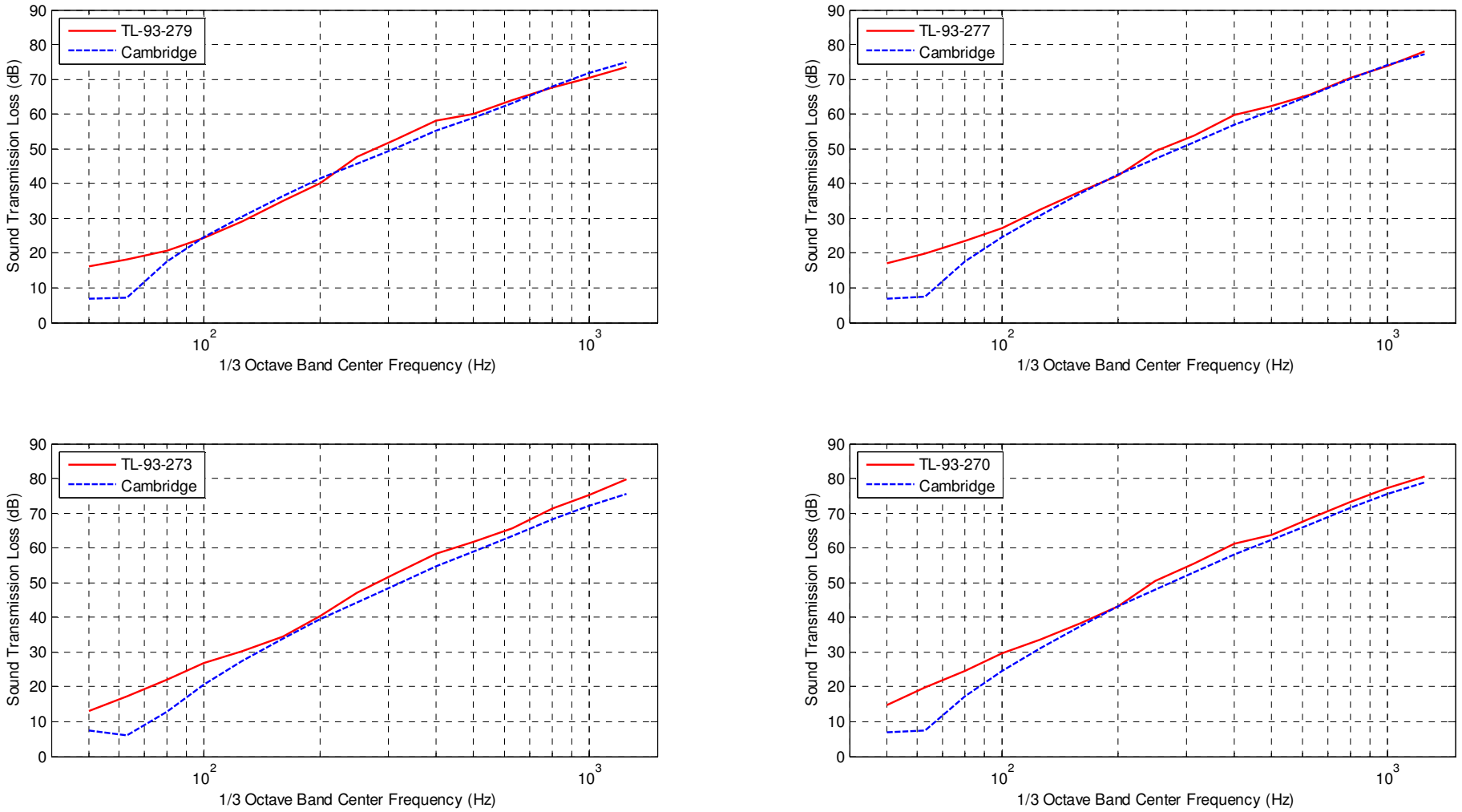

Figure 54 Predicted and measured STL for TL-93-279, TL-93-277, TL-93-273, TL-93-270

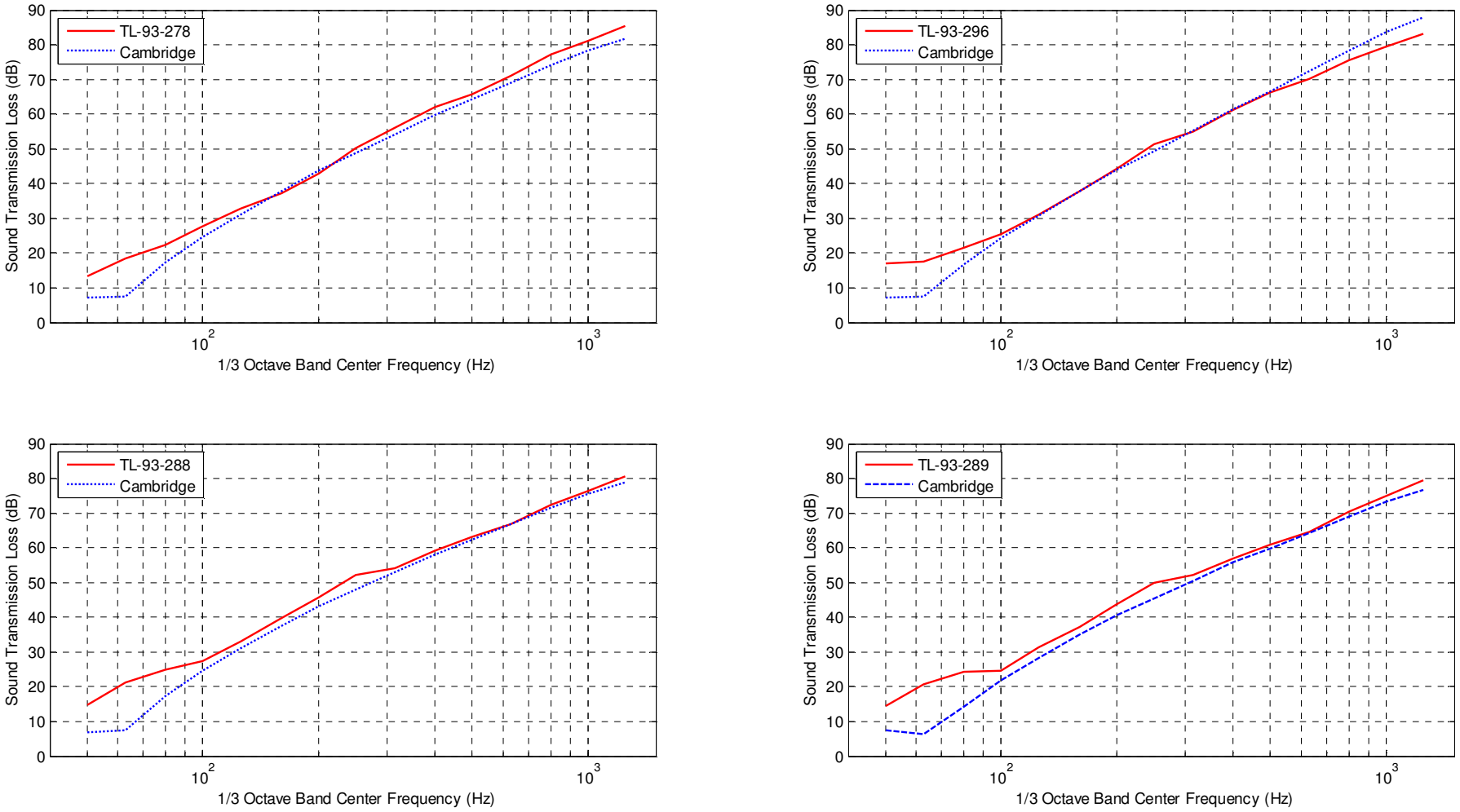

Figure 55 Predicted and measured STL for TL-93-278, TL-93-296, TL-93-288, TL-93-289

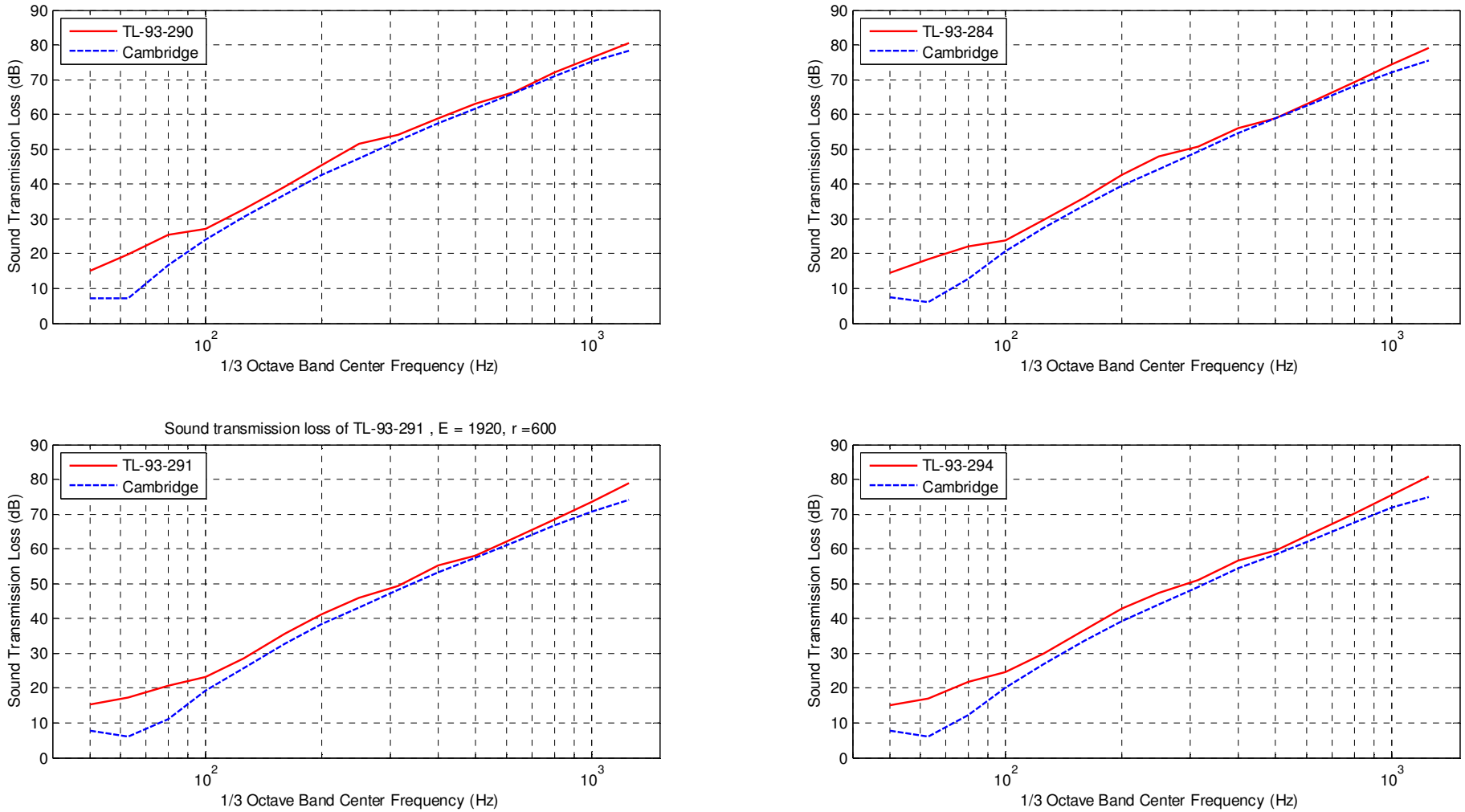

Figure 56 Predicted and measured STL for TL-93-290, TL-93-284, TL-93-291, TL-93-294

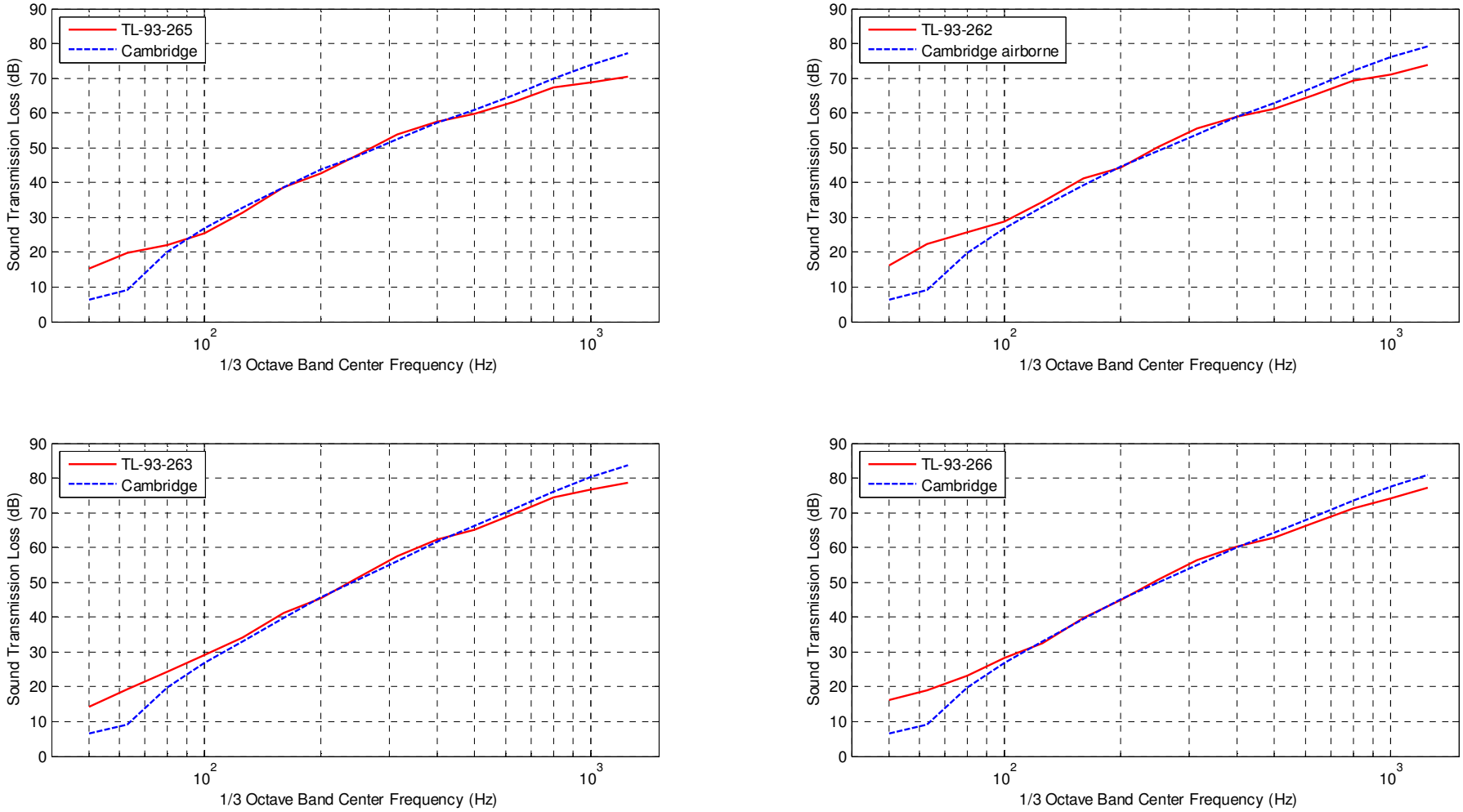

Figure 57 Predicted and measured STL for TL-93-265, TL-93-262, TL-93-263, TL-93-266

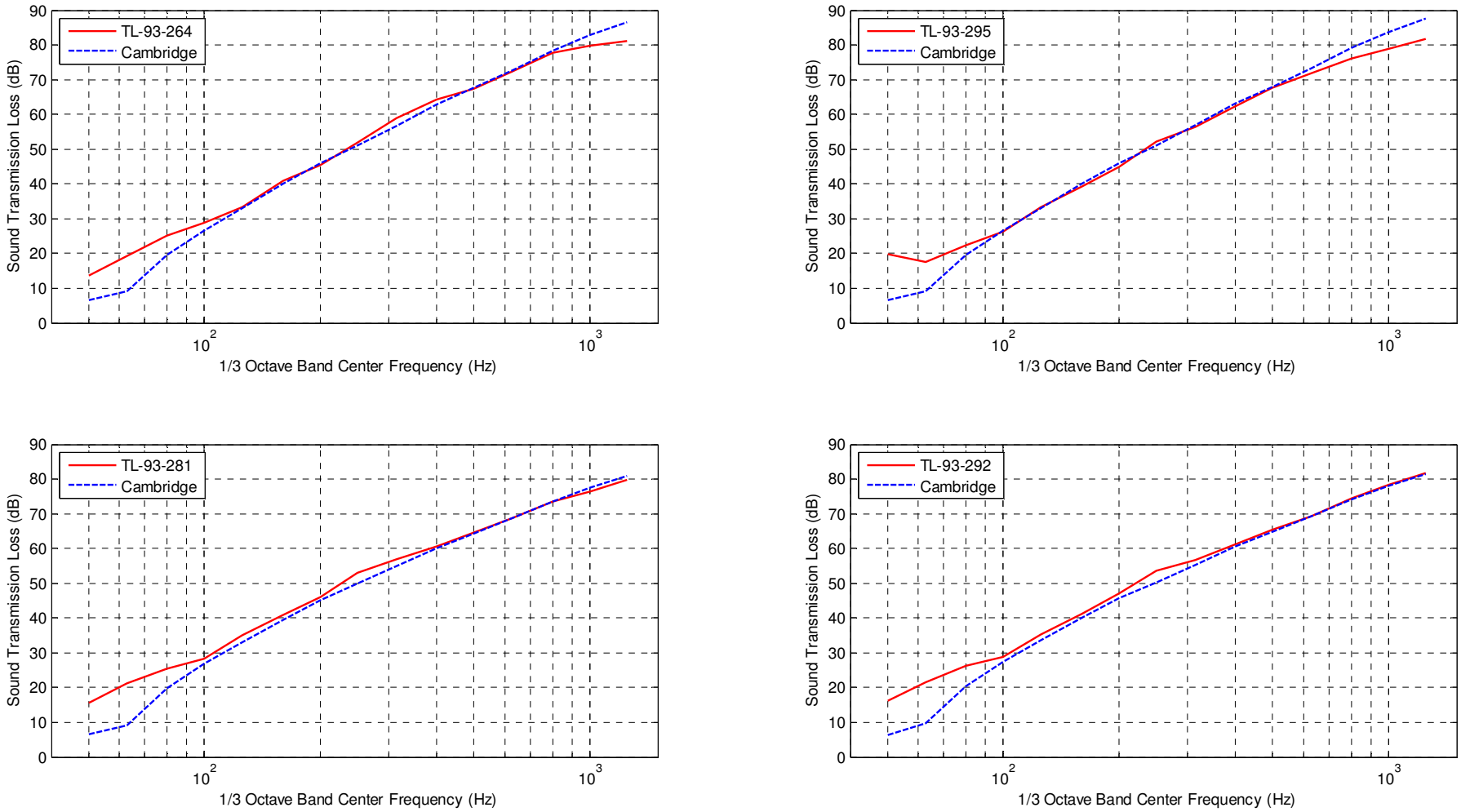

Figure 58 Predicted and measured STL for TL-93-264, TL-93-295, TL-93-281, TL-93-292

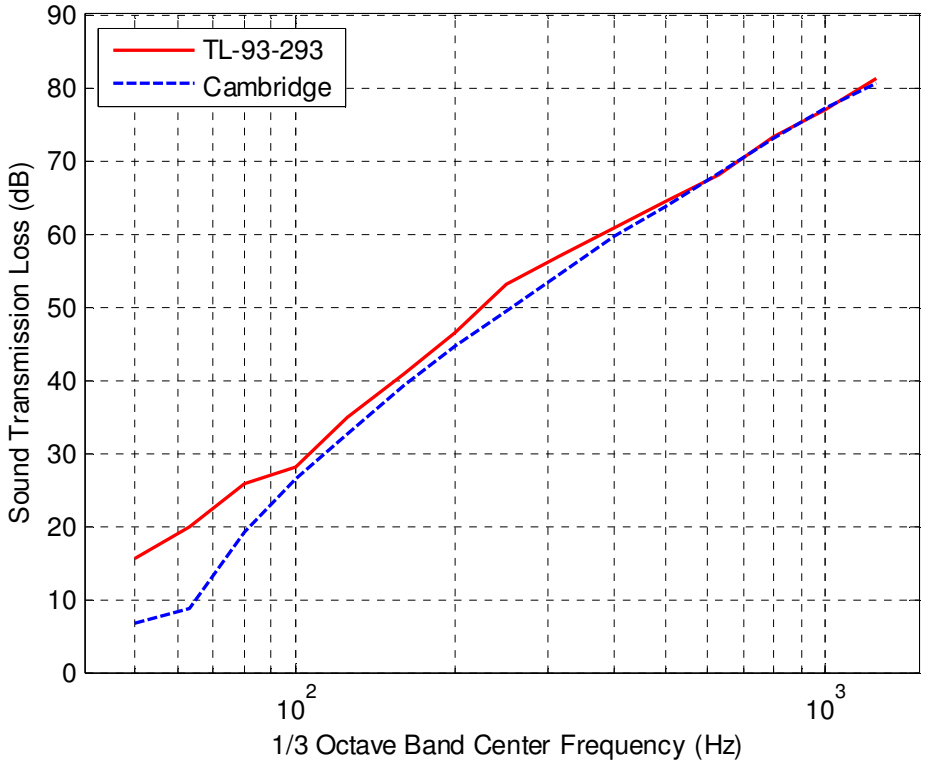

Figure 59 Predicted and measured STL for TL-93-293

Appendix C: Predicted and measured STL through double glazed windows

Comparisons between the measured and predicted results for Quirt's (1981) measured the STL through different double glazed window systems are given within this section. The results shown in Figure 60 are for double glazed windows with 3 mm thick window panes with different cavity depths, while the results shown in Figure 61 and Figure 62 are for 4 mm thick double window panes.

In order to obtain the prediction results shown in this section it was assumed that the compliance of the window frame, $C_m = 0$ Pa^{-1} and the distance between the window frames was 0.67 m for the structure borne transmission, while the airflow resistivity $\Xi = 50$ Ns/m^4 , the resistance $r = 600/\rho_o c$ and the length of the cavity $l = 0.625$ m was used for the airborne sound transmission.

The results shown for both the 3 and 4 mm thick windows indicate that as the depth of the cavity is increased the sound transmission is better predicted by the structure borne sound prediction model. At the smaller cavity depths the airborne sound transmission model does provide a reasonable prediction of the STL. A plausible explanation for these trends was given in Section 9.1.

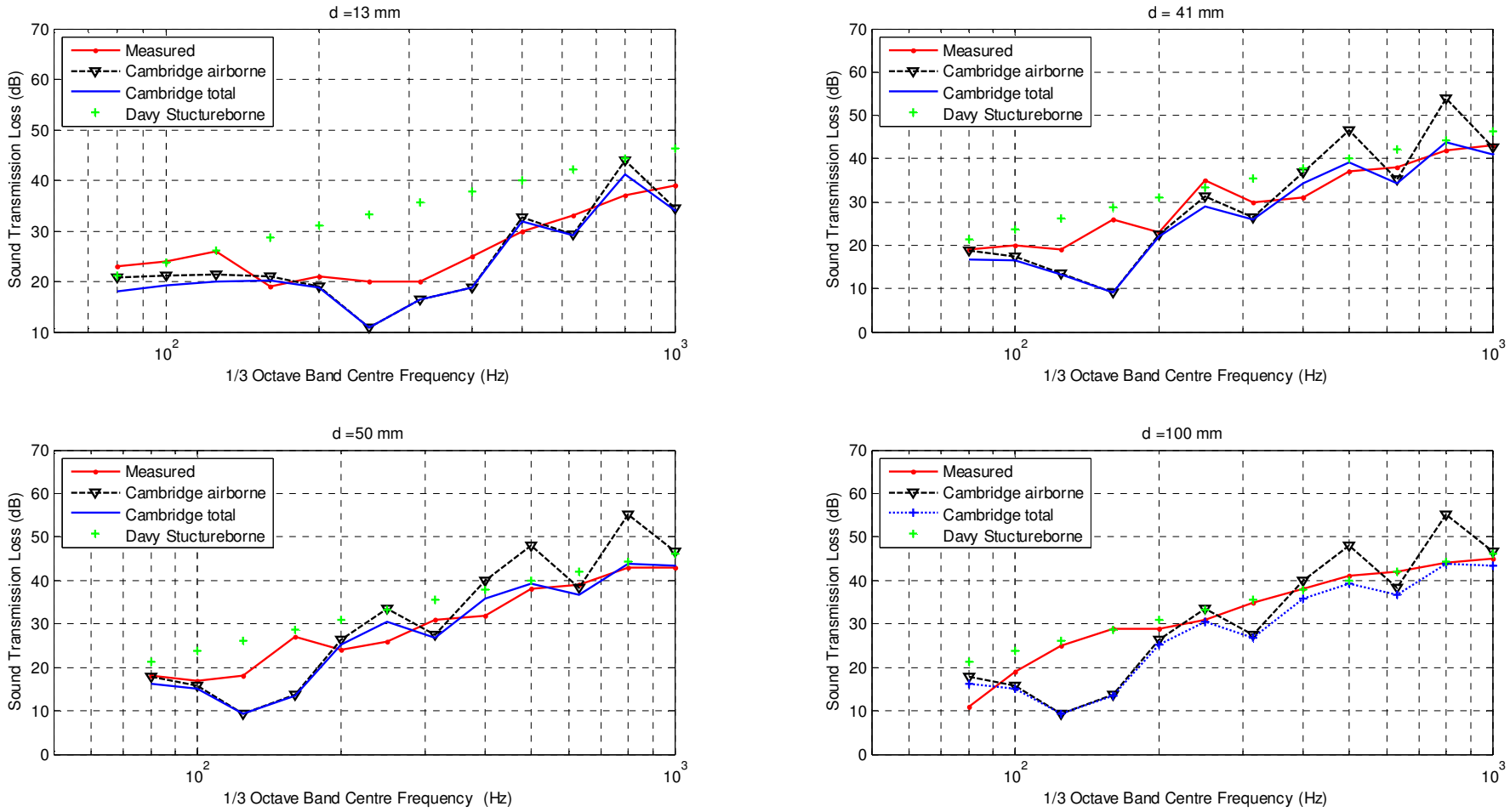

Figure 60 NRCC measured STL and predictions for a 3 mm thick double glazed system with 13, 41, 50 and 100 mm cavity depth

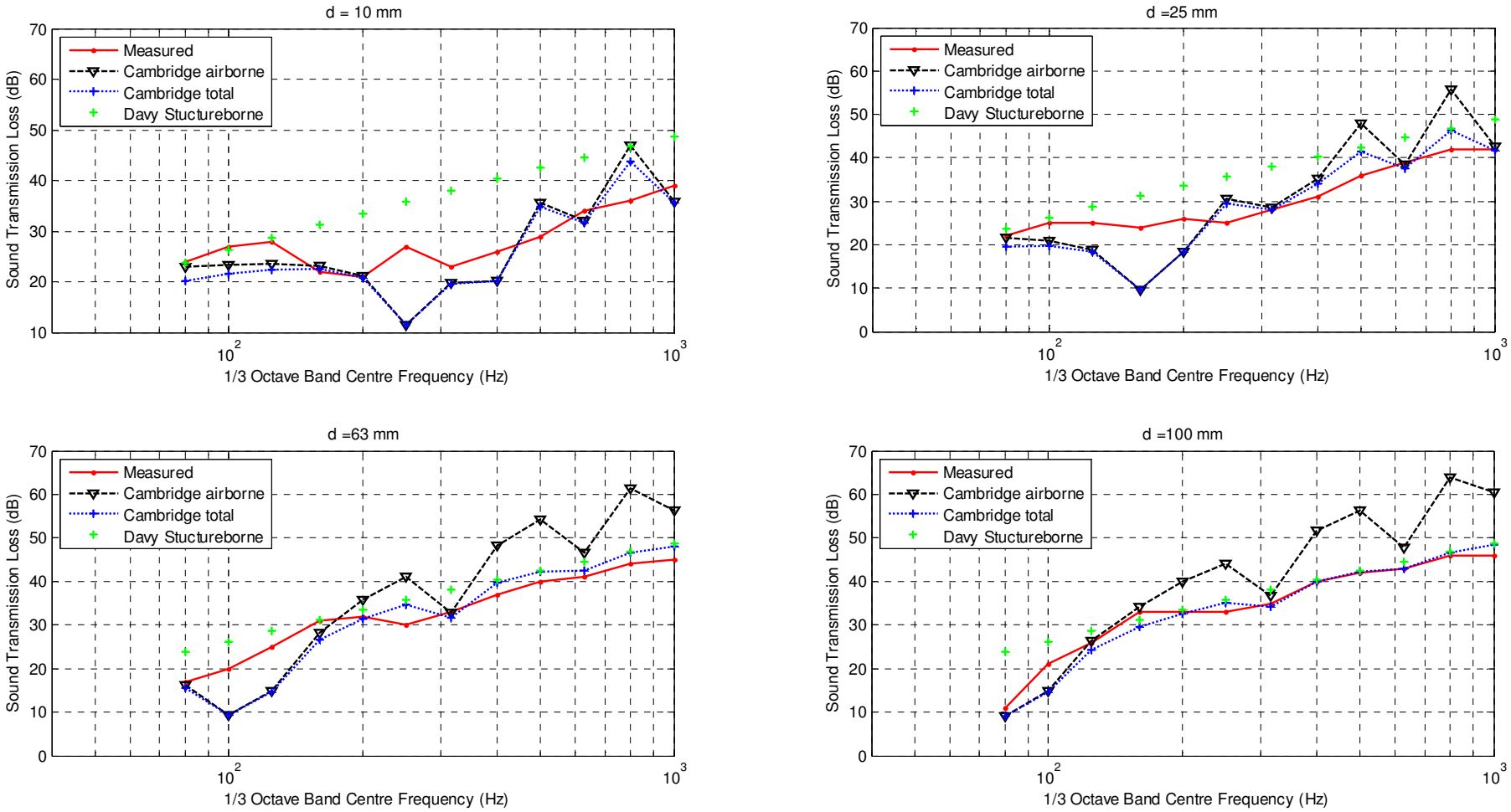

Figure 61 NRCC measured STL and predictions for a 4 mm thick double glazed system with 10, 25, 63 and 100 mm cavity depth

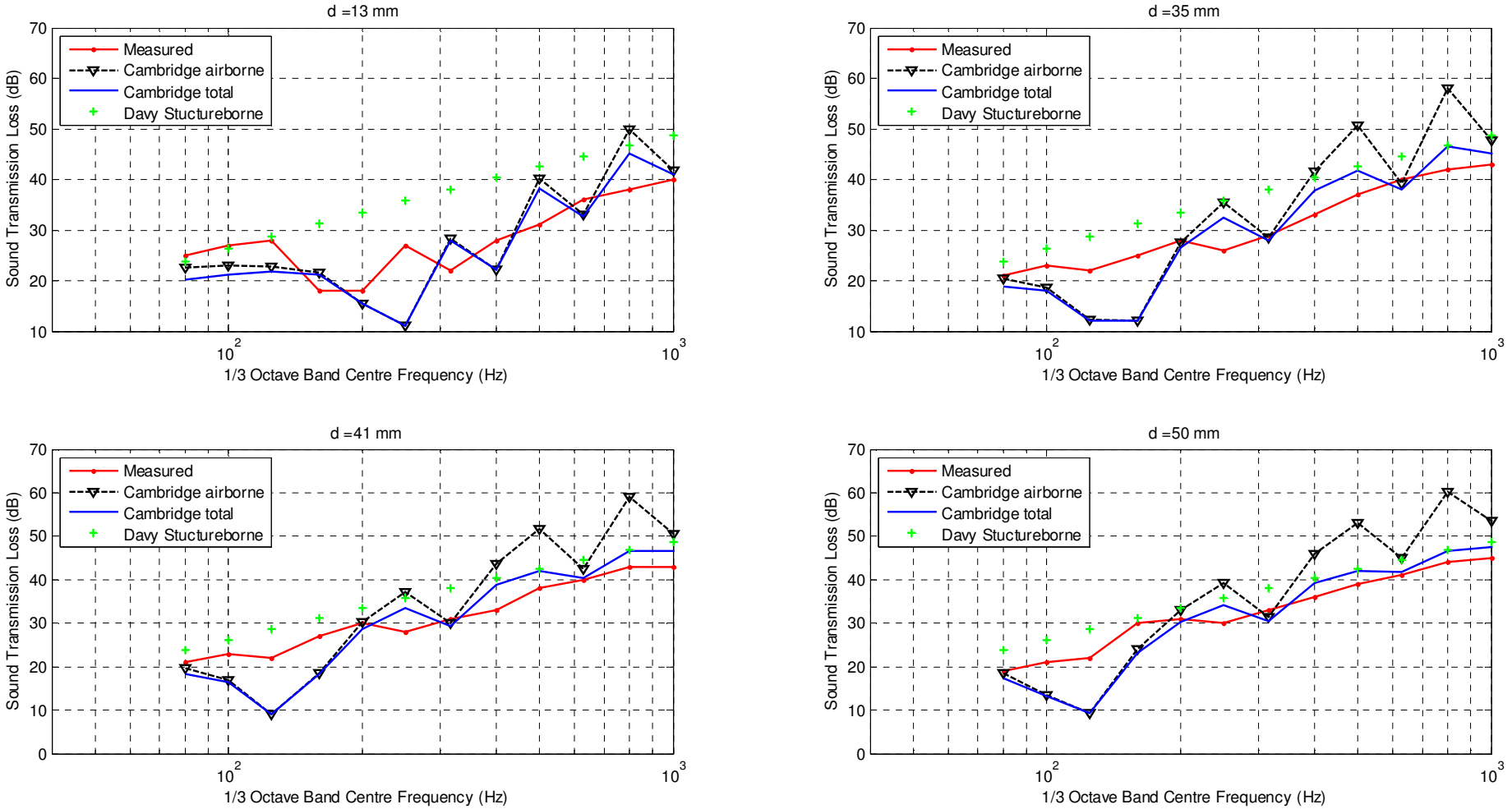

Figure 62 NRCC measured STL and predictions for a 4 mm thick double glazed system with 13, 35, 41 and 50 mm cavity depth

References

Abramowitz, M., and Stegun, I. A. (**1965**). *Handbook of mathematical functions with formulas, graphs and mathematical tables* (Dover Publications New York).

Allard, J. F. (**1987**). "Anisotropy effect in glass wool on normal impedance in oblique incidence," J. Sound Vib. **114**, 233-238.

Allard, J. F. (**1993**). *Propagation of sound in porous media: modelling sound absorbing materials* (Elsevier Applied Science, London).

Au, A. C. K., and Byrne, K. P. (**1987**). "On the insertion losses produced by plane acoustic lagging structures " J. Acoust. Soc. Am. **82**, 1325-1333.

Au, A. C. K., and Byrne, K. P. (**1990**). "On the insertion losses produced by acoustic lagging structures which incorporate flexurally orthotropic impervious barriers," Acust. **70** 284-291.

Bazley, E. N. (**1966**). *The airborne sound insulation of partitions* (Her majesty's stationery office London).

Beranek, L. (ed). (**1971**). *Noise and vibration contol* (McGraw-Hill Inc, New York).

Beranek, L. L., and Work, G. A. (**1949**). "Sound insulation through multiple structures containing flexible blankets," J. Acoust. Soc. Am. **21**, 419-428.

Bies, D. A., and Hansen, C. (**2009**). *Engineering noise control, theory and practice* (Taylor & Francis, New York).

Blanchard, P., Devaney, R., L, and Hall, G., R (**1998**). *Differential equations* (Brooks/Cole Publishing Company, Pacific Grove CA).

Bolton, J. S., Shiau, N. M., and Kang, Y. J. (**1996**). "Sound transmission through multi-panel structures lined with elastic porous materials " J. Sound Vib. **191**, 317-347.

Bravo, J. M., Sinisterra, J., Uris, A., Llinares, J., and Estelles, H. (**2002**). "Influence of air layers and damping layers between gypsum boards on sound transmission," Appl. Acoust. **63**, 1051-1059.

Brüel, P. V., and Rasmussen, G. (**1959**). "Free field response of condensr of condenser microphones," Brüel and Kjær Technical Review, Part 1, No. 1-1959, pp 12-17, Part 2-1959, pp.1-15.

Brunskog, J. (**2005**). "The influence of finite cavities on the sound insulation of double-plate structures " J. Acoust. Soc. Am. **117**, 3727-3739.

Burke, S. (**1983**). "The absorption of sound by anisotropic porous layers " in *106th Meeting of the ASA November 1983* (San Diego, California).

Chapra, S. C., and Canale, R. P. (**2002**). *Numerical methods for engineers with software and programming applications* (Mc Graw Hill, Boston).

Craik, R. J. M. (**2001**). *Sound transmission through buildings using the Statistical Energy Analysis* (Ashgate Publishing Limited Aldershot).

Craik, R. J. M. (**2003**). "Non-resonant sound transmission through double walls using Statistical Energy Analysis " Appl. Acoust. **64**, 325-341.

Craik, R. J. M., and Wilson, R. (**1995**). "Sound transmission through masonry cavity walls " J. Sound Vib. **179**, 79-96.

Cremer, L. (**1942**). "Theorie der schalldämmung sände bei schrägem einfall (Theory of sound insulation of a panel at oblique sound incidence)," Akustische Zeitschrift **7**, 81-104.

Cremer, L., Heckl, M., and Petersson, B. A. T. (**2005**). *Structure borne sound: Structural vibrations and sound radiation at audio frequencies* (Springer, Berlin, Heidelberg, New York).

Cremer, L., and Müller, H. A. (**1982**). *Prinicples and applications of room aoustics Volume 2* (Applied Science Publisher, London and New York).

Cummings, A., and Mulholland, K. A. (**1968**). "The transmission loss of finite sized double panels in a random incidence sound field " J. Sound Vib. **8**, 126-133.

Davy, J. L. (**1990a**). "A model for predicting the sound transmission loss of walls " in *Institution of Engineers Australia, Vibration and Noise Conference* (Melbourne).

Davy, J. L. (**1990b**). "Predicting the sound transmission of cavity walls " in *National Conference Australian Acoustical Society*

Davy, J. L. (**1991**). "Predicting the sound insulation of stud walls " in *Inter-noise 91*.

Davy, J. L. (**1998**). "Problems in the theoretical prediction of sound insulation " in *Internoise 98* (Christchurch, New Zealand).

Davy, J. L. (**2004**). "The radiation efficiency of finite size flat panels " in *Proceedings of Acoustics* (Australian Acoustical Society Gold Coast, Australia).

Davy, J. L. (**2009a**). "The directivity of the sound radiation from panels and openings," J. Acoust. Soc. Am. **125**, 3795-3805.

Davy, J. L. (**2009b**). "The forced radiation efficiency of finite size flat panels that are excited by incident sound " J. Acoust. Soc. Am. **126**, 694-702.

Davy, J. L. (**2009c**). "Predicting the sound insulation of walls " Build. Acoust. **16**, 1-20.

Davy, J. L. (**2010**). "The improvement of a simple theoretical model for the prediction of the sound insulation of double leaf walls " J. Acoust. Soc. Am. **127**, 841-849.

Ding, H., and Jacobsen, F. (**1994**). "Comparison of sound transmission loss between the sound intensity method and the conventional two room method in the laboratory " in *Inter-noise 94* (Yokohama-Japan).

Donato, R. J. (**1972**). "Sound transmission through a double leaf wall " J. Acoust. Soc. Am. **51**, 807-815.

Dowell, E. H. (**1978**). "Reverberation time, absorption and impedance," J. Acoust. Soc. Am. **64**, 181-191.

Elmallawany, A. (**1982**). "Improvement of the method of Statistical Energy Analysis for the calculation of sound insulation at low frequencies " Appl. Acoust. **15**, 341-245.

EN12354-1:2000. "Building acoustics: Estimation of acoustic performance of buildings from the performance of elements-Part 1: Airborne sound insulation between rooms " (European Committee for Standardization).

Fahy, F. (**1985**). *Sound and structural vibration: Radiation, transmission and response* (Academic Press, London).

Fahy, F. (**1995**). "Sound intensity " (E & FN Spon, London).

Fausti, P., Pompoli, R., and Smith, R. (**1999**). "An intercomparison of laboratory measurements of airborne sound insulation of lightweight plasterboards " Journal of Building Acoustics **6**, 127-140.

Finnveden, S. (**2007**). "Two observations on the wave approach to SEA," in *14th International Congress on Sound and Vibration* (Cairns, Australia).

Ford, R. D., Lord, P., and Williams, P. C. (**1967**). "The influence of absorbent linings on the transmission loss of double-leaf partitions," J. Sound Vib. **5**, 22-28.

Gerretsen, E. (**1979**). "Calculation of the sound transmission between dwellings by partitions and flanking structures " Appl. Acoust. **12**, 413-433.

Gerretsen, E. (**1986**). "Calculation of airborne and impact sound insulation between dwellings " Appl. Acoust. **19**, 245-264.

Gösele, V. K. (**1980**). "Zur Berechnung der Luftschalldämmung von doppelschaligen Bauteilen (ohne Verbindung der Schalen) (On the calculation of the dampening of air-borne sound by laminated building components)," Acust. **45**, 218-227.

Gösele, V. K., and Gösele, U. (**1977**). "Einfluß der Hohlraumdämpfung auf die Steifigkeit von Luftschichten bei Doppelwänden (Influence of cavity volume damping on the stiffness of air layers in double walls)," Acust. **38**, 159-166.

Gradshteyn, I. S., and Ryzhik, I. M. (**1980**). *Table of integrals, series and products* (Academic Press New York).

Green, W. D., and Cameron, W. S. (**1982a**). "Sound transmission loss of gypsum wallboard partitions. Report #1. Unfilled steel stud partitions " J. Acoust. Soc. Am. **71**, 90-96.

Green, W. D., and Cameron, W. S. (**1982b**). "Sound transmission loss of gypsum wallboard partitions. Report #2. Steel stud partitions having cavity filled with glass fiber batts " J. Acoust. Soc. Am. **71**, 902-907.

Green, W. D., and Cameron, W. S. (**1982c**). "Sound transmission loss of gypsum wallboard partitions. Report #3. 2*4 in. wood stud partitions " J. Acoust. Soc. Am. **71**, 908-914.

Gu, Q., and Wang, J. (**1983**). "Effect of resilient on sound transmission loss of metal double stud panel partitions " Chinese J. Acoust **113**.

Halliwell, R. E., Nightingale, T. R. T., Warnock, A. C. C., and Birta, J. A. (**1998**). "Gypsum board walls: Transmission loss data " (Internal report IRC-IR-761, National Research Council Canada).

Hamada, Y., and Tachibana, H. (**1985**). "Analysis of sound transmission loss of multiple structures by four-terminal network theory," in *Proceedings of Internoise 85* (Munich, Germany).

Hart, W., Noel, Bruce, D., Robert, Bommer, S., Arno, and Lefkowitz, A., Kimberly (**2010**). "+6 dB? The effect of pressure doubling on exterior to interior transmission loss values," in *Noise-Con 2010* (Baltimore, Maryland).

Heckl, M. (**1964**). "Einige Anwendungen des Reziprositätsprinzips in der Akustik (Some applications of the reciprocity principle in acoustics)," Frequenz **18**, 299-304.

Heckl, M. (**1981**). "The tenth Sir Richard Fairey memorial lecture: Sound transmission in buildings " J. Sound Vib. **77**, 165-189.

Hongisto, V. (**2006**). "Sound insulation of double panels - comparison of existing prediction models," Acta Acustica United With Acustica **92**, 61-78.

Hongisto, V., Lindgren, M., and Helenius, R. (**2002**). "Sound insulation of double walls - an experimental parametric study," Acta Acustica United With Acustica **88**, 904-923.

Hopkins, C. (**2007**). *Sound insulation* (Elsevier, Oxford).

Irvine, L. K., and Richards, L. R. (**1998**). *Acoustics and noise control handbook for architects and builders* (Krieger publishing company, Malabar Florida).

Jacobsen, F., and Ding, H. (**1996**). "Observations of the systematic deviations between the results of the conventional method and the sound intensity method of measuring transmission loss " in *Inter-noise 96* (Liverpool).

Jacobsen, F., and Juhl, P. (**2010**). "Radiation of sound," http://server.elektro.dtu.dk/ftp/fja/radiation.pdf.

Josse, R., and Lamure, C. (**1964**). "Transmission du son par une paroi simple (Sound transmission by a single wall)," Acust. **14**, 266-280.

Kang, H.-J., Ih, J.-G., Kim, J.-S., and Kim, H.-S. (**2000**). "Prediction of sound transmission loss through multilayered panels by using Gausian distribution of directional incident energy," J. Acoust. Soc. Am. **107**, 1413-1420.

Kihlman, T. (**1967**). "Sound radiation into a rectangular room. Applications to airborne sound transmission in buildings " Acust. **18**, 11-20.

Kropp, W. (**2003**). "Technical Acoustics 1: Propagation and radiation of structure borne sound (Lecture note 8)," (Chalmers University of Technology Department of Applied Acoustics Gothenburg).

Kurra, S., and Arditi, D. (**2001a**). "Determination of sound transmission loss of multilayered elements Part 1: Predicted and measured results " Acust. **87**, 582-591.

Kurra, S., and Arditi, D. (**2001b**). "Determination of sound transmission loss of multilayered elements part 2: An experimental study " Acust. **87**, 592-603.

Lait, J. C. S., Burgess, M. A., Narang, P. P., and Mikl, K. (**1991**). "Transmission loss measurements: Comparisons between intensity and conventional methods " in *Inter-noise 91* (Australia).

Leppington, F. G., Broadbent, E. G., and Heron, K. H. (**1982**). "The acoustic radiation efficiency of rectangular panels " Proceedings of the Royal Society of London.Series A, Mathematical and Physical Sciences **382**, 245-271.

Leppington, F. G., Broadbent, E. G., Heron, K. H., and Susan, M. M. (**1987**). "Resonant and non-resonant acoustic properties of elastic panels. II. The transmission problem " Proceedings of the Royal Society of London.Series A, Mathematical and Physical Sciences **412**, 309-337.

Ljunggren, S. (**1991**). "Airborne sound insulation of thin walls " J. Acoust. Soc. Am. **89**, 2324-2337.

London, A. (**1949**). "Transmission of reverberant sound through single walls " US Department of Commerce National Bureau of Standards **42**, 605-615.

London, A. (**1950**). "Sound transmission through double Walls," J. Acoust. Soc. Am. **22**, 270-279.

Loney, W. (**1971**). "Effect of cavity absorption on the sound transmission loss of steel-stud gypsum wallboard partitions," J. Acoust. Soc. Am. **49**, 385-390.

Loney, W. (**1973**). "Effect of cavity absorption and multiple layers of wallboard on sound-transmission loss of steel-stud partitions," J. Acoust. Soc. Am. **53**, 1530-1534.

Lund, J., and Bower, K., L (**1992**). *Sinc methods for quadrature and differntial equations* (Society for Industrial and Applied Mathematics Philadelphia).

Lyon, R. H., and Maidanik, G. (**1962**). "Power flow between linearly coupled oscillators " J. Acoust. Soc. Am. **34**, 623.

Mahn, J., and Pearse, J. (**2008**). "On the probablility density functions of the terms described by the EN12354 prediction model " Build. Acoust. **15**, 263-287.

Maidanik, G. (**1962**). "Response of ribbed panels to reverberant acoustic fields," J. Acoust. Soc. Am. **34**, 809-826.

Matlab (**2012**). "Matlab 2012a help file " (The MathWorks, InC).

Meyer, E. (**1935**). "Die Mehrfachwand als akustisch-mechanische drosselkette (Multiple walls as acoustic-mechanical inductor)," Elektr Nachrichtentech **12**, 393.

Morse, P. M. (**1939**). "Some aspects of the theory of room acoustics " J. Acoust. Soc. Am. **11**, 56-66.

Mulholland, K. A. (**1971**). "Sound insulation measurements on a series of double plasterboard panels with various infills " Appl. Acoust. **4**, 1-12.

Mulholland, K. A., Parbrook, H. D., and Cummings, A. (**1967**). "The transmission loss of double panels " J. Sound Vib. **6**, 324-334.

Mulholland, K. A., Price, A. J., and Parbrook, H. D. (**1968**). "Transmission loss of multiple panels in a random incidence field " J. Acoust. Soc. Am. **43**, 1432-1435.

Muller, G. G., Black, R., and Davis, T. E. (**1938**). "The diffraction produced by cylindrical and cubical obstacles and by circular and square plates " J. Acoust. Soc. Am. **10**, 6-13.

Narang, P. P. (**1993**). "Effect of fiberglass density and flow resistance on sound transmission loss of cavity plasterboard walls," Noise Control Engineering Journal **40**, 215-220.

Narang, P. P. (**1995**). "Material parameter selection in polyester fibre insulation for sound transmission and absorption " Appl. Acoust. **45**, 335-358.

New Zealand Department of Building and Housing (**2006**). "Compliance document for New Zealand building code," in *Clause G6 airborne and impact sound*

Nicolas, J., and Berry, L. J. (**1984**). "Propagation du son et effet de sol (Sound propagation and ground effect)," Revnue d'Acoustique, 191-200.

Northwood, T. D. (**1966**). "Transmission loss of plasterboard walls " (National Research Council Canada, Ottawa).

Novak, R. A. (**1992**). "Sound insulation of lightweight double walls " Appl. Acoust. **37**, 281-303.

Ookura, K., and Saito, Y. (**1978**). "Transmission loss of multiple panels containing sound absorbing materials in a random incidence field " in *Inter Noise 78* (San Francisco, USA), pp. 637-640.

Pan, J. (**1992**). "The forced response of an acoustic-structural coupled system " J. Acoust. Soc. Am. **91**, 949-956.

Pan, J., and Bies, D. A. (**1988**). "An experimental investigation into the interaction between a sound field and its boundaries," J. Acoust. Soc. Am. **83**, 1436-1444.

Pan, J., and Bies, D. A. (**1990**). "The effect of fluid-structural coupling on sound waves in an enclosure: Theoretical part " J. Acoust. Soc. Am. **87**, 691-707.

Prasetiyo, I., and Thompson, D. J. (**2012**). "Effect of finite air cavity and steel studs on sound transmission loss of lightweight double panel systems," in *Euronoise* (European Acoustics Association, Prague).

Price, A. J., and Crocker, M. J. (**1970**). "Sound transmission through double panels using Statistical Energy Analysis " J. Acoust. Soc. Am. **47**, 683-693.

Quirt, J., D (**1981**). "Measurement of the sound transmission loss in windows," in *Building Research Note 172* (Institute for Research in Construction, National Research Council Canada).

Quirt, J. D., and Warnock, A. C. C. (**1993**). "Influence of sound-absorbing material, stud type and spacing, and screw spacing on sound transmission through double-panel wall specimen " in *Inter-noise 93* (Leuven-Belgium).

Radinowitz, S. (**1993**). "How to find the square root of a complex number," Mathematics and Informatics Quarterly, 54-56.

Rasmussen, B. (**2010**). "Sound insulation between dwellings- Requirements in building regulations in Europe " Appl. Acoust. **71** 373-385.

Rasmussen, B., and Rindel, J. H. (**2005**). "Concepts for evaluation of sound insulation of dwellings-from chaos to consensus," in *Forum Acusticum* (Budapest), pp. 2081-2092.

Rindel, J. H. (**1975**). "Transmission of traffic noise through windows, influence of incident angle on sound insulation in theory and experiment " (Technical University of Denmark, Lyngby).

Rindel, J. H. (**2006**). *Chapter 5: Double Constructions* (E-mail to Cambridge).

Royar, J. (**2007**). "Different influence of mineral wool airflow resistivity on performance of sound transmission loss constructions," in *Inter-noise 2007* (Istanbul, Turkey).

Rudder, F. (**1985**). "Airborne sound tranmission loss characteristics of wood-frame construction," (Center for Building Technology, National Bureau of Standards Gaithersburg, MD), pp. 1-28.

Sato, H. (**1973**). "On the mechanism of outdoor noise transmission through walls and windows- A modification of infinite wall theory with respect to radiation of transmitted wave " The Acoustical Society of Japan **29**, 509-516.

Sewell, E. C. (**1970**). "Transmission of reverberant sound through a single-leaf partition surrounded by an infinite rigid baffle " J. Sound Vib. **12**, 21-32.

Sharp, B. H. (**1973**). "A study of techniques to increase the sound insulation of building elements " (US Department of Housing and Urban Development.).

Sharp, B. H. (**1978**). "Prediction methods for the sound transmission of building elements," Noise Control Engineering **11**, 53-63.

Sivian, L. J., and O'Neil, H. T. (**1932**). "On the diffraction caused by rigid circular plate, square plate and semi-finite screen," J. Acoust. Soc. Am. **3**, 483-510.

Smith, P. W. (**1962**). "Response and radiation of structural modes excited by sound " J. Acoust. Soc. Am. **34**, 827.

Smith, R. (**1997**). "Sound transmission through lightweight parallel plates " in *Department of Building Engineering and Surveying* (Heriot-Watt University Edinburg).

Spanier, J., and Oldham, K. (**1987**). *An atlas of functions* (Hemisphere Publishing Corporation, New York).

Stenger, F. (**1993**). *Numerical methods basen on Sinc and analytic functions* (Springer-Verlag, New York).

Sum, K. S., and Pan, J. (**1998**). "A study of the medium frequency response of sound field in a panel-cavity system " J. Acoust. Soc. Am. **103**, 1510-1519.

Sum, K. S., and Pan, J. (**2002**). "On the steady-state and the transient decay methods for the estimation of reverberation time," J. Acoust. Soc. Am. **112**, 2583-2588.

Sum, K. S., and Pan, J. (**2003**). "Some aspects of coupling-induced sound absorption in enclosures " J. Acoust. Soc. Am. **114**, 666-676.

Tomlinson, D., Craik, R. J. M., and Wilson, R. (**2004**). "Acoustic radiation from a plate into a porous medium " J. Sound Vib. **273**, 33-49.

Uris, A., Cervera, F., and Llinares, J. (**2000**). "Sound transmission loss of lightweight double walls filled with polyurethane foam," Noise Control Engineering Journal **48**, 5-7.

Uris, A., Llopis, A., and Llinares, J. (**1999**). "Effect of the rockwool bulk density on the airborne sound transmission of lightweight double walls," Appl. Acoust. **58**, 327-331.

Uris, A., Llopis, A., and Llinares, J. (**2001**). "Technical note: The influence of insulation thickness and number of layers of gypsum wall board on lightweight partition sound transmission loss," Noise Control Engineering Journal **49**, 238-240.

Utley, W. A., Cummings, A., and Parbrook, H. D. (**1969**). "The use of absorbent material in double leaf wall constructions " J. Sound Vib. **9**, 90-96.

Utley, W. A., and Mulholland, K. A. (**1968**). "The transmission loss of double and triple walls " Appl. Acoust. **1**, 15-20.

Vigran, T. E. (**2009**). "Predicting the sound reduction index of finite size specimen by a simplified spatial windowing technique," J. Sound Vib. **325**, 507-512.

Villot, M., and Guigou-Carter, C. (**2005**). "Using spatial windowing to take the finite size of plane structures into account in sound transmission," in *NOVEM* (Biarritz, France).

Villot, M., Guigou, C., and Gagliard, L. (**2001**). "Predicting the acoustical radiation of finite size multi-layered structures by applying the spatial windowing on infinite structures " J. Sound Vib. **245**, 433-455.

Warnock, A. C. C. (**2010**). "Sound transmission loss measurements: Personal communication via A. Warnock and J. Davy," (National Research Council of Canada).

Warnock, A. C. C., and Quirt, J. D. (**1995**). "Sound transmission through gypsum board walls " in *Inter-noise 95* (Newport Beach, CA, USA).

White, P. H., and Powell, A. (**1965**). "Transmission of sound and vibration through a Rectangular Double Wall " J. Acoust. Soc. Am. **40**, 821-832.

Wilson, R. (**1992**). *Sound Transmission Through Double Walls* (Heriot-Watt University).

World Health Organization (**1999**). *Guidlines for community noise* (World Health Organization Geneva).

World Health Organization regional office for Europe (**2011**). *Burden of disease from envionmental noise qualifications of healthy life years lost in Europe* (World Health Organisation Bonno).

Zaborov, V. I., and Klyachko, L. N. (**1967**). "Optimum parameters of double walls," Soviet Physics-Acoustics **13**, 113-114.